Universidade do Minho

Escola de Engenharia

Luís Carlos Rodrigues Moreira

Assist-As-Needed EMG-based Control Strategy for Wearable Powered Assistive Devices

Dissertação de Mestrado

Mestrado Integrado em Engenharia Biomédica

Ramo Eletrónica Médica

Trabalho realizado sob a orientação de

Professora Doutora Cristina P. Santos, Universidade do Minho

Doutora Joana Sofia Campos Figueiredo, Universidade do Minho

Doutora Elena García Armada, Consejo Superior de Investigaciones Científicas – Universidad Politécnica de Madrid

Dezembro de 2019

ACKNOWLEDGMENTS

Firstly, I want to thank my parents and brother for all the support, conditions, comfort and emotional strength that was given to me over the last five years. All the academic success was achieved because of your presence.

I would like to thank my advisor, Professor Cristina P. Santos, for the opportunity to work on this project, for all the guidance and motivational conversations towards the achievement of the main goals.

To my co-worker, Doctor Joana Figueiredo, I want to thank for all the availability, for give me the best advices, for being a constant support along this dissertation and for all the patience. You are an example to follow.

Thanks to my lab colleagues for all the good daily disposition, coffees, game of cards and for all the delicious Wednesday' snacks.

To the best friends that Braga gave me, João Mendes Lopes, Cristiana Pinheiro, Margarida Machado, Ana Pereira, Carla Pereira, Luciana Meneses and Pedro Mouta. We started together and we will continue always together. When and where is the next dinner? You are great people!

To all my musician friends of Banda Musical e Cultural da Vila de Rio de Moinhos, thank you for all the moments out of the work, for all the social meetings, barbecues and good music that we made together.

Last but not least, I have to thank my girlfriend, Mariana Costa, for being present in all the most important moments of my life, for giving the support and the strength to never give up and for all the times that you said "Força Engenheirinho!". You were essential in the success of this journey.

Thank you very much,

Luís Moreira

STATEMENT OF INTEGRITY

I hereby declare having conducted this academic work with integrity. I confirm that I have not used plagiarism or any form of undue use of information or falsification of results along the process leading to its elaboration.

I further declare that I have fully acknowledged the Code of Ethical Conduct of the University of Minho.

RESUMO

A assistência e reabilitação robótica usando dispositivos de assistência ativos vestíveis (WPADs), como ortóteses e exosqueletos, tem crescido na área da reabilitação com o fim de recuperar e aumentar a função motora de sujeitos com alterações neurológicas. Estes dispositivos devem fornecer uma assistência personalizada, uma vez que a condição física e a fadiga muscular variam de paciente para paciente. Nesta área, sinais de eletromiografia (EMG) têm sido usados para controlar WPADs, dada a sua capacidade de inferir a intenção de movimento do utilizador. Contudo, em casos de deficiência motora, os sinais de EMG apresentam menor amplitude quando comparados com sinais de EMG em condições saudáveis e, portanto, o uso de WPADs geridos por sinais de EMG pode não oferecer a assistência que o paciente necessita.

O principal objetivo desta dissertação visa o desenvolvimento de uma estratégia de controlo baseada em EMG capaz de fornecer assistência quando necessário, para futura integração num sistema ortótico ativo e inteligente (SmartOs). Para atingir este objetivo foram desenvolvidos e validados os seguintes elementos: **(i)** sistema de EMG para adquirir sinais de atividade muscular dos músculos mais relevantes no movimento da articulação do tornozelo; **(ii)** ferramenta de *machine learning* para estimação do binário da articulação do tornozelo para servir como referência na estratégia de controlo; e **(iii)** ferramenta de estimação do binário real do tornozelo considerando sinais de EMG dos músculos *Tibialis Anterior* (TA) e *Gastrocnemius Lateralis* (GASL) e ângulo real do tornozelo.

O sistema de EMG apresentou correlações satisfatórias com um sistema comercial. O binário de referência para o tornozelo foi gerado com base no ângulo de referência da mesma articulação, velocidade de marcha (de 1 até 4 km/h) e dados antropométricos (alturas de 1.51 m até 1.83 e massas de 52.0 kg até 83.7 kg), usando cinco algoritmos de *machine learning*: *Support Vector Machine*, *Random Forest*, *Multilayer Perceptron*, *Long-Short Term Memory* e *Convolutional Neural Network*. CNN apresentou a melhor performance, prevendo binários de referência do tornozelo com um fit entre 74.7 e 89.8 % e Normalized Root Mean Square Errors (NRMSE) entre 3.16 e 8.02 %. A estimativa do torque com base em sinais de EMG requer a inclusão de um maior número de músculos, uma vez que sinais de EMG dos músculos TA e GASL não foram suficientes.

PALAVRAS-CHAVE

Dispositivos de Assistência Ativos Vestíveis, Estratégia de Controlo baseada em EMG, Modelos de Regressão, Eletromiografia, Reabilitação da Marcha

ABSTRACT

Robotic-based gait rehabilitation and assistance using Wearable Powered Assistive Devices (WPADs), such as orthosis and exoskeletons, has been growing in the rehabilitation area to recover and augment the motor function of neurologically impaired subjects. These WPADs should provide a personalized assistance, since physical condition and muscular fatigue modify from patient to patient. In this field, electromyography (EMG) signals have been used to control WPADs given their ability to infer the user's motion intention. However, in cases of motor disability conditions, EMG signals present lower magnitudes when compared to EMG signals under healthy conditions. Thus, the use of WPADs managed by EMG signals may not have potential to provide the assistance that the patient requires.

The main goal of this dissertation aims the development of an Assisted-As-Needed (AAN) EMG-based control strategy for a future insertion in a Smart Active Orthotic System (SmartOs). To achieve this goal, the following elements were developed and validated: **(i)** an EMG system to acquire muscle activity signals from the most relevant muscles during the motion of the ankle joint; **(ii)** machine learning-based tool for ankle joint torque estimation to serve as reference in the AAN EMG-based control strategy; and **(iii)** a tool for real EMG-based torque estimation using *Tibialis Anterior* (TA) and *Gastrocnemius Lateralis* (GASL) muscles and real ankle joint angles.

EMG system showed satisfactory pattern correlations with a commercial system. The reference ankle joint torque was generated based on predicted reference ankle joint kinematics, walking speed information (from 1 to 4 km/h) and anthropometric data (body height from 1.51 m to 1.83 m and body mass from 52.0 kg to 83.7 kg), using five machine learning algorithms: Support Vector Regression (SVR), Random Forest (RF), Multilayer Perceptron (MLP), Long-Short Term Memory (LSTM) and Convolutional Neural Network (CNN). CNN provided the best performance, predicting the reference ankle joint torque with fitting curves ranging from 74.7 to 89.8 % and Normalized Root Mean Square Errors (NRMSEs) between 3.16 and 8.02 %. EMG-based torque estimation beneficiates of a higher number of muscles, since EMG data from TA and GASL are not enough to estimate the real ankle joint torque.

KEYWORDS

Wearable Powered Assistive Devices, EMG-based Control Strategy, Regression Models, Electromyography, Gait Rehabilitation

CONTENTS

LIST OF FIGURES

LIST OF TABLES

List of Abbreviations and Acronyms

A	Non-linear shape factor
AAN	Assist-As-Needed
ADAM	Adaptive Moment Estimation
AI	Artificial Intelligence
AL	*Adductor Longus*
ANN	Artificial Neural Networks
BF	*Biceps Femoris*
CCU	Central Controller Unit
CNN	Convolutional Neural Network
DT	Decision Trees
EMC	EMG Model-based Control
EMG	Electromyography
fEMG	Fine-wire EMG
FEL	Feedback-Error Learning
F^{max}	Maximum isometric muscle fiber force
F^{mt}	Muscle-tendon unit force

FR	Frequency Response
GAS	*Gastrocnemius*
GASL	*Gastrocnemius Lateralis*
GASM	*Gastrocnemius Medialis*
GM	*Gluteus Maximus*
GOF	Goodness of fit
GRA	*Gracilis*
HS	Heel-Strike
iEMG	Intramuscular EMG
ISCI	Incomplete Spinal Cord Injury
ISw	Initial Swing
L_o^m	Optimal Muscle Fiber Length
L_{slack}	Optimal Length of the Tendon
LMT	Musculotendon Length
LR	Load Response
LSTM	Long-Short Term Memory
MA	Moment Arm
MLP	Multilayer Perceptron
MSt	Mid Stance
MSw	Mid Swing
NRMSE	Normalized Root Mean Square Error
$\boldsymbol{\phi}$	Pennation angle
PID	Proportional Integral Derivative
PMC	Proportional Myoelectric Control
PSw	Pre-Swing

QF	*Quadriceps Femoris*
R	Correlation Coefficient
R^2	Coefficient of Determination
RBFNN	Radial Basis Function Neural Network
RF	Random Forest
RF	*Rectus Femoris*
RMSE	Root Mean Square Error
RMSJ	Root Mean Square Jerk
RQ	Research Question
sEMG	Surface EMG
SM	*Semimembranosus*
SmartOS	Smart Active Orthotic System
SOL	*Soleus*
ST	*Semitendinosus*
SVR	Support Vector Regression
TA	*Tibialis Anterior*
TF	*Tensor Fasciae*
TSt	Terminal Stance
TSw	Terminal Swing
VI	*Vastus Intermedius*
VL	*Vastus Lateralis*
v^m	Maximal speed of the muscle
VM	*Vastus Medialis*
WPAD	Wearable Powered Assistive Device
γ	Optimal Fiber Length

CHAPTER 1 – INTRODUCTION

This dissertation presents the work developed in the scope of the fifth year of the Integrated Master's in Biomedical Engineering during the academic year of 2018/19.

During the first semester, skills in the field of the human gait cycle were achieved at Marsi Bionics S.L. in Madrid, Spain, integrated into an ERASMUS placement program. With this experience, it was possible to learn competences regarding the human gait pattern based on the analysis of its main characteristics and strategies. As a result, a hybrid dynamic and kinematic model to simulate a healthy human gait cycle was constructed, fed and validated with data collected at the gait laboratory of the company.

The work presented in this dissertation was developed during the second semester and the concepts acquired in the first semester were fundamental to achieve the main goals of this project. This dissertation was developed at BiRD LAB (Biomedical Robotic Devices Laboratory) of the Center of MicroElectroMechanical Systems (CMEMs), at University of Minho, Braga, Portugal. This dissertation addresses the development of a control strategy for personalized human gait rehabilitation with a Wearable Powered Assistive Device (WPAD). To achieve this goal, an Assisted-As-Needed (AAN) EMG-based control strategy was projected, combining concepts of machine learning, to predict the reference gait kinematics and kinetics oriented to the user, with the development of musculoskeletal models to determine the real gait kinematics and kinetics of the user in real-time.

1.1. Motivation

According to [1], stroke events correspond to the **second leading cause of death** and the **third leading cause of disability** in the world. The phenomenon behind these episodes is related to the absence of oxygen in the brain tissue due to a rupture of an artery in the brain (hemorrhagic stroke) or due to a blocking in the blood flow (ischemic stroke) [2]. Based on [3], **63% of the stroke survivors** cannot walk without external support, not being able to perform their daily life activities. Consequently, the patient's quality life is affected due to social and work exclusion, costly medical assistance and early retirement [4].

The hemiparesis and hemiplegia are the two major consequences derived from a stroke. Hemiparetic patients exhibit weakness on one side of the body, whereas hemiplegic patients present complete paralysis on one side of the body. With this information, the residual lower limb muscle force of the hemiparetic patients can be considered into their gait rehabilitation [5].

The lower limbs rehabilitation has been changed in the last years, to deal with **(i)** the disadvantages associated with the inter- and intra-therapist variances; **(ii)** the dependency of the malleability of the patient's joint (commonly affected by spasticity); and **(iii)** the absence of precise and repeatable movements during therapy. For this purpose, in the rehabilitation area, the robotic assistance integrating **WPADs**, such as orthosis and exoskeletons, has steadily gained importance [6].

The first generation of WPADs for lower limbs, integrating trajectory tracking control strategies, is responsible to concern a cyclic pattern to the user, based on pre-programmed trajectories [7]. However, in these cases, the patient participation is reduced, since the effort required by the user to perform the walking motion is small. According to [8], [9], the rehabilitation process is more efficient if the encouragement of the patient participation is achieved. On the other side, it was already proved that these trajectory tracking strategies, when applied to hemiparetic patients, are not efficient in the rehabilitation context [10], [11]. In such circumstances, the incapacity level varies from patient to patient and it also varies during the rehabilitation process. From this perspective, since the physical condition and muscular fatigue comprehend different aspects that modify from patient to patient, a personalized assistance should be provided [12].

A human-machine interaction has been highlighted by applying bioinspired control architectures with **user-oriented assistive control strategies** integrated in WPADs. Moreover, these control strategies are designed to consider information about the user's motor condition and motion intention, by using bio-signals acquired with biomedical sensors [13]. In this context, **Electromyography (EMG)** signals have been

widely used since they can forecast information related to the user's motion intention, namely 20 – 100 ms before the user's lower limb motion [6], [14], [15]. In this sense, the provision of functional assistance is possible if **EMG-based assistive control strategies** are implemented into WPADs, avoiding the muscle atrophy.

1.2. Problem Statement

Notwithstanding the EMG-based control assistive strategies help to avoid muscle atrophy, this strategy is destinated to follow the intentions of the user. However, in cases of impairments of the lower limbs, the muscle weakness results in lower EMG signals when compared to EMG signals from healthy subjects [16]. Consequently, the use of EMG-based control strategies to manage the assistance delivered by WPADs may not provide the assistance that the patient needs to walk [17]. To combat this phenomenon, while considering the patient motion intention, studies have proposed **AAN control strategies** to provide the assistance needed by the patient to perform the walking motion [6].

The conventional AAN strategies consider the trajectory of the user's lower limbs and a predefined reference trajectory, not considering the human condition and motion intention [6]. Due to this, there are difficulties related to **(i)** the synchronism between the reference trajectory and the user's movement; and **(ii)** the adaptation of the reference trajectory according to the user-specific needs and intentions [18]. These drawbacks can be overpassed using EMG signals, taking advantage of their anticipatory performance, by the construction of an **AAN EMG-based control strategy**. Moreover, the EMG signals can be useful as a metric of the muscle weakness and, thus, when integrated in AAN control strategies, a personalized assistance could be provided [13].

This dissertation explores the potential of AAN strategies based on EMG signals for a future integration into a WPAD, in order to provide a personalized assistance in real-time, considering the physical condition and the motion intention of each user.

1.3. Goals and Research Questions

The ultimate goal of this dissertation aims the development of an AAN EMG-based control strategy towards the personalized rehabilitation of the ankle joint using **Smart Active Orthotic System (SmartOs)**. The strategy should be adapted for each user, providing only the required assistance in real-time.

The development of EMG-based control strategies requires the conversion of EMG signals into joint torques, particularly ankle joint torques [14], [19]. On the other side, the joint torques are dependent on

the joint kinematics and, thus, to perform the ankle joint torques prediction for specific subjects, the ankle joint kinematics should be well adapted. For this purpose and considering the main goal of this project, several objectives were established:

- **Objective 1:** To perform a literature search to collect the main control strategies already developed to assist and to restore the lower limbs functions, using EMG signals. Perform a literature search to collect the most relevant works to convert EMG signals into joint torque values. This objective is addressed in Chapter 2.
- **Objective 2:** To develop an EMG system to monitor the muscular activity of lower limb muscles, particularly the most important muscles responsible for the ankle motion. The system must correctly detect the muscle activations with low noise and with few motion artifacts. Validate the effectiveness of the developed EMG system with a commercial solution. This objective is addressed in Chapter 3.
- **Objective 3:** To implement and validate an effective method to estimate a reference joint position trajectory, namely ankle joint kinematics, tackling the variability of the walking speed and subject anthropometric data. This objective is addressed in Chapter 4.
- **Objective 4:** To develop and validate an automatic and accurate machine learning-based method to estimate a reference joint torque trajectory, considering the user-oriented reference joint kinematics and the variability of the walking speed and subject anthropometric data. This objective is addressed in Chapter 5.
- **Objective 5:** To implement and validate an efficient method to estimate the real user's joint torque, based on EMG signals and joint angles towards the implementation of the AAN EMG-based strategy. This objective is addressed in Chapter 6.

With this dissertation, four Research Questions (RQs) were identified and answered, in order to complete the main challenges of the project:

- **RQ1:** Which are the contributions and the main differences of the EMG-based control and the AAN EMG-based control strategies?
- **RQ2:** Is it possible to obtain joint torque measures only using EMG signals?
- **RQ3:** Is it possible to predict reference walking kinematics and kinetics trajectories relying exclusively on the walking speed and anthropometric data?

- **RQ4:** Can EMG-based torque estimation strategy present a good performance?

1.4. Contributions

The main contributions of this dissertation are:

- A descriptive literature review reporting the assistive control strategies based on EMG signals and integrated into WPADs;
- A descriptive literature review reporting the EMG-based torque estimation methods;
- A tool to estimate reference ankle joint position trajectories based on the walking speed and anthropometric data;
- A machine learning-based method for reference ankle joint torque estimation considering user-oriented reference ankle joint kinematics trajectories, walking speed and anthropometric data;
- A method to perform an EMG-based torque estimation using EMG signals and real ankle joint position trajectories, towards the implementation into a WPAD destinated for ankle joint assistance and rehabilitation.

Furthermore, the developed work allowed the publication of four conference papers:

- Moreira, L., Pinheiro, C., Lopes, J. M., Sanz-Merodio, D., Figueiredo, J., Santos, C. P., & Garcia, E. (2019). Study of Gait Cycle Using a Five-Link Inverted Pendulum Model: First Developments. In 2019 IEEE 6th Portuguese Meeting on Bioengineering (ENBENG) (pp. 1–4). IEEE. https://doi.org/10.1109/ENBENG.2019.8692451
- Lopes, J. M., Moreira, L. Pinheiro, C., Sanz-Merodio, D., Figueiredo, J., Santos, C. P., & Garcia, E. (2019). Three-Link Inverted Pendulum for Human Balance Analysis: A Preliminary Study. In 2019 IEEE 6th Portuguese Meeting on Bioengineering (ENBENG) (pp. 1–4). IEEE. https://doi.org/10.1109/ENBENG.2019.8692531
- Pinheiro, C., Lopes, J. M., Moreira, C., Sanz-Merodio, D., Figueiredo, J., Santos, C. P., & Garcia, E. (2019). Kinematic and kinetic study of sit-to-stand and stand-to-sit movements towards a human-like skeletal model. In 2019 IEEE 6th Portuguese Meeting on Bioengineering (ENBENG) (pp. 1–4). IEEE. https://doi.org/10.1109/ENBENG.2019.8692569
- Fernandes, P. N., Figueiredo, J., Moreira, L., Félix, P., Correia, A., Moreno, J. C., & Santos, C. P. (2019). EMG-based Motion Intention Recognition for Controlling a Powered Knee Orthosis. In 2019 IEEE International Conference on Autonomous Robot Systems and Competitions (ICARSC) (pp. 1–6). IEEE. https://doi.org/10.1109/ICARSC.2019.8733628

- Moreira, L., Figueiredo, J., Garcia, E. & Santos, C. P. (2020). Myoelectric Control Strategies Applied in Powered Lower Limb Assistive Devices: A Review. In Robotics and Autonomous Systems (Submitted).

1.5. Thesis Outline

This dissertation is organized in the following seven chapters.

Chapter 2 presents the state of the art addressed to four main points: **(i)** the main muscles responsible for the lower limbs joint motion; **(ii)** the most used EMG systems to acquire EMG signals; **(iii)** the EMG-based control and AAN EMG-based control strategies already implemented and integrated into WPADs to restore the lower limbs functions; and **(iv)** the EMG-based torque estimation methods already developed.

Chapter 3 exhibits an insight about SmartOs architecture, presenting information about its constituent hardware and software. It is also presented the proposed AAN EMG-based control strategy and the chapter ends with the hardware of the EMG system developed in this dissertation.

Chapter 4 presents a regression model to generate reference ankle joint kinematics, based on walking speed and anthropometric data. Additionally, it describes the data acquisition protocol to validate all the algorithms developed in this dissertation.

In Chapter 5, machine learning algorithms are developed and validated to predict the ankle joint torques, that will be used as a reference parameter on the control strategy proposed in Chapter 3.

Chapter 6 presents the validation of the results obtained in Chapter 4 and Chapter 5, where the output results obtained in Chapter 4 serve as input data to the best algorithm developed in Chapter 5. Moreover, the chapter describes the implemented algorithm responsible for EMG-based real joint torque estimation and presents its validation.

Lastly, Chapter 7 presents the main conclusions of this master dissertation, the research questions are answered and topics for a future work are proposed.

CHAPTER 2 – STATE OF THE ART

This chapter begins with a brief description of the healthy and the pathological walking motion, identifying the main muscles affected by a stroke event and the main muscles responsible for the motion of the knee and ankle joints. Subsequently, commercial EMG systems are presented, as well as their main characteristics. It is followed by an exhaustive review of the control strategies already developed and applied into WPADs, using EMG signals to assist and restore the lower limbs functions. At last, studies related to the conversion of the EMG signals into torque values are also presented, since most of the EMG-based control strategies perform this conversion [14], [19].

2.1. Physiological Aspects

Stroke events cause functional or neuromuscular changes, depending on the location of the affected area of the brain. According to [16], [20], these changes are related to a loss of strength in the hemiparetic leg, being verified weakness in the flexor muscles and spasticity in the extensor muscles, causing an increase of the joint stiffness. Studies concluded that, generally, in stroke survivors, the *Soleus* (SOL) and *Gastrocnemius* (GAS) muscles (responsible for the plantar flexion motion of the ankle joint) are contracted due to spasticity, while the *Tibialis Anterior* (TA) muscle (responsible for the dorsiflexion motion of the same joint) remains weak [2], [16], [20], [21]. This is the main reason of the drop foot disorder in patients that suffered a stroke event [22]. Regarding the knee joint, the knee extensors (*Vastus Medialis* (VM), *Vastus Lateralis* (VL), *Vastus Intermedius* (VI) and *Rectus Femoris* (RF)) exhibit spasticity and the knee flexors (*Biceps Femoris* (BF), *Semitendinosus* (ST) and *Semimembranosus* (SM)) are weak, being

verified a knee hyperextension and a decrease in the flexion movement of this joint during the gait cycle [16], [20], [21]. In this sense, considering the muscles affected by stroke events and according to [23], the muscles that provide more information about the **ankle joint** motion are the **TA** muscle for dorsiflexion and the **SOL** or the **GAS** muscles for plantar flexion. Concerning the **knee joint**, the muscles that present more information are the **BF** muscle for flexion and the **VM** and the **RF** muscles for extension.

2.2. Electromyographic Signals

2.2.1. Overview

The contraction and the relaxation episodes of the muscles are controlled by the nervous system, through electric signals delivered by the neurons to the muscles. This electrical activity can be recorded using EMG, providing a powerful forecast information related to the motion intention of the user [6], [14], [15], [24].

EMG signals can be measured using needles inserted directly in the muscles (**intramuscular EMG – iEMG**, also known as **fine-wire EMG – fEMG**) or using electrodes placed on the skin (**surface EMG - sEMG**). The choice of the method to measure the electrical activity of the muscles depends on the properties of the muscles to study. Comparing both, the first enounced method presents less cross-talk, since it receives lower muscle activities of the muscles around the desired muscle [25]. However, due to the difficulty of insertion, greater invasiveness and higher cost, this method is not normally used in EMG studies [25], [26]. In contrast, **sEMG technique is commonly used**, since it is non-invasive, practical, inexpensive and it may be used by non-clinical assessors. In addition, some studies reported that this method, when applied to the SOL, GAS and TA muscles, presents EMG amplitudes similar to iEMG and a negligible value of cross-talk [27]–[29].

Regarding the sEMG (referred as "EMG" along this dissertation), there are two configurations to adopt, namely the **monopolar** and the **bipolar**. The monopolar configuration uses two electrodes: detection electrode placed on the skin, above the muscle in study; and a reference electrode that should be placed on an electrically neural tissue or a bone [30]. However, according to [31], this configuration is not recommended, since the signal-noise ratio and the spatial resolution of the EMG signals are reduced, when compared to EMG acquisitions performed with bipolar configurations. On the other side, the bipolar configuration uses three electrodes: two detection electrodes placed above the target muscle, distanced by 10 - 20 mm [32], [33] and a reference electrode. In this sense, the **bipolar configuration is**

preferable, since the common noise of both detection electrodes is eliminated, increasing the signal-noise ratio and producing a cleaner EMG signal [33], [34].

2.2.2. Commercial Systems

The characteristics of the EMG signals are well established in the literature and the most relevant are the amplitude range between ±10 mV, the response frequency between 0 and 500 Hz with the dominant energy between 50 and 150 Hz and the stochastic nature, characterized by a Gaussian distribution function [35].

Delsys, Noraxon, MotionLab, Plux, BTS Bioengineering, Contemplas, Cometa, Biopac, Shimmer, Cadwell, Myontec and Athos are examples of companies that produce EMG acquisition systems able to acquire EMG signals with the aforementioned characteristics. An EMG acquisition system can reach the tens of thousands of euros and, thus, depending on the finality of each project, it is required to analyze the specifications of each system. Table 1 summarizes the main characteristics of the 4 more used commercial EMG acquisition systems.

Table 1. EMG systems specifications

	Delsys [36], [37]	**Noraxon** [38]	**Motion Lab** [39]	**MuscleBAN** [40], [41]
EMG Signal Input Range	± 11 mV	± 24 mV	± 250 mV	*
Resolution	16 bits	16 bits	16 bits	16 bits
EMG Signal Bandwith	20 – 450 Hz	Minimum: 20 – 500 Hz Maximum: 5 – 1500 Hz	10 – 2000 Hz	1 – 1000 Hz
Sampling Rate	2000 Hz	2000 Hz or 4000 Hz	4000 Hz	4000 Hz
Transmission Range	40 m	40 m	18 m	10 m
Gain	1	1	10 – 500	1100
Sensor Size	27 x 37 x 13 mm	24 x 37 x 16 mm	38 x 19 x 9 mm	28 x 70 x 12 mm
Mass	14 g	14 g	20 g	25 g
Autonomy	2 – 3 h	8 h	*	8 h
Temperature Range	5 – 45 degrees Celsius	0 – 38 degrees Celsius	20 – 40 degrees Celsius	*

*Information not specified

2.3. Assistive Control Strategies

In this section, the control strategies involving EMG signals to control WPADs found on literature are analyzed, covering the EMG-based control and the AAN EMG-based control strategies. This information is useful to determine which strategies were already developed, which of them yielded the best results and which are the methodologies required to achieve proper rehabilitation outcomes.

The implemented search methodology was based on an electronic literature search on IEEE, Web of Science, and Scopus. The keywords used were: ["EMG based control"], ["EMG based control lower limbs"], ["AAN EMG based control"] and ["assist as needed EMG based control"]. Hyphens were also used, for example ["EMG-based control"] to consider all the search possibilities, as well as the extension of EMG: electromyography. The inclusion criteria were based on four assumptions. The control strategy must: **(i)** be in real-time; **(ii)** be applied only for lower limbs; **(iii)** use WPADs and **(iv)** use EMG readings to control WPADs.

For a better comprehension of the information collected, two tables were constructed to extract the data related to EMG-based control strategies (Table 2) and AAN EMG-based control strategies (Table 3).

2.3.1. EMG-based Control Strategies

The EMG-based control strategies use EMG signals to detect the user's motion intentions to control the WPADs always following the EMG signals collected [19]. From the literature search, two control methods were found involving EMG signals: **Proportional Myoelectric Control** (PMC) and **EMG Model-based Control** (EMC).

A. Proportional Myoelectric Control

In [42], an ankle orthosis was developed using two artificial pneumatic muscles to simulate the SOL and the TA muscles. They implemented a PMC strategy that adjusts proportionally the air pressure delivered to both artificial muscles according to their EMG signals. Clinical results involving two subjects with Incomplete Spinal Cord Injury (ISCI) demonstrated a positive modification of muscle recruitment during the walking assisted by the ankle orthosis.

Another proportional method was proposed by [43] to control the HAL-3 exoskeleton to assist the hip and the knee joint. They presented a calibration method to find two proportional gains for each joint, one for flexion and other for extension motion and, thus, the assistance torque of each joint only depends on the contribution of each muscle. The effectiveness of the methodology was tested during walking and standing up test. Information about the ground reaction force was also considered to avoid the user's

discomfort. An identical strategy was developed by [13]. They found two constant parameters to estimate the user's knee joint torque directly, in order to control a powered knee orthosis, according to the user's motion. Results from healthy walking in a treadmill indicated that the PMC strategy (active condition) requires less effort from the users than passive conditions, presenting smaller levels of muscular activity.

In [44], another PMC strategy was proposed, using EMG and joint angle data to control a powered ankle exoskeleton. These data were converted into torque values, based on a linear proportional model developed by [45]. Experiments performed in eight healthy volunteers showed that the level of muscular activity of the muscles decreased with the assistance of the exoskeleton, whereas the joint angles were controlled.

B. EMG Model-based Control

EMC is a strategy that uses models driven by EMG signals, such as musculoskeletal or empirical models (topics covered in the next section), to map the user's motion intentions into assistive commands, in order to control WPADs.

The most used musculoskeletal model to control WPADs using EMG signals was established by [46] and developed by [47]. Based on this model, it is possible to obtain the joint torque considering the EMG signals of the muscles of the joint in the study, the joint angles, and specific muscle parameters found in calibration steps [47]. Other models were developed based on this one, minimizing the model uncertainty [48]–[50].

Using the Hill-type muscle model developed by [47], in [51], a knee electrical orthosis controlled by the user's intentions was proposed. The outputs of the model were the user joint torque and the stiffness trend index. With these two variables, the user joint angle and stiffness were determined and, thus, the torque that should be applied by the orthosis was also determined. The performance of the method was evaluated in a healthy subject performing the sit-to-stand and stand-to-sit movements, showing a good adaptation of the controller, since the user's torque under assistance conditions was reduced. In [44], based on [47], [48], an ankle power-assist orthosis robot was controlled using EMG data and joint angles. Concerning the calibration process, only three parameters were identified: **(i)** the maximum isometric muscle fiber force, F^{max}; **(ii)** the optimal fiber length, L_o^m; and, **(iii)** a non-linear shape factor, A. An assistant ratio with four levels was defined to achieve the assistance torque, when multiplied by the torque predicted by the musculoskeletal model. Experiments performed in eight healthy volunteers showed that as the assistant ratio increased, the level of muscular activity of the muscles decreased, as well as the level of movement stability, which is in accord with [52].

As empirical models, neuro-Fuzzy methods have been explored in this field. This approach was developed in [53] and quoting the explanation presented by [54], "*A fuzzy controller consists of four main blocks: the fuzzification block, which interprets the inputs; the fuzzy-rules block, which holds the knowledge of how to control the system; an interface mechanism to select which rule should be implemented; and the defuzzification block which converts the fuzzy results into desired output signals*". In [53], the inputs of the fuzzification block were the EMG signals acquired from eight muscles (presented in Table 2). The EMG signals were converted into torque values, based on twenty fuzzy IF-THEN control rules (fuzzy-rules block), according to the fuzzy linguistic variables developed. To each control rule, a value of torque was attributed (selection of the rule to implement and access to the defuzzification block). To test the effectiveness of the EMG-based controller, experiences were carried out with a healthy subject, who performed the sitting down and standing up motion under normal and tired physical condition. Under assisted conditions, the hip and knee joint angles were controlled, and the activity levels of the muscles were reduced.

In [55], it was reported that the joint torque generated to perform different motions depends on the joint angle. For this purpose, the joint angles were considered, along with the EMG signals to estimate the joint torque. A change in the control approach developed by [53] was made, avoiding the fuzzy IF-THEN control rules to obtain the hip and knee joint torque directly. A real-time neuro-fuzzy muscle-model matrix modifier with five layers was proposed, where the inputs were the hip and the knee joint angles. Results, from three healthy male subjects demonstrated a reduced muscle level activation, indicating that the model adopted itself to each user.

Recently, in [11], it was developed another method to estimate the hip and knee joint torques using EMG signals, joint angles, velocities, and accelerations to control a knee orthosis. These signals were converted into torque values, through a Radial Basis Function Neural Network (RBFNN). A two-step learning strategy was developed to improve the accuracy of the estimation. This method was proposed to estimate the joint torque with practicability and adaptivity, where there was no necessity of model calibrations and where the model should be updated in real-time. Experiments including four subjects performing the swing motion showed that this model can obtain the joint torque without calibration steps.

Table 2. EMG-based control strategies

Study	Control Method	Joint	Muscles	Participants (number)	Results
[42]	PMC	Ankle	SOL and TA	ISCI (2)	Recruitment of the muscles, during the walking motion
[43]	PMC	Hip Knee	BF, VM, *Gluteus Maximus* (GM) and RF	Healthy (1)	Decrease in the levels of muscular activity
[13]	PMC	Knee	ST, SM, VL and VM	Healthy (2)	Decrease in the levels of muscular activity
[44]	PMC	Ankle	TA and GAS	Healthy (8)	Decrease in the levels of muscular activity
[51]	EMC	Knee	RF, VM, VL, BF, SM and ST	Healthy (1)	Decrease in the levels of muscular activity
[44]	EMC	Ankle	TA and GAS	Healthy (8)	Decrease in the levels of muscular activity
[53]	EMC	Hip Knee	*Tensor Fasciae* (TF), RF, VL, VM, *Adductor Longus* (AL), *Gracilis* (GRA), BF and ST	Healthy (1)	Decrease in the levels of muscular activity
[55]	EMC	Hip Knee	TF, RF, VL, AL, GRA, VM, BF, ST	Healthy (3)	Decrease in the levels of muscular activity
[11]	EMC	Hip Knee	*Quadriceps Femoris* (QF) and BF	Healthy (4)	Decrease in the levels of muscular activity

2.3.2. AAN EMG-based Control Strategies

Further studies have been explored AAN EMG-based control strategies by providing the assistance required by the user while considering his/her motion intention from EMG signals [17]. With this control strategy, the patient can perform the walking motion correctly, based on a human-machine interaction, regaining autonomy to move [56].

C. Fleischer *et al.* [17], [57], [58] presented the first works in this field, developing a control strategy able to provide an additional torque upon the knee joint torque of the user, estimated through EMG signals. This control strategy is composed by two loops: the outer loop and the inner loop. In the outer loop, the processed EMG signals, along with the joint angles, are converted into knee torque values of the wearer through a musculoskeletal model [48]. These knee joint torques are multiplicated by an amplification factor, defined as a support ratio, varying from 0 to 1 to set the target joint torque. The inner loop provides the real knee torque based on force sensors connected between the orthosis and the

actuator. Consequently, the controller sends a control signal to the orthosis to diminish the difference between the current and the target torques, achieved with the inner and the outer loop, respectively. Experiments with a healthy subject showed a decreased muscle activation when the support ratio increases, since the user is benefitting from the support provided. However, the interaction between the user and the WPAD showed operating issues, such as oscillations in the knee torque provided when fast movements are performed for the maximum the support ratio.

Later, in [56], [59], [60], another AAN EMG-based control strategy was developed, integrated into a knee joint actuated orthosis. EMG signals along with the knee angles, acted as inputs in an EMG-Driven Musculoskeletal model [49] to obtain the user's knee joint torque. The desired torque was estimated by inverse dynamics. In this sense, the torque delivered by the orthosis is inversely amplificated or reduced with respect to the user's knee joint torque. Different experimental tests were performed in the three works to evaluate the robustness of the implementation. In [59], with the user in a sitting position, three tests were made: **(i)** subject in passive mode; **(ii)** subject developing a considerable torque level; and, **(iii)** subject developing less torque level. When the user develops an enough effort/torque to complete a specific task, the assistance torque decreases, whereas if the user does not develop enough torque to complete a task, not performing the desired trajectory, the assistance torque increases. During these three experiments, the Root Mean Square Error (RMSE) between the current knee joint position and the desired one was below 0.7 °. Experiments with the user performing step movements indicated a RMSE below 2.71 °, between the current and the desired knee joint position [60]. The robustness related with external disturbances was tested in [56], with the orthosis providing a greater torque to drive the system to the desired trajectory. In these cases, RMSE equal to 6.81 ° were achieved.

Table 3. AAN EMG-based control strategies

Study	Control Method	Joint	Muscles	Participants (number)
[57]	EMC	Knee	RF, VL and ST	Healthy (1)
[58]	EMC	Knee	RF, VM, VL, SM, ST and BF	Healthy (1)
[17]	EMC	Knee	RF, VM, VL, SM, ST and BF	Healthy (1)
[59]	EMC	Knee	RF, VL, SM, ST and BF	Healthy (1)
[60]	EMC	Knee	RF, VL, SM, ST and BF	Healthy (1)
[56]	EMC	Knee	RF, VL, SM, ST and BF	Healthy (1)

2.3.3. Discussion

The reviewed control strategies, presented in Table 2 and Table 3, were designed to help the lower limbs performing certain motions, in real-time. According to [61], these control strategies may be categorized in assistance or rehabilitation strategies, as follows. An assistance strategy is generally used in subjects with lower limb impairments, to enable a performance similar to the performance of healthy individuals. On the other hand, rehabilitation strategies are defined as a method to rehabilitate and re-train the lower limb capabilities of subjects who suffered an injury.

The four PMC methods presented in [13], [42]–[44] have different purposes. Studies [13], [43], [44] revealed that the developed control strategy generated lower levels of muscular activity, whereas the joint trajectories were correctly executed. In contrast, in [42], experiments realized in ISCI patients showed a recruitment of the muscles after using the WPAD controlled by a PMC. These findings demonstrate that the works developed by [13], [43], [44] and the strategy proposed in [42] could be suitable for lower limb assistance and rehabilitation, respectively.

Concerning the EMC strategies, they were divided into two categories: the musculoskeletal and the empirical models. All the reviewed model-based control strategies contributed to lower limb assistance, since the levels of muscular activity decreased, while the joint angles were controlled. Both of the musculoskeletal models proposed in [44], [51], were based on [47]. In spite of showing a decreased muscular activity, the study [44] reported that as the amplification factor increases, the instability of the control system also increases. This fact was rectified in [51], since there is no amplification factors in the control strategy.

The PMC strategies and the musculoskeletal models presented [13], [42]–[44], [51] require calibration steps to determine proportional gains or model parameters, respectively. These calibration steps are realized with the users performing specific movements, such as isometric contractions or walking. This procedure may present a methodological issue when applied to pathological individuals because some of them may not be able to perform these motions due to muscular weakness.

On the other hand, the empirical models do not depend on calibration steps. Previous studies [11], [53], [55] demonstrated that the levels of muscular activity decreased when using WPAD controlled by empirical models. Thus, these strategies could be useful to assist lower limbs with moderate impairments. However, some limitations were notified in [11], namely a resistance offered by the orthosis during the motion, that could be related to the generation of torque by other muscles (not the QF, neither the BF). In this sense, an alternative to improve the effectiveness of empiric models aims the use of a higher number of EMG electrodes to map the user intentions correctly.

Furthermore, the works developed by [17], [56]–[60] reveal to be a suitable approach to assist and rehabilitate the knee joint, when the user requires support. Based on the results, two situations were verified: **(i)** if the support ratio provided by the WPAD increases, the user's torque decreases, but the knee joint angle remains equal; and (ii) if the support ratio decreases, the user's torque increases and the knee joint angle remains equal once again. This indicates that the AAN strategy provides the assistance to perform the movements when required, offering great potential to motor rehabilitation and user's motor autonomy. Nonetheless, the muscle model should be improved and suitable for each muscle, in order to consider different activation delays of each muscle.

Based on the AAN EMG-based model strategies already developed, it is concluded that if the user does not perform any movement, the exoskeleton provides the enough amount of torque to complete the desired knee joint trajectory. On the other hand, if the wearer has an electric signal associated, the exoskeleton only provides a torque upon the user's torque, in order to achieve a correct knee joint trajectory.

2.4. EMG-based Torque Estimation

Most of the implemented control strategies involved the joint torque estimation of the real user's joint torque, based on the EMG signals acquired from specific muscles. For this purpose, a literature search was made to review the methods applied to convert the EMG signals into torque values, namely **proportional gain methods**, **musculoskeletal models** and **empirical models**, as presented in Table 4.

2.4.1. Proportional Gain Methods

The studies developed by [13], [43], [44] followed the same methodology to obtain the joint torque, based on a proportional gain method. They carried out a calibration step to find proportional gains per joint, for flexion and extension motions. For this purpose, the participants had to maintain a fixed joint angle, while the orthosis/exoskeleton actuator performed a fixed torque value. This process implied that the participant needed to perform a joint torque to maintain the required joint angle. At the same time, the EMG signals were read and, a proportional gain that relates the EMG signals with the joint torque was found. In the three works, the estimated joint torque was similar to the real one. In [13], a Normalized Root Mean Square Error (NRMSE) and a phase delay between the measured torque and the estimated torque was were calculated, achieving values of 12 % and 22 ms, respectively. In [44], the RMSE and the Root Mean Square Jerk (RMSJ) between the estimated and the measured torque was 3.56 ± 0.63 Nm and 2.85 ± 0.78 Nm, respectively.

2.4.2. Musculoskeletal Models

The Hill-type model proposed by [46] and developed in [47] was the first musculoskeletal model proposed to estimate joint torque using EMG signals and joint angles. Further variations of this model have been developed, improving the calibration process, in order to minimize the model uncertainty. In this calibration process, muscle parameters are identified to construct the model, following a trade-off between the accuracy of the model and its complexity [51].

Based on [46], [47], the work of [48] predicts the knee joint torque, using EMG signals from thirteen muscles and the knee joint angles. Eighteen parameters were found in the calibration process to construct the model. Among these parameters, the force produced by the muscle-tendon unit (F^{mt}), depends on the pennation angle (ϕ) that depends on L_o^m. Consequently, L_o^m is function of the percentage change in optimal fiber length, γ. This percentage was varied in this study to investigate the importance of a correct calibration step in musculoskeletal models. The feasibility of the conversion was assessed by six subjects, who performed approximately 204 tasks, including dynamometer, running and sidestepping trials. Coefficient of determination (R^2) of 0.91 ± 0.04 was obtained between the knee joint torque predicted by the model and by inverse dynamics. A mean residual error below 0.2 Nm/kg normalized to body weight was achieved. These results were obtained with γ = 15 %. When γ was set to 0 %, a R^2 of 0.85 was obtained, showing the sensitivity of the model to the parameters of the calibration step.

Based on the works developed by [47], [48], other six works were developed aiming the simplification of the model, the reduction of the conversion time and the reduction of the conversion errors. In [62] the user motion intentions for the knee joint were mapped, using EMG signals (listed in Table 4) and knee joint angles. At the same time, the joint angles and the ground reaction forces served as input to the seven-link biomechanical model (composed by two legs with feet, shanks, thighs and the torso) to obtain the knee joint torque through inverse dynamics. When compared to [48], only two parameters were calibrated (presented in Table 4). The effectiveness of the methodology was evaluated in one healthy subject during stepping up stairs and with flexion and extension motions of the knee joint. A good correlation between both joint torques was achieved, but the amplitudes of the curves were different in some cases.

The study advanced by [49] considered fewer calibration parameters than [48], aiming the reduction of the time of the EMG-based torque conversion. For this purpose, the tendon strain parameter (found in the calibration process of [48]) was neglected, since this parameter represents only 3.3 % of the tendon length when a maximum isometric force is generated. This neglection allows the estimation

of the L_0^m without the time-consuming Runge-Kutta-Fehlerg integration, proposed in [48]. Considering the estimated and the experimental knee joint torque, a correlation coefficient (R) of 0.892 ± 0.047 and a RMSE of 8.10 ± 1.02 Nm, when a healthy subject performed 10 gait trials. Moreover, the calibration was completed in 63.4 ± 1.20 s and the joint torque estimation in this simplified model took 0.0630 s, whereas the complete model [48] took 3 h and 0.691 ± 0.0146 s to accomplish the same the calibration and the estimation tasks, respectively.

Inspired in the model developed by [47], in [51] the knee joint torques were estimated, using the EMG signals of six muscles (listed in Table 4) and the knee joint angles. Eight parameters were determined in the calibration process (also presented in Table 4), since the authors considered this number as an acceptable tradeoff between the complexity of the model and its uncertainty. Experiments were carried out with a healthy subject performing flexion and extension movements of the knee joint. A NRMSE between the torque obtained with the model and the measured torque from inverse dynamics was 12.4 %.

Moreover, in [63], a musculoskeletal model was developed, based on the Hill-type muscle model developed by [48]. EMG data were recorded from three muscles of a healthy person, along with the joint angles and they acted as input in the model. In the calibration step, four parameters were identified, as presented in Table 4. The RMSE and the R^2 were calculated to evaluate the model performance, obtaining values below 1.99 Nm and an average of 0.89, respectively.

In [44], in addition to the developed linear proportional model, an EMG-driven Hill-type neuromuscular model was also proposed, based on [47]. Two muscles were used to perform the conversion and only three parameters were determined in the calibration process. The effectiveness of the conversion was tested in eight healthy subjects, performing maximum isometric voluntary contractions at different angles. RMSE of 3.49 ± 0.57 Nm and RMSJ of 1.21 ± 0.51 Nm were obtained between the estimated and the measured torque.

An EMG-driven musculoskeletal model was proposed in [64], in real-time, to predict the user intentions of the ankle and knee joint motions. This musculoskeletal model was based on [48], where the EMG signals and the ankle and knee joint angles are the model's inputs. This methodology was implemented in a Raspberry Pi 2 to investigate the computational cost. Three different tasks were performed by five different participants: (i) walking at self-selected speed, (ii) knee squat, and (iii) calf rise motion. The estimated torques by the musculoskeletal model were compared with the calculated joint torques using inverse dynamics. The results of the EMG-driven model were presented in 2.7 ± 0.48 ms. RMSE were always below 0.37 ± 0.12 Nm/kg and the smallest value observed was 0.01 ± 0.01 Nm/kg.

Pearson coefficients were also calculated and the values were always above 0.43 ± 0.36, and the highest correlation value obtained was 0.9 ± 0.07.

2.4.3. Empirical Methods

From the literature research, it was verified that empirical methods, such as neuro-fuzzy models [53], [55] and neural networks [11], [65], [66] have been applied to estimate the joint torque based on EMG signals.

Study [53] only used EMG data of eight muscles as input in a neuro-fuzzy model to obtain the hip and knee joint torques. To construct this model, twenty fuzzy IF-THEN control rules were defined and a value of joint torque was matched. In [55], the EMG signals along with the joint angles served as input to obtain the joint torque. In both works is not presented the comparison between the real torque and the estimated torque. When performing different movements, if the EMG signals were reduced, the research concluded that the EMG-based controller is adapted to the user.

A Multilayer Perceptron (MLP) neural network was developed in [66] to estimate the knee joint torque. EMG data normalized to the maximal isometric activation, along with the body mass, height, age, gender, joint velocity, and joint position were entered as input variables in the three-layer neural network. The second layer was composed by a variable number of hidden units. The third layer estimated joint torque of the knee joint. The results (R = 0.96) demonstrated the effectiveness of this neural network to estimate the knee joint torque. Later, in [65], the authors improved the MLP presented in [66]. First, the research concluded that how many more muscles were incorporated, better results are achieved. Second, better results were obtained when normalized data at each isometric angle was used in training process of the neural network, because it was proved that the curve of the normalized joint torque at each angle is similar to the curve of the normalized EMG. Third, results pointed out that MLP neural network has a better joint torque estimation when compared with other neural networks, such as Fully Connected Cascade. At last, five neurons in the second layer were found as the best number of hidden units.

A RBFNN with a two-step learning strategy was developed by [11] to convert the EMG signals into torque values. The performance of the methodology was evaluated through simulations and experiments with four healthy subjects only for the swing phase. A RMSE of 2 Nm and a R higher than 0.8 were found, between the measured and the estimated joint torque.

Table 4. Methods to convert EMG signals into joint torque values

Study	Conversion Method	Used in Control?	Calibration Parameters	Inputs	Joint	Muscles	Participants (number)	Results
[43]	Proportional Gain Method	Yes	Two gain parameters/joint	EMG data	Hip Knee	BF, VM, GM and RF	Healthy (1)	*
[13]	Proportional Gain Method	Yes	Two gain parameters/joint	EMG data	Knee	VL, VM, SM and ST	Healthy (2)	NRMSE = 12 % Phase delay = 22 ms
[44]	Proportional Gain Method	Yes	One gain parameter/joint	Joint angles and EMG data	Ankle	TA and GAS	Healthy (8)	RMSE = 3.56 ± 0.63 Nm RMSJ = 2.85 ± 0.78 Nm
[48]	Musculoskeletal Model	No	Eighteen parameters **	Joint angles and EMG data	Knee	Thirteen muscles **	Healthy (6)	R^2 = 0.91 ± 0.04 Mean Residual Error/body weight < 0.2 Nm/kg
[62]	Musculoskeletal Model	No	F^{max}, F^{mt}, and A	Joint angles and EMG data	Knee	*	Healthy (*)	Good correlation between the shape of the knee joint torque obtained by inverse dynamics and by the EMG-based model
[49]	Musculoskeletal Model	No	F^{max}, F^{mt}, L_0^m, ϕ and maximal speed of the muscle (v^m)	Joint angles and EMG data	Knee	SM, ST, BF, Sartorius (SAR), TF, GRA, VL, VM, VI, RF, Gastrocnemius Medialis (GASM) and Gastrocnemius Lateralis (GASL)	Healthy (1)	R = 0.892 ± 0.047 RMSE = 8.1 ± 1.02 Nm Calibration time = 63.4 ± 1.20 s Joint torque estimation time = 0.0630 s
[51]	Musculoskeletal Model	Yes	F^{max}, F^{mt}, L_0^m, ϕ, A and three constants	Joint angles and EMG data	Knee	RF, VM, VL, BF, SM and ST	Healthy (1)	NRMSE = 12.4 %

[63]	Musculoskeletal Model	No	F^{max}, F^{mt}, Lo^{m}, ϕ	Joint angles and EMG data	Knee	RF, VM and VL	Healthy (1)	RMSE = 1.99 R^2 = 0.89
[44]	Musculoskeletal Model	Yes	F^{max}, F^{mt}, Lo^{m} and A	Joint angles and EMG data	Ankle	TA and GAS	Healthy (8)	RMSE = 3.49 ± 0.57 Nm RMSJ = 1.21 ± 0.51 Nm
[64]	Musculoskeletal Model	No	F^{max}, F^{mt}, Lo^{m} and A	Joint angles and EMG data	Ankle and Knee	BF, GASL, GASM, GRA, RF, SAR, SOL, SM, VL, VM, TA, Peroneus Longus (PL) and Peroneus Tertius (PT)	Healthy (5)	Joint torque estimation time = 2.7 ± 0.48 ms RMSE < 0.37 ± 0.12 Nm/kg Pearson correlations > 0.43 ± 0.36
[53]	Empirical Model	Yes	***	EMG data GRF data	Hip Knee	TF, RF, VL, VM, AL, GRA, BF and ST	Healthy (1)	*
[55]	Empirical Model	Yes	***	Joint angles and EMG data	Hip Knee	TF, RF, VL, AL, GRA, VM, BF and ST	Healthy (3)	*
[66]	Empirical Model	No	***	Body mass, body height, age, gender, joint velocity, joint position and EMG data	Knee	VL and BF	Healthy (20)	R = 0.96
[65]	Empirical Model	No	***	Body mass, body height, age, gender, joint velocity, joint position and EMG data	Knee	VL, BF, RF, VM and ST	Healthy (1)	• More muscles imply a better joint torque estimation; • The data should be normalized at each isometric angle; • The second layer should have five neurons.

[11]	Empirical Model	Yes	***	Joint angles, velocities and EMG data	Hip	QF and BF	Healthy (4)	RMSE < 2 Nm R > 0.8

* Not specified

** Consult [48] for more information

*** Not Required

2.4.4. Discussion

Among the different strategies, three methods were identified to convert the EMG signals into joint torque values: **Proportional Gain Methods**, **Musculoskeletal Models** and **Empirical Methods**.

It was reported by [46], [67] that the muscle activation, the architectural and biomechanical properties of the muscle fibers and tendons are determinant factors in the force of muscle-tendon units. For this purpose, in a study developed by [68], reported that only the use of EMG signals in proportional gain method is not enough to predict the torque of the ankle joint. Moreover, [69] reported that the proportional torque control only using EMG values is not reliable for two-fold reasons: **(i)** the human body muscles and coactivation effects are exclusive from person to person; and **(ii)** the EMG readings are dependent on the electrodes placement, location and skin impedance. Study [70] showed the differences between using only EMG signals and motion data fusion (EMG and other sensors data), concluding that the fusion of biomechanical data with EMG signals improves joint torque estimation. Additionally, study [43] combined floor reaction force with EMG signals to improve the hip torque at extension motion and consequently, overcome the user discomfort during stance phase.

Regarding the musculoskeletal models [44], [48], [49], [51], [62]–[64], there are several factors to consider to obtain a good EMG-torque conversion, as follows: the number of calibration parameters to find, the number of muscles to acquire the EMG signals, the complexity and the accuracy of the model, and the time to perform the conversion. The complexity of the model increases with the increment of **(i)** the number of calibration parameters; and **(ii)** the number of muscles. Consequently, the computational burden will increase. The works developed by [48], [62] are not capable to perform the conversion in real-time, in contrast with the works developed later by [44], [49], [51], [63], [64]. The real-time conversion is an important aspect to consider when it is desired to assist patients using EMG signals in torque controllers.

As already referred, the proportional gain and the musculoskeletal methods require calibration steps that may not be realized by pathological individuals. For this purpose, the empirical models, as the ones presented in [11], [53], [55], [65], [66], can be a suitable strategy to convert the EMG signals into torque values, avoiding calibration steps.

In the study developed by [65], some improvements in a MLP neural network were done. It was reported that the number of muscles, the inputs normalization and the number of hidden units had a strong impact in the performance of the conversion. However, the dataset used to construct the neural network presented twenty subjects where the age range of the participants, as well as the range of physical activity of the participants was small. Moreover, the EMG-torque conversion implemented in both

works [65], [66] is not completed in real-time. In [11], the joint torque is obtained through a RBFNN, where the increment of the number of muscles leads good results without calibration steps. However, the error of the torque estimation increases when the hip movement of the orthosis's joint changed its direction. At last, this methodology was only developed for the swing phase, requiring more advances to cover all the gait cycle.

2.5. General Conclusions

There is interest in using EMG signals to control WPADs, since they are directly related to user motion intention. Two types of control strategies integrating EMG data were identified, the **EMG-based control** and the **AAN EMG-based control**. Both strategies contributed to muscular activity improvement and endurance. EMG-based control strategies can be used to re-train the lower limbs of patients with impairments. However, it is not expectable that these strategies have the potential to assist their motor condition. **AAN EMG-based control strategies have the potential to assist and rehabilitate the lower limbs**, such that the user can achieve autonomy to perform their daily life activities, in contrast to EMG-based control strategies. It is expectable that the integration of AAN EMG-based control strategies into WPADs may foster motor assistance, re-train, rehabilitation and autonomy when applied to disabled users. However, validation tests with pathological subjects are still missing to validate this phenomenon. Furthermore, until the moment, there is no explanation by the existence of AAN EMG-based control strategies only destinated to the knee joint.

Further, this review concluded that most of the control methods which use EMG signals to control WPADs convert these EMG signals into torque values. There is evidence that only **EMG readings are not enough to obtain the accurate values of joint torques**, being necessary to fuse EMG data with biomechanical data, such as, joint angles, velocities, accelerations. Moreover, to perform the EMG-based torque estimation in AAN EMG-based control strategies, it was noticed that only musculoskeletal models were used.

Overall, this dissertation aims the development of an AAN EMG-based control strategy destinated to the ankle joint assistance, using a musculoskeletal model fed with EMG signals, joint angles and velocities to perform the EMG-based torque estimation, since there were not found literature evidences of the use of these strategies to assist the referred joint.

CHAPTER 3 – SYSTEM OVERVIEW

In this chapter, it is presented an overview relative to the orthotic system used in this dissertation to assist individuals with disabilities in the ankle joint. The control architectures already implemented in this orthotic system are briefly explained and the AAN EMG-based control strategy is proposed. At last, the chapter ends with the description of the constructed EMG acquisition system, that represents an essential element of the proposed control strategy.

3.1. SmartOs Description

SmartOs is a WPAD embedded with wearable sensors destinated to the analysis and control of the gait motion. SmartOs was developed in [71] and it presents the capacity of providing a personalized and repetitive gait training, such as joint trajectory tracking control, to assist the user according with its needs and to enable the abnormal gait pattern correction, such as drop foot gait in stroke survivors. Besides that, this WPAD invokes the user participation, in order to rehabilitate the ankle joint, by considering the user's motion intention based on muscular information (an example of an EMG-based control strategy) and it was designed to achieve walking speeds ranging from 0.5 to 1.6 km/h [71]. Moreover, SmartOs also present a biofeedback system integrated in its architecture to accelerate the familiarization of the user to itself and to accelerate the gait recovery.

The conceptual design of SmartOs is presented in Figure 1 and a brief explanation of each block is provided. Nonetheless, the scope of this dissertation is the projection of an AAN EMG-based control strategy that has not yet been developed.

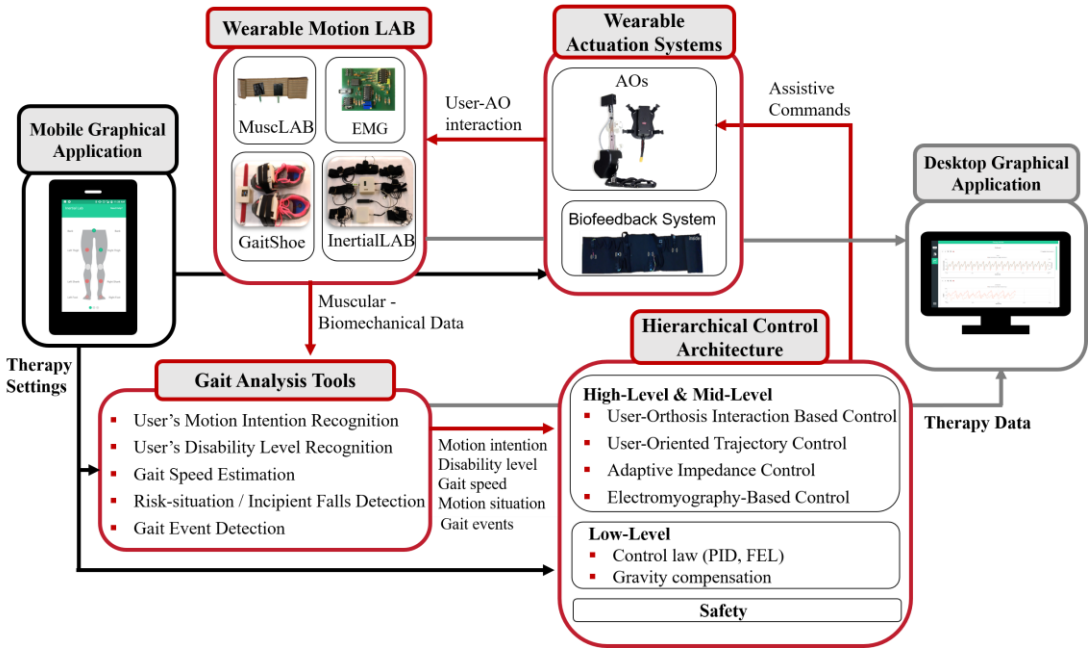

Figure 1. Conceptual design of SmartOs [71].

SmartOs presents two graphical interfaces (**Mobile** and **Desktop Graphical Applications**) that were established via wireless technology enabling an intuitive utilization, considering therapists or a technician as possible users. In order to provide a user-oriented assistance, the Mobile Graphical Application was developed to configure the system with the subject data (e.g. body height) and to configure the assistance settings, selecting the speed, the gravity compensation tool, the stiffness and the therapy mode. All configured information is transmitted via Bluetooth to the Central Controller Unit (CCU) of SmartOs, that includes a Raspberry Pi 3, a single board computer with 1 GB of RAM and a quad-core processing unit (1.2 GHz, 64 bit CPU).

Desktop Graphical Application provides a real-time displaying from the user, allowing a real-time monitorization.

The time-effective walking assistance in SmartOs is possible due to the presence a **Bioinspired Hierarchical Control Architecture**, organized from the low-level (comprehending the Proportional Integral Derivative (PID) and Feedback-Error Learning (FEL) controllers) to the high-level modules. This last module presents high-level controls that are executed in the CCU of SmartOs. CCU enables the gait analysis performed by **Gait Analysis Tools** and it is responsible to establish external communications with other applications. To generate control commands, the walking pattern is continuously analyzed based on gait tools. This time-effective gait analysis and monitorization of the user's motor status is performed with recourse to wearable, ergonomic and stand-alone sensors, exhibited in the **Wearable Motion LAB** block.

In Chapter 2, it was referred that subjects with muscle atrophy present EMG signals that are weaker than the EMG signals of healthy subjects. Thus, the use of EMG-based control strategies (already implemented in the high-level of SmartOs) could not be efficient. Moreover, it was seen that a user-oriented control strategy considering the user's needs, such as an AAN EMG-based control strategy, may enhance motor assistance, rehabilitation and autonomy when applied to disabled users. However, this control strategy has not yet been developed, neither applied in SmartOs. Thus, the focus of this dissertation consists into develop an AAN EMG-based control strategy, aiming its future implementation in the high-level module of SmartOs. In this sense, in this chapter, the proposed control strategy is presented, ending with the construction of an improved EMG system, in order to acquire EMG signals to serve as input in the proposed strategy.

3.2. Proposed AAN EMG-based Control Strategy

To implement an AAN control strategy, it is required to predict the ankle joint trajectory that a subject should perform (reference trajectory) and compare it with an ankle joint trajectory that the subject is performing (real trajectory), in real-time. Since the parameter to control is the joint torque, it is required to **predict the reference ankle joint torque that a specific subject should perform** (Figure 2), in order to **compare with the real joint torque that the subject is performing**. The input data to achieve the reference joint torque will be discussed in Chapter 4 and Chapter 5.

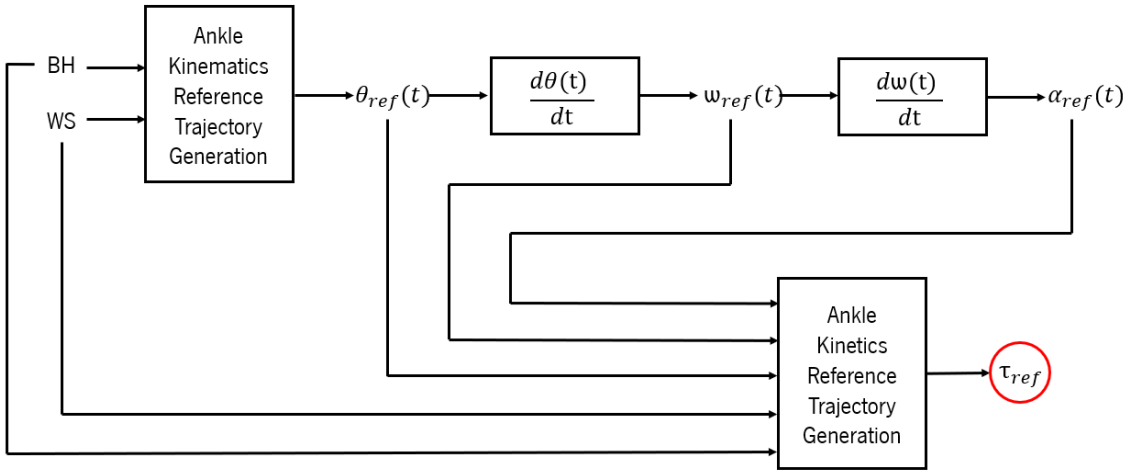

Figure 2. Proposed reference joint torque estimation diagram, where BH, WS, $\theta_{ref}(t)$, $\omega_{ref}(t)$, $\alpha_{ref}(t)$ and $\tau_{ref}(t)$ correspond to Body Height, Walking Speed, reference joint angle, angular velocity, angular acceleration and reference joint torque, respectively.

In AAN EMG-based control strategy, the user's motor intentions are estimated based on EMG signals. There are numerous methods to convert these signals into real joint torques performed by the user, also considering the joint angles, as presented in Chapter 2. Thus, the determination of the torque

of a specific joint in real-time conditions can be performed, as represent by Figure 3. This conversion is the focus of Chapter 6.

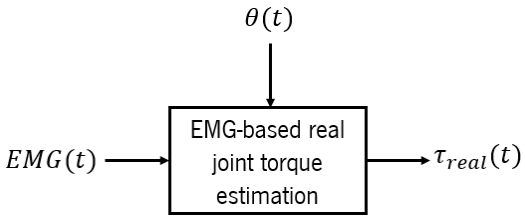

Figure 3. Proposed real joint torque ($\tau_{real}(t)$) estimation based on EMG signals (EMG(t)) and real joint angles ($\theta(t)$).

With these two blocks, the real and the reference joint torque can be determined and, therefore, it is possible to relate both, as presented by Figure 4.

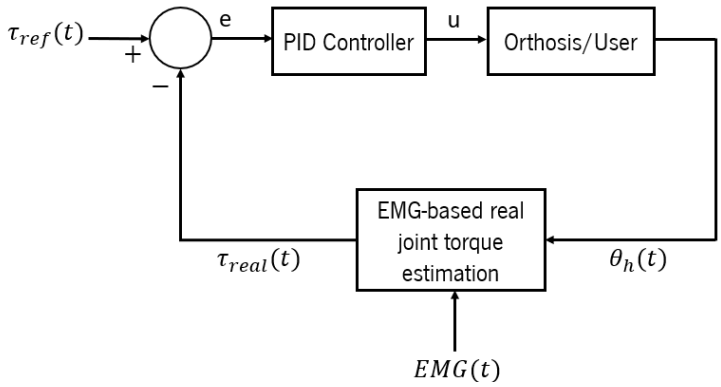

Figure 4. Proposed AAN EMG-based control strategy.

The comparison between the real and the reference torque produces an error, *e*, that acts as input in the PID Controller. Based on this error, this last block produces a control command, *u*, that is interpreted by the DC motor of SmartOs, producing a value of torque corresponding to *u*. The angle performed by the ankle joint, θ_h, is measured through a precision potentiometer with resolution of 0.5 ° and this angle is responsible to close the loop, since it is used, along with the EMG signals, to determine the real joint torque performed by the user.

3.3. Wired EMG Acquisition System

Considering the necessity of an EMG acquisition system in the proposed control architecture, in the following sub-sections, the hardware of the EMG boards responsible to acquire EMG signals is presented. These signals will be acquired using a STM324F4 – Discovery development board that integrates a STM32F407VGT microcontroller [72].

Furthermore, the protocol created to validate the system will be presented and the section ends with the discussion of the obtained results.

3.3.1. Hardware Specifications

A. Electrode Configurations

The bipolar configuration was chosen in this dissertation, along with a differential amplification, in order to suppress signals common to both detection electrodes, such as AC signals and EMG signals from distant muscles. Moreover, with this arrangement, EMG signals from muscles close to the detection electrodes will be amplified with better signal-noise ratio along with an increase in the spatial resolution of the EMG signal [31].

B. Instrumentation Amplifier

In a bipolar configuration, a differential amplifier is required to introduce a gain with respect to a difference between two signals. In this sense, it was used a Low-Power Instrumentation Amplifier - INA128. This operational amplifier was selected due to its low offset voltage, high common-mode rejection ratio (CMRR), low input bias current and low quiescent current, which eliminates most of the noise of the signal. Moreover, this operational amplifier enables an easily adjustable gain, conferring the features referred above. The main characteristics of this component are presented in Table 5.

Table 5. INA128 main features

Parameter	Value	Units
Offset Voltage	50	µV
Quiescent Current	700	µA
Input Bias Current	5	nA
CMRR	120	dB

A gain of 50 was chosen, enabling an amplification of the EMG signal without introducing too much noise. Besides that, to increase the performance of all components in the circuit, two capacitors were placed in the power supply lines.

C. Bandpass Filter

According to [31], [35], the typical frequency of the EMG signals varies between 0 to 500 Hz. However, due to the movement artifacts with low frequencies, it is recommended to filter the EMG signal with a high-pass filter with a cut-off frequency between 10 and 20 Hz. In addition, to avoid aliasing and to remove the noise of frequencies above 500 Hz, it is also recommended to apply a low-pass filter with a cut-off frequency of 500 Hz [31].

In this sense, an active second order high-pass filter and a low-pass filter of Sallen-Key with cut-off frequencies of 20 Hz and 500 Hz, respectively, were implemented. These filters were chosen, because they present a better frequency response when compared with passive filters, allowing a better rejection of the undesired frequencies and a lower attenuation of the desired frequencies [73]. Both filters were dimensioned considering the damping ratio, trying to avoid unwanted oscillations during the performance of the system.

D. Notch Filter

In the case of this EMG system be supplied by the power lines, it should be able to clean the noise introduced by power lines, with a dominant component at 50 Hz. In this sense, an active second order notch filter with cutoff frequency of 50 Hz was implemented.

E. Non-Inverting Summing Amplifier

Typically, the EMG signals range from –10 mV to 10 mV and, since that this signal will be acquired and processed in a microcontroller, it is required to create an amplification stage. In previous developments, it was observed a little offset component different from subject to subject. In this sense, it was developed a summing amplifier to remove this offset component with a potentiometer of 2.2 kΩ. Moreover, to miniaturize the system, the rectification of the signal will be done in software. Thus, the non-inverting summing amplifier is also useful to introduce an offset component to the signal, considering its maximum signal range allowed to avoid the saturation. In this case, a DC offset component of 1.65 V was chosen, since the minimum and maximum voltage allowed by the processing unit ranges from 0 V to 3.3 V [72]. To confer a gain to the EMG signal, a potentiometer of 1 MΩ was used, allowing an adjustable gain from 1 to 200.

Note that all the filters and the non-inverting summing amplifier used a high precision operational amplifier, the OPAx277. These operational amplifiers were selected, since they present ultralow offset voltage, high CMRR, low bias current, low quiescent current and a wide supply range. The main characteristics of this amplifier are presented in Table 6.

Table 6. OPAx277 main features

Parameter	Value	Units
Offset Voltage	10	μV
CMRR	140	dB
Input Bias Current	1	nA
Quiescent Current	800	μA/amplifier
Supply Range	±2 to ±18	V

F. Voltage Limiter

Finally, a voltage limiter circuit was implemented, in order to protect the inputs of the processing unit. However, it was not used a typical buffer configuration supplied between the referred voltages. Aiming the protection of the operational amplifier, a non-inverting amplifier with a diode Zener of 2.7 V placed on the input of the amplifier was implemented. Thus, the inputs of the processing unit, as well as the inputs of the operational amplifier are protected. Moreover, in this stage a gain of 2 was conferred to the signal.

G. Final System

Before the practical hardware implementation, the filters were projected on *National Instruments*: *MULTISIM* software. Once implemented, the expected and the theoretical frequency responses of the system were compared and the results are presented in Figure 5.

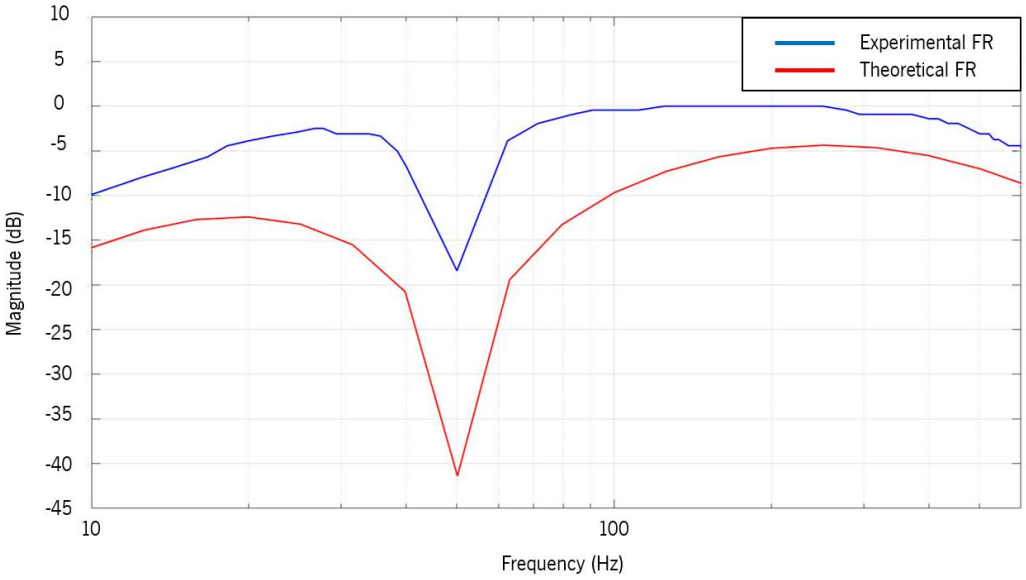

Figure 5. Theoretical and experimental frequency response (FR) of the Sallen-Key high-pass and low-pass filters, along with the notch filter.

Analyzing Figure 5, differences with respect to the attenuation levels between the experimental and theoretical implementations are visible. Based on the theoretical FR, it would be expectable to achieve higher levels of attenuation in the desirable range of frequencies. However, despite of lower levels of attenuation have been verified experimentally, this phenomenon does not compromise the proper functioning of the projected system. Moreover, the experimental attenuation levels introduced by the filters at frequencies ranging from 80 to 300 Hz are better than the expected ones, since at these frequencies, the signal is not attenuated.

The final EMG system can be seen in Figure 6. Since this system was designed to acquire EMG signals from only one muscle, other boards must be used to acquire signals from other muscles. Thus, an input/output supply was projected to supply energy between consecutive boards.

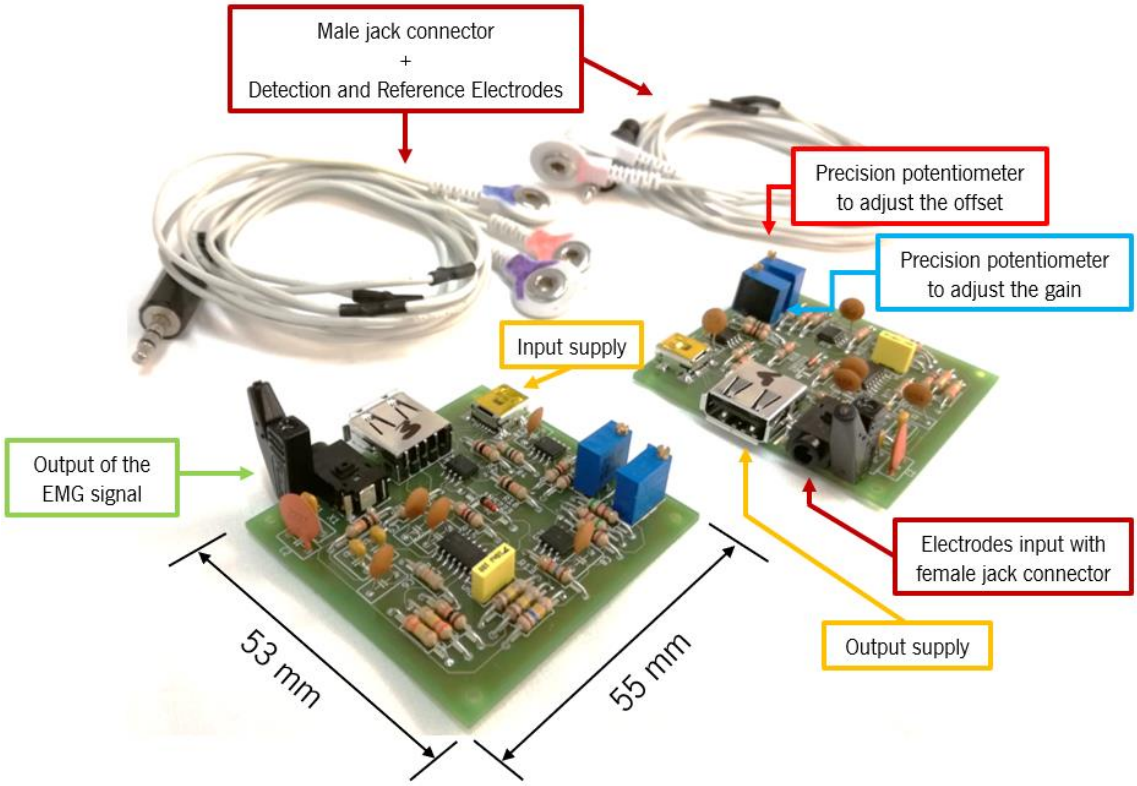

Figure 6. Final EMG system.

3.3.2. Experimental Validation Protocol

To analyze the feasibility of the developed EMG system, a validation trial was performed with a healthy male subject (with 23 years old, height of 1.70 m and weight of 78.1 kg) walking in a treadmill at 1 km/h, for 1 minute. The choice of the walking speed was based on the minimum (0.5 km/h) and maximum (1.6 km/h) range of speeds allowed in SmartOs [71]. The MuscleBAN EMG system of [40]

was used as ground truth. The detection electrodes were placed on the TA muscle and the reference electrode was placed on the knee, as exhibited in Figure 7.

Figure 7. Electrode configuration adopted for a validation test to measure the electrical activity of the TA muscle.

3.3.3. EMG Signal Processing

During the data collection, EMG data from ten gait cycles were acquired. To this data, the DC offset component of 1.65 V introduced in hardware was removed to achieve a signal with null mean. Then, the rectification of the signal was performed, taking the absolute value of the signal. The envelope of the EMG signal was determined using the Root Mean Square (RMS) value of the signal with a 300 ms movable window. The RMS feature was used to create the EMG envelop since it is the most suitable method to represent a physical meaning of muscle force [74]. To confirm this fact, a recent study showed that the RMS method is better correlated with the muscle contraction force when compared with other methods, such as mean absolute value, median frequency and mean power frequency, since an increase/decrease of the muscle force contraction is more easily detected with RMS value [75]. The choice of the window length (below 300 ms) was based on [76]. Higher values of window length do not cause an increase of the information. In some cases, it was reported that an extreme increase of the window length could produce a loss of information [76].

3.3.4. Results and Discussion

Results of the experimental validation trial are presented in Figure 8, where it is possible to verify that the signals acquired with the projected EMG boards present a considerable correlation level with the signals acquired with the system of [40]. Notwithstanding the ground truth system enable a better

muscular activation detection (verified by the higher amplitude voltage), comparing both systems, the muscular activations are detected at the same instant, conferring robustness to the constructed EMG system. Besides the comparison of the EMG signals acquired with different systems, another comparison was performed, in order to analyze the feasibility of the measure based on literature evidences. In this sense, the black perimeter delimited in Figure 8 was zoomed and the EMG signals of both systems were filled. The reason why this perimeter was chosen is because the range time selected corresponds to a single gait cycle.

The EMG signals inside the zoomed perimeter were compared with literature EMG signals of a subject walking freely and, based on the results, it is possible to infer that the signals acquired with the proposed EMG system are similar to the expected ones.

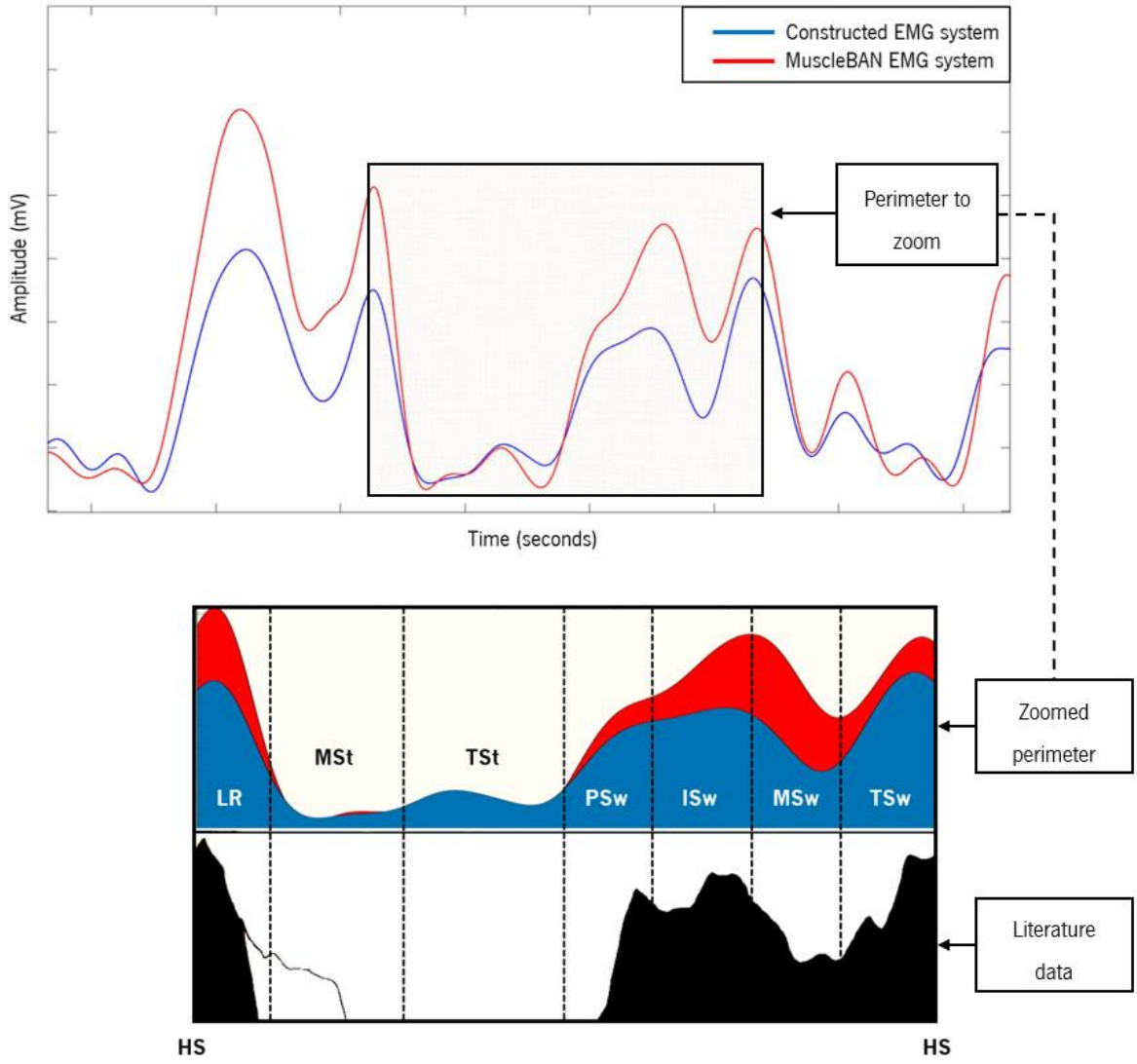

Figure 8. EMG signals acquired with the projected EMG system (blue line) and with a system from [40] (red line). The black signal represents the Literature data, where HS, LR, MSt, TSt, PSw, ISw, MSw and TSw mean Heel Strike, Load Response, Mid Stance, Terminal Stance, Pre-Swing, Initial Swing, Mid Swing and Terminal Swing, respectively.

3.4. General Conclusions

In this chapter, the main characteristics and strategies presented in SmartOs were presented. Since it was identified the necessity to construct an user-oriented strategy, an AAN EMG-based control approach was proposed, aiming its future insertion into the presented WPAD.

Furthermore, an EMG acquisition system was constructed to acquire signals from the main muscles reviewed in Chapter 2. A good correlation between the signals acquired with the constructed EMG system and the acquisition system of [40] was found. Moreover, the signals acquired with the developed EMG system were also compared with literature evidences with respect to the activation of the TA along a single stride. With the achieved results, it was concluded that the EMG system was correctly projected and it can be used and integrated in the proposed AAN EMG-based control strategy.

Once constructed the EMG system to collect EMG signals from the muscles of interest, another requirement of the proposed AAN EMG-based control strategy is the prediction of user-oriented reference walking kinematics and kinetic trajectories, that will be the focus of the Chapter 4 and Chapter 5, respectively.

CHAPTER 4 – ANKLE KINEMATICS TRAJECTORY GENERATION

To implement the AAN EMG-based control strategy, it is required to predict the ankle joint torques, to serve as the reference in the proposed architecture. Since the joint torque is associated with the joint kinematics [77], a fundamental step to predict the ankle joint torque consists of the generation of ankle joint kinematics for each subject. Moreover, in this field, some works already reported the possibility to model ankle joint angles based on the walking speed [78], [79].

For this purpose, it is necessary an ankle kinematics prediction model based on well-known data from the subject. In this sense, body height and body mass, as well as the walking speed are possibilities to accomplish this issue. From this perspective, this chapter is focused on the generation of reference ankle joint kinematics along the gait cycle, oriented to the subject.

4.1. Introduction

Usually, pre-recorded joint trajectories of healthy individuals represent the most used method to create joint kinematics in the sagittal plane to serve as reference in assistance applications of the human gait. These trajectories are normally recorded at slow (3.2 – 5.0 km/h), normal (5.0 – 6.5 km/h) and fast (6.5 – 7.5 km/h) speeds [80]. However, the walking speed of stroke, or ISCI, or Parkinson survivor is, approximately, from 1.8 km/h to 2.5 km/h [81]. A possible solution to overcome this issue could be the recording of joint trajectories using numerous walking speeds, in order to construct a huge database to be used as reference in gait assistant applications. However, this solution is not suitable due to the high time consumption of the data collection and large amount of data, becoming impracticable to

advance with this approach. In this direction, regression models have been proposed to enable the prediction of joint kinematics trajectories during gait cycle [78], [79], [82].

According to [78], the **ankle angle waveform during gait cycle presents a linear and quadratic relationship with the walking speed**. In this sense, if joint trajectories of healthy individuals at slow walking speeds are used as reference in control strategies integrated into WPADs, the assistance will not be efficient, because people with neurological injuries prefer lower walking speeds and, consequently, different joint trajectories. For this reason, in [78], four regression equations based on the walking speed were developed to predict the peaks of the ankle joint dorsiflexion and plantar flexion during the stance and swing phases. The R^2 was used as metric to evaluate the accuracy of the model. However, the highest values obtained were 0.1110, demonstrating unsatisfactory results. The equations and the results obtained by [78] can be consulted in Table 7, where v represents the walking speed.

Table 7. Regression equations and the correspondent results, achieved in [78], for each peak of the ankle joint angle

Parameter	Equation	R^2
Peak Ankle Plantar Flexion (Stance Phase)	$-1.7583v + 9.190961$	0.0496
Peak Ankle Dorsiflexion (Stance Phase)	$-2.4v + 13.62415$	0.105
Peak Ankle Plantar Flexion (Swing Phase)	$3.7834v + 12.88073$	0.0870
Peak Ankle Dorsiflexion (Swing Phase)	$4.16v^2 - 10.7498v + 10.03869$	0.111

Contrary to the four equations presented by [78], in [79], only one regression equation was developed considering the linear and quadratic relationship between the walking speed and the ankle joint ankle. Better results were achieved using the equation exhibited in Table 8.

Table 8. Regression equation and the correspondent results, achieved in [79], where *a*, *b* and *c* represent regression coefficients of the model

Parameter	Equation	RMSE
θ	$av^2 + bv + c$	2.79 ± 2.05°

In accordance with other studies, the effect of the body height in the construction of the ankle trajectory is not relevant [80]. However, in [82], it was reported that if the **variability of the body height is higher**, this parameter may present a **larger effect on the ankle trajectory**. Based on this suggestion, in this dissertation, the body height was added to the equation presented in Table 8, as proposed by [82]. Thus, the ankle joint trajectories are dependent on the walking speed and body height of each subject. With this approach, the necessity of recording joint trajectories at many different body heights and

different walking speeds is avoided. The results of this approach are compared and validated with data acquired with a motion-capture system (Oqus; Qualysis – Motion Capture System, Göteborg, Sweden) under specific experimental conditions.

4.2. Methods

4.2.1. Data Acquisition

The ground truth data were collected during locomotion tests. Despite only lower limbs joint kinematic and anthropometric data are required, joint kinetic and EMG data were also collected, being useful data for the next chapters.

A. Volunteers

The study was performed with sixteen adult subjects (8 males and 8 females with mean age of 23.8 ± 2.02 years, mean weight of 67.5 ± 10.8 kg and mean height of 1.69 ± 0.109 m), with no evidence of any type of physical and physiological disorder that could interfere with their walking pattern, performed walking tests. The minimum and maximum body height registered in the data collection was **1.51 and 1.83 m**, respectively and, consequently, **the reconstruction of the ankle joint trajectories can only be performed in this range.**

B. Materials

The data acquisition was performed using a motion-capture system with 12 cameras (Oqus; Qualysis – Motion Capture System, Göteborg, Sweden), acquiring at 200 Hz, five force platforms embedded in the floor (with characteristics presented in Table 9), acquiring at 200 Hz and an 8-channel wireless electromyograph (Delsys, Massachussetts, United States of America) [37], acquiring at 2000 Hz.

Table 9. Force plates used in the data acquisition

Force Plate System	Model	Quantity
Bertec, Ohio, United States of America	FP4060	2
Bertec, Ohio, United States of America	FP6090	2
Kistler, Winterthur, Switzerland	9281 EA – FP4060	1

C. Subject Preparation

The Newington-Helen Hayes model was adopted as marker set, integrating four more markers placed in trochanter, medial tuberosity of the femur, medial malleolus and in the first metatarsal head to obtain results more accurate [83]. In this sense, a total of **24 reflective markers** were used. In relation to the EMG signals, they were extracted from TA, GASL, BF and VL of both legs. Both markers and EMG sensors are presented in Figure 9.

Figure 9. EMG sensors and markers placement on the user's body.

First, the user was instrumented with EMG sensors. Then, two maximum voluntary contractions were performed for each muscle, in order to normalize all the EMG data to the maximum isometric contraction registered. After this step, the 24 reflective markers were placed on the body and then, the subjects were asked to perform a standing static calibration with their arms crossed in front of the chest, looking forward and with their feet in a comfortable position, aligned with the shoulders. This step was useful to fit the anthropometric data to the body model of the acquisition system.

D. Walking Experiments

All subjects were instructed to perform 10 walking trials on a 10-meter flat surface with 5 embedded force platforms, at seven different speeds (**1.0, 1.5, 2.0, 2.5, 3.0, 3.5 and 4.0 km/h**), controlled with a metronome. Between each speed change, the subjects rested for one minute and they performed a habituation trial to become acquainted with the new walking speed.

E. Data Collection and Processing

The data collected were the joint angles, angular velocity and angular acceleration for ankle, knee and hip joints, the ground reaction force and the EMG data from TA, GASL, BF and VL.

Following the data collection of joint angles, the kinematic and kinetic data were filtered with a low-pass Butterworth filter. The cutoff frequency chosen was 6 Hz, since in [84], a frequency around 6 and 7 Hz was determined as the optimal cutoff frequency to smooth trajectories during the walking motion. Regarding the EMG data, a band-pass filter with 20 and 450 Hz as cutoff frequencies was applied to the raw data. Further, the EMG envelop was determined using the RMS value of the signal with a 300 ms movable window.

In this chapter, only ankle joint position trajectories will be used. The kinetic and EMG data will be useful for the Chapters 5 and 6.

4.2.2. Regression Model Implementation

The implementation of the regression model to estimate ankle joint trajectories during walking motion was performed using *MATLAB*® and it was inspired in the work developed in [82]. Based on the collected kinematic data, the ankle joint angles were split into individual gait cycles, where the first sample corresponds to the heel-strike event. For each trial (that represents a single gait cycle), the joint angle values and the instant frame at seven key-events (listed in Table 10) were extracted.

Table 10. Key-events considered to construct the ankle joint angle

Key-event	Instant of the stride
1	Heel-Strike
2	Minimum Angle of the Stance Phase
3	Minimum Angular Velocity of the Stance Phase
4	Maximum Angle of the Stance Phase
5	Minimum Angle of the Swing Phase
6	Maximum Angle of the Swing Phase
7	Heel-Strike

To detect all these events, two strategies were adopted: **(i)** creation of a detection algorithm based on the second derivative of the ankle joint angle (angular velocity); **(ii)** creation of a detection algorithm with reference to the maximums and minimums peaks of the ankle joint angle.

In both strategies, the 1st and the 7th event correspond to the first and final samples of each trial, respectively. In case **(i)**, the events number 2, 4, 5 and 6 were extracted based on a zero-cross detection. Every time that the angular velocity of the ankle joint crossed the zero value, an event was marked. To distinguish between a dorsiflexion or a plantar flexion event, the previous and the next samples in relation

to the zero-cross value were also considered. If the previous and the next samples corresponded to positive and negative values, respectively, a dorsiflexion event was considered, whereas if the previous and the next samples correspond to negative and positive values, respectively, a plantar flexion event was marked. Only two plantar flexion and two dorsiflexion events must be detected. At last, the event number 3 corresponds to the minimum angular velocity between the minimum (second event) and the maximum angle of the stance phase (forth event). Figure 10 presents the detection of all key-events using the strategy **(i)**.

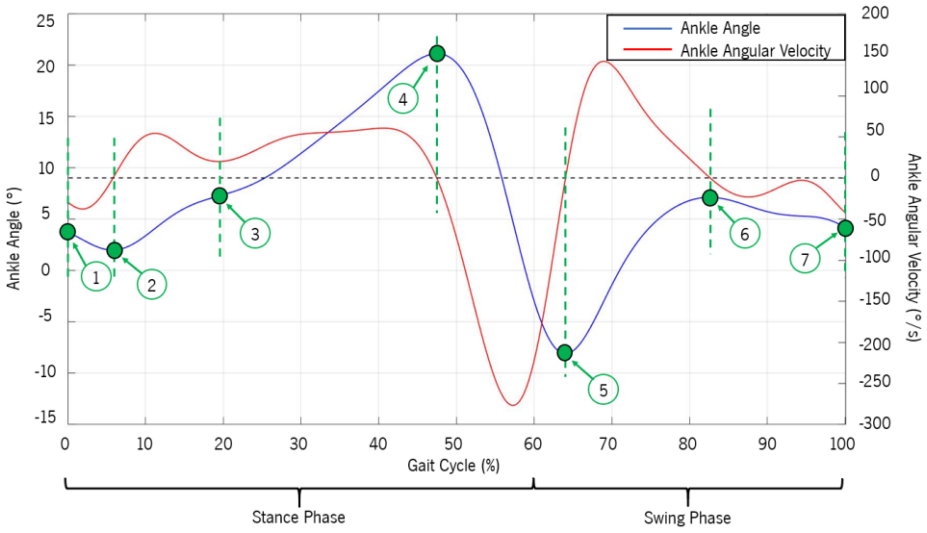

Figure 10. Identification of the seven key-events enounced on Table 10, for a walking speed of 4 km/h.

However, mainly at slow walking speeds, the event detection procedure does not work efficiently due to irregularities in the pattern of the ankle joint angles and angular velocities collected, as presented in Figure 11.

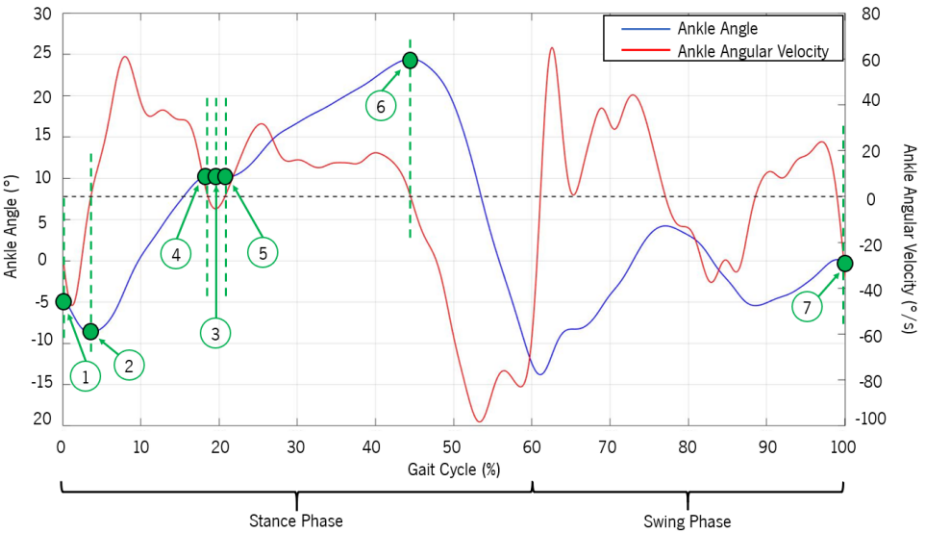

Figure 11. Poor identification of the seven key-events enounced on Table 10, for a walking speed of 1 km/h.

To avoid the untruth event detection, strategy **(ii)** was developed. This algorithm is a simpler solution to identify the 2nd, 4th, 5th and 6th events. The 2nd and the 5th events represent the instants where maximum plantar flexion is verified during the stance and the swing phases, respectively. The maximum dorsiflexion during the same phases corresponds to the 4th and 6th events, respectively. In this sense, a simple max-min algorithm can be used to identify these events. Initially, to detect these four events, each stride was split into two phases (Phase 1 and 2), according to Figure 12. To perform this division, the instant frame where the minimum value of angular velocity occurs (that represents, approximately, the transition from stance phase to swing phase) was fixed. At this instant frame, a black dashed line was traced, giving rise to the blue and green sides, that represent Phase 1 and 2, respectively (Figure 12). With this division, the minimum and the maximum of both phases can easily be identified. Thus, the events number 2, 4, 5 and 6 are correctly identified. As in case strategy **(i)**, the event number 3 corresponds to the minimum angular velocity detected between the 2nd and the 4th events.

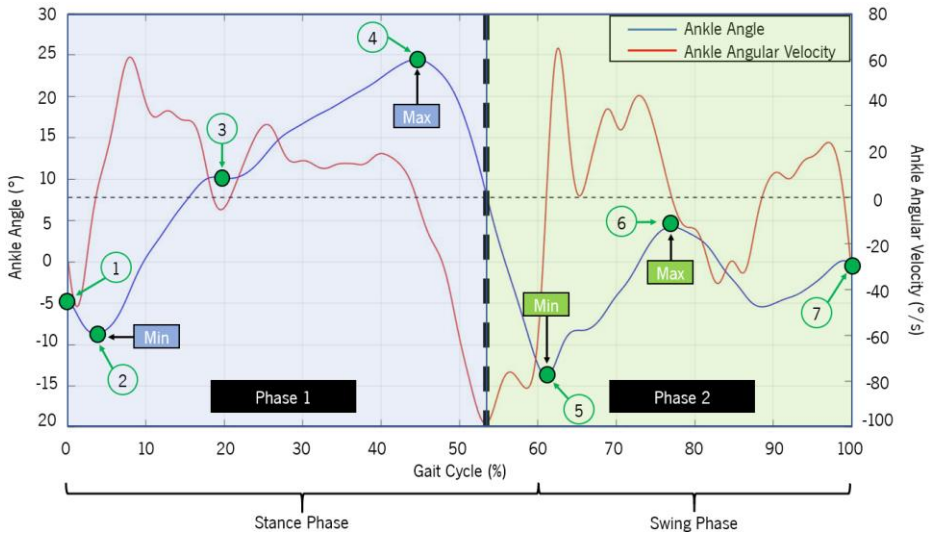

Figure 12. Gait Cycle division based on the minimum of angular velocity.

The regression model used to predict two parameters (**joint angles** and **instant frames**) at each key-event is represented by Equation (1):

$$y_i = \beta_1 + \beta_2 v + \beta_3 v^2 + \beta_4 l \quad (1)$$

Where y_i is a parameter that represents the joint angle or the instant frame for each key-event i = 1, 2, 3, 4, 5, 6, 7, v represents the walking speed and l is the body height of each subject. The parameters $\beta_{1,2,3,4}$ consist in the regression coefficients found with recourse to a **Robust Least Squares** fitting with a **bisquare weighting function**. This method was chosen because, according with [85], it attributes smaller weights to points that are farther from the fitted line (designed as outliers), minimizing their contribution.

The best β parameters were found using a cross-validation method to confer robustness to the regression model. A total of 56 β parameters were found, being 28 to estimate the joint angles and the other 28 to estimate the instant frame at each key-event, covering all the heights and walking speeds in study. These parameters can be consulted in Table 11.

Table 11. Regression coefficients for angle and instant frame estimation

Parameter	Key-event	β_1	β_2	β_3	β_4
Angle	1	2.38	-1.97	0.236	1.97
	2	3.22	-2.20	0.590	-3.61
	3	26.9	-4.41	0.644	-7.93
	4	44.5	-2.03	0.301	-13.5
	5	-59.8	23.0	-3.50	8.25
	6	6.41	2.00	-0.616	0.112
	7	1.95	-1.46	0.109	2.01
Instant Frame	1	1.00	0.00	0.00	0.00
	2	-49.1	17.4	-2.31	51.6
	3	192	-9.72	-0.134	51.3
	4	402	-3.43	1.12	47.4
	5	696	-44.5	6.73	14.4
	6	724	-89.8	17.0	119
	7	1.00	0.00	0.00	0.00

After the prediction of the joint angles and the instant frames at each key-event, it was used a **Modified Akima cubic Hermite interpolation** to create a continuous trajectory, which, according with [82] is better for control. This Modified Akima cubic Hermite interpolation is based on piecewise functions of polynomials and it was chosen since this method does not produce continuous trajectories with high oscillations, neither flattened trajectories.

4.2.3. Regression Model Evaluation Metrics

Since the intra-subject variation in amplitude and timing was small, the prediction of the ankle angle was compared with the mean of the trials for each subject. In this sense, the performance of the regression model was evaluated based on four metrics: **RMSE**, **R**, **Goodness of Fit (GOF)** and **NRMSE** between the predicted and the experimental ankle angle. The first two evaluation metrics were calculated to compare the results of the implemented regression model with the results of [82]. Equations (2) and (3) present the formulas to calculate the GOF and the NRMSE, respectively. Regarding the GOF, this

metric is useful to perceive the performance of the fit, where $-\infty$ represents a very poor fit and 100 % corresponds to a perfect fit.

$$GOF = \left(1 - \left(\frac{\|y_{ref} - y\|}{\|y_{ref} - \overline{y_{ref}}\|}\right)\right) \times 100 \quad (2)$$

Where y_{ref} symbolizes the real parameter (angle or instant frame), $\overline{y_{ref}}$, represents the mean of the real parameter and y is the estimated parameter.

The NRMSE is useful to provide a percentage of the RMSE in the range of the experimental data, where 0 % is the best case to achieve.

$$NRMSE = \frac{RMSE}{max_{y_{ref}} - min_{y_{ref}}} \times 100 \quad (3)$$

In Equation (3), $max_{y_{ref}} - min_{y_{ref}}$ represents the range of the real parameter.

4.3. Results and Discussion

The results of the ankle angle prediction are exhibited in Table 12, presenting the mean and the standard deviation of the four metrics: RMSE, R, GOF and NRMSE.

Table 12. Results of the ankle joint angle prediction

RMSE (°)		R		GOF (%)		NRMSE (%)	
Validation mean (std) *	Test	Validation mean (std)	Test	Validation mean (std)	Test	Validation mean (std)	Test
3.99 (1.20)	4.01	0.930 (0.0482)	0.925	48.4 (21.5)	47.3	13.8 (6.33)	14.1

* Where std means standard deviation

Based on the collected results, it is concluded that the regression model offers satisfactory performances. Comparing the RMSE and R results to those achieved in [82], the performances of both implementations are comparable. The RMSE results obtained in this dissertation are similar to those achieved in [82], whereas the R results obtained in this dissertation provided an increment of 0.14 upon the R results of [82], approximately. Furthermore, since the walking speed presents a greater contribution in the prediction of the joint angles, the effect of its variation was evaluated. To perform this analysis, boxplots were constructed for each walking speed, since these graphics indicate how each metric is spread out. The results are presented in Figure 13.

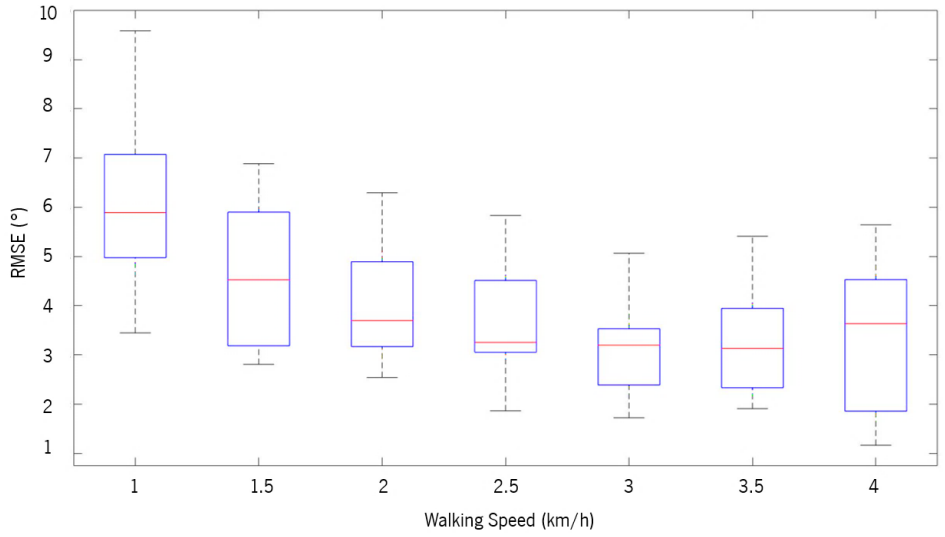
RMSE (°)
10
9
8
7
6
5
4
3
2
1
1
1.5
2
2.5
3
3.5
4
Walking Speed (km/h)

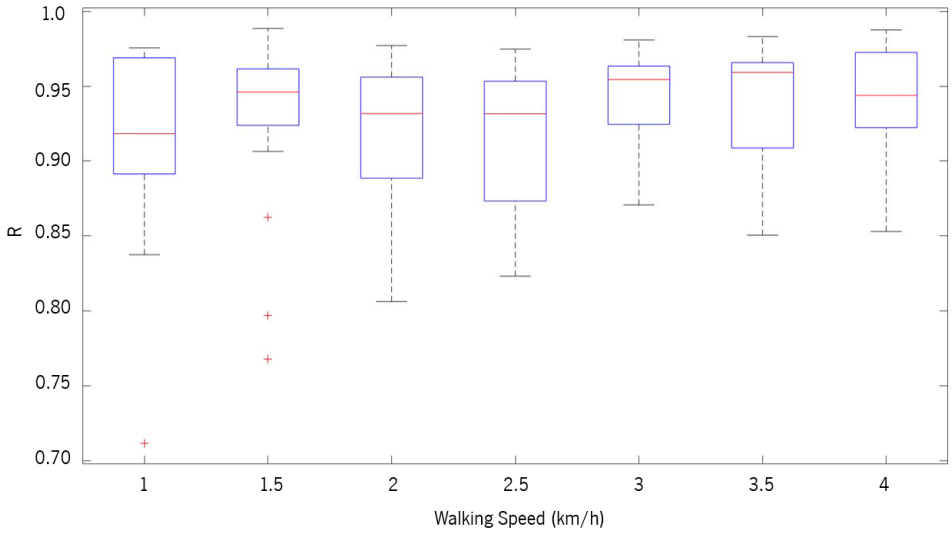
R
1.0
0.95
0.90
0.85
0.80
0.75
0.70
1
1.5
2
2.5
3
3.5
4
Walking Speed (km/h)

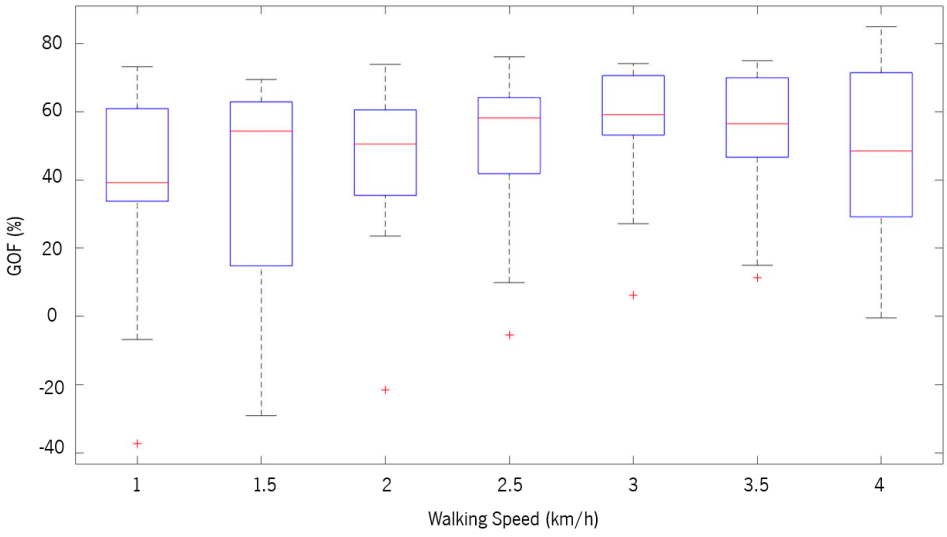
GOF (%)
80
60
40
20
0
-20
-40
1
1.5
2
2.5
3
3.5
4
Walking Speed (km/h)

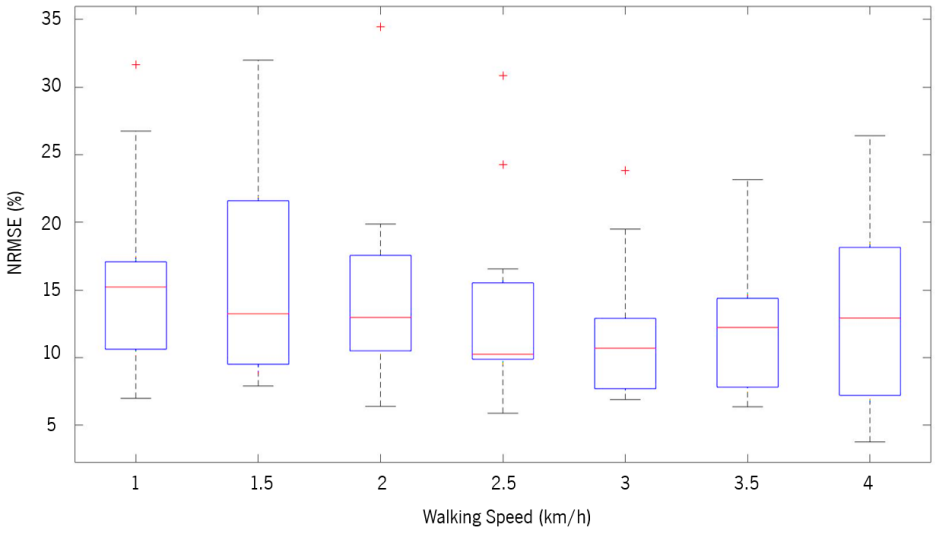

Figure 13. Boxplots of the RMSE, R, GOF and NRMSE with the walking speed variation.

In accordance with the results presented in Figure 13, it is possible to verify that, at slow walking speeds (below 2.5 km/h), the regression model presents higher prediction errors, therefore, less capacity to produce a good fit with the real ankle joint curve. This phenomenon was also reported by [82]. In this dissertation, these errors at slow walking speeds can be related with the data collection, because some subjects reported more difficulties into maintain the equilibrium during walking trials at slow walking speeds. During the data collection, it was verified that these subjects spent more time in the stance phase to maintain the equilibrium. Consequently, the angle value of the sixth key-event (maximum peak of plantar flexion) increases and it occurs later, as exhibited in Figure 14.

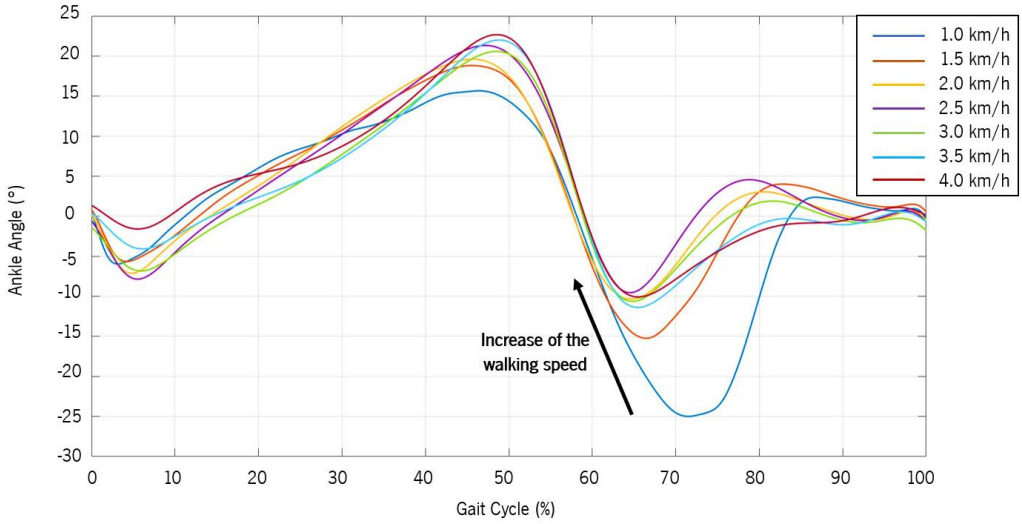

Figure 14. Collected ankle joint angle curves at different walking speeds, for a single subject.

At slow walking speeds, nearly 61 % of the gait cycles presented not only this phenomenon, but also a plantar flexion peak inferior to – 15 degrees (that corresponds to the typical angle value of plantar

flexion) and 31 % exhibit a peak below – 25 degrees. In this sense, the regression model learns these wrong values (derived from the loss of balance during the data collection) as the suppose values to attribute to new input data from subjects walking at slow speeds. However, there were participants that presented a walking pattern more stable and, thus, they did not demonstrate joint angles below – 15 degrees. From this perspective and considering most of the peak values of plantar flexion at slow speeds, when the data of these individuals act as input in the regression model, it is expectable that low values of plantar flexion are predicted. In fact, this phenomenon occurred, as evidenced by an example in Figure 15 – a), producing outliers, low values of GOF and R and high values of RMSE and NRMSE. On the other side, as the walking speed increases, better ankle angle predictions were observed. Figure 15 – b) represents the best reconstruction achieved, that is confirmed by the highest value of GOF and R and one of the lowest values of RMSE and NRMSE.

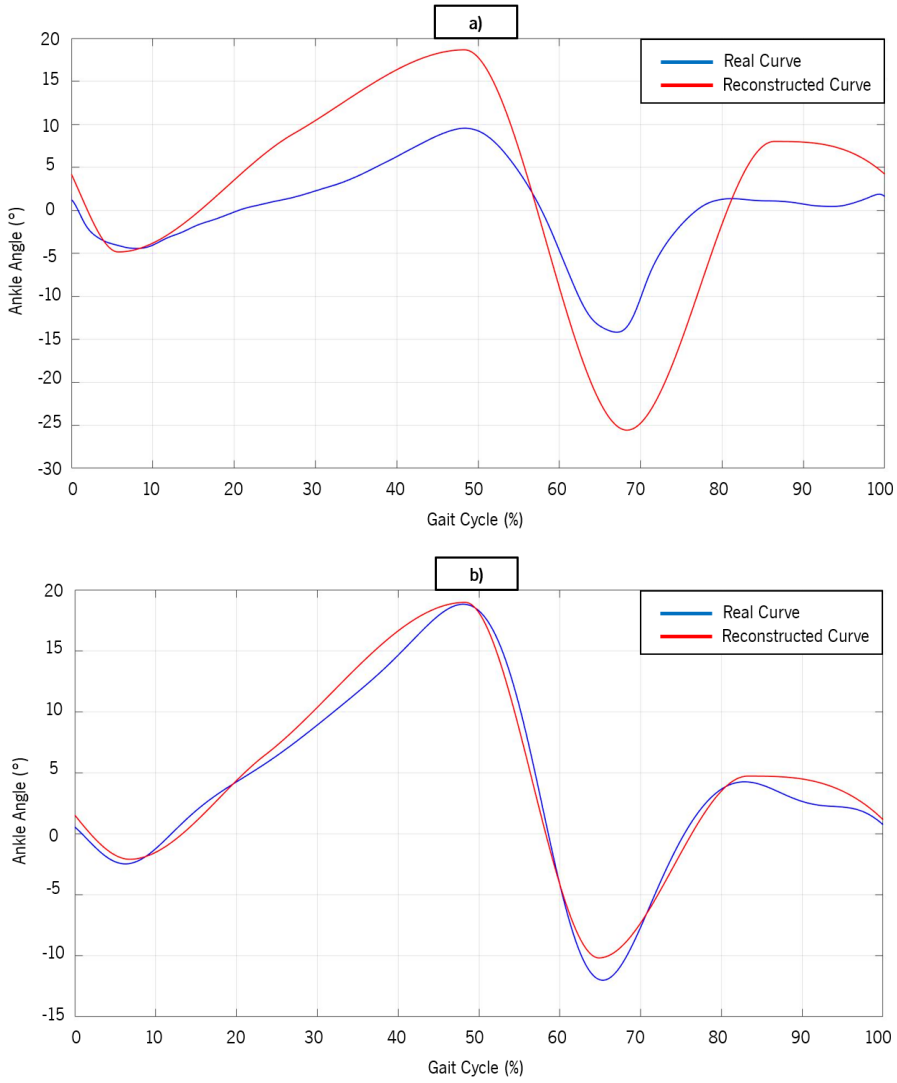

Figure 15. Worst (**a)**) and best (**b)**) ankle joint angle prediction achieved for a walking speed of 1 km/h (RMSE of 9.58 °, R of 0.918, GOF of - 37.3 % and NRMSE of 31.7 %) and for a walking speed of 4 km/h (RMSE of 1.16 °, R of 0.988, GOF of 85.0 %, NRMSE of 3.78 %), respectively.

Despite the best result has been achieved for a walking speed of 4 km/h, based on Figure 13, the **walking speed that is able to produce results with a smaller error distribution is 3 km/h**, because at this velocity, **99.3 % of the predictions present a RMSE below 5 °, a R between 0.871 and 0.981, a GOF from 30 to 70 % and a NRMSE below 20 %.**

Additionally, there is another limitation in the current regression model. The proposed methodology will provide the same ankle joint trajectories for individuals with the same body height, walking at the same walking speed. However, based on the data collected, it is seen that the inter-subject variation for individuals in the same conditions is considerable. This phenomenon can be visualized in Figure 16. In this sense, as future work, a user-oriented regression method should be developed, in order to consider more characteristics of the subjects (e.g. body mass), constructing different joint trajectories for subjects in the same conditions.

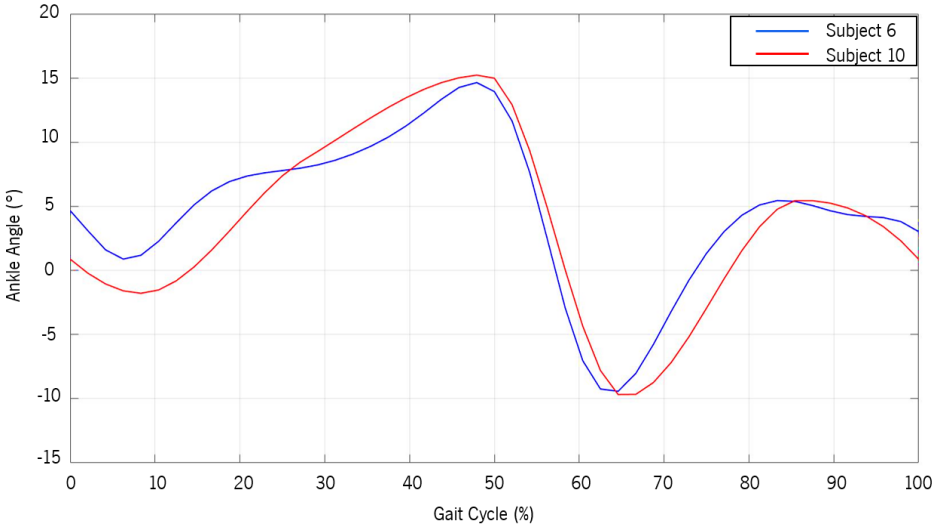

Figure 16: Subject 6 and 10 with a body height of 1.80 m, walking with a speed of 4 km/h.

4.4. General Conclusions

In this chapter, a regression model was implemented to generate reference ankle joint trajectories in the sagittal plane for subjects with body heights from 1.51 m to 1.83 m and walking speeds from 1 to 4 km/h, according to the walking speed and body height of each subject. The results were satisfactory and similar to the results achieved in [82]. However, improvements are needed. The reasons that justify improvements can be related with two facts: the **data collection** and the **regression model**. If the data collection had been performed in a treadmill, certainly, the stability of the subjects walking at slow speeds would not have been compromised. Therefore, the ankle joint data derived from the walking motion would not have been so irregular. Furthermore, using the proposed regression model, subjects in the same conditions of speed and body height will acquire the same walking trajectory. However, it was seen that

the inter-subject variation is significant and, for this reason, it is recommended to develop a model oriented to the user, considering more data, such as body mass.

CHAPTER 5 – ANKLE KINETICS TRAJECTORIES GENERATION

This chapter focuses on modeling of reference ankle joint torques based on five inputs, namely the reference ankle joint angles determined in the Chapter 4 and their derivatives (angular velocity and acceleration), body height of the subject and walking speed. The chapter starts with a brief explanation of the dependency of the joint torque on the body mass and then, machine learning methods used to create the reference joint torques are presented. At last, the results of each model are exhibited, compared and discussed, ending the chapter with the best approach to model the reference ankle joint torque. In this context, with the current and the previous chapter, the creation of reference ankle joint torques based on the walking speed, body height and body mass of each subject can be achieved.

5.1. Introduction

In the Chapter 4, based on [78], [82] and according to the achieved results, it was seen that the ankle joint kinematics during the gait cycle depends on the walking speed and the body height. Besides that, during the walking motion, the ankle plantar flexors muscles are responsible for providing the support required to boost the body forward [86]. In this sense, with an increase of the body mass, it is expectable that the support given by the ankle joint should be higher, increasing the muscle function and the joint torque and power. Some studies already verified that the ankle joint kinetics depends not only on the walking speed, but also on the body mass [87]–[89]. Thus, in this dissertation, all the joint torques were normalized by the body mass.

In the last years, studies have revealed that machine learning algorithms have capacity to model nonlinear relationships of data from the walking motion. In this field, most of these machine learning algorithms are selected to classify and to recognize locomotion modes [90]–[92]. There is no evidence of the use of machine learning were found to predict joint kinetics oriented to the subject during gait cycle. In this connection, this chapter focuses on the use of different machine learning algorithms to model the ankle joint kinetics.

To explore the relation between variables, two approaches of machine learning can be used: **supervised** and **unsupervised** learning techniques. A supervised learning technique develops a prediction model, using a training dataset with a relation between the input and the output data. Then, this developed model can predict the output for a new dataset and its generalization capacity with high predictive accuracy is dependent of the variance of the training dataset. On the other hand, in unsupervised learning techniques, the learning process is based on learning patterns through grouping instances. While supervised learning techniques comprehend regression and classification algorithms, unsupervised learning techniques correspond to dimensionality reduction or clustering [93]. Thus, supervised learning techniques are used in this chapter to predict the reference ankle joint torque.

5.2. Methods

In this section, different regression models are implemented to achieve the most proximal ankle joint torque for each subject. Based on a literature search, the most investigated machine learning approaches used in regression problems include **Support Vector Machine** (SVR), **Random Forest** (RF) and **Artificial Neural Networks** (ANN). In the field of ANN, MLP neural networks and Deep Learning architectures, including Long-Short Term Memory (LSTM) and Convolutional Neural Networks (CNN), have been widely used to solve regression problems [65], [66], [94]–[96]. In this sense, these regression models (SVR, RF, MLP, LSTM and CNN) were implemented, trained and optimized in *MATLAB*® and the best method was chosen to predict the reference ankle joint torque.

5.2.1. Regression Models

A. Support Vector Regression

As in Support Vector Machine, developed by [97], SVR is widely used in regression problems due to its greater capacity of generalization [93], [98]. This technic is characterized to map a lower-dimensional data into a high-dimensional feature space using kernel methods to achieve higher accuracies. The most commonly used kernels of this method are linear, polynomial and gaussian or radial

basis function. However, there is no evidence about the best kernel to use. In SVR, the train is performed using a symmetrical loss function. During this process, a flexible tube (ε-tube) is formed around the estimated function and the main objective of this method is to find the tube with the minimal width (ε - epsilon) that approximates the continuous-valued function, penalizing points outside the tube and providing no penalization to the points inside. At the same time, the model complexity and the prediction of the error are balanced. In addition to the great generalization capacity with high accuracy, the dimensionality of the input data does not affect the complexity of the model and, since it is less sensitive to the noise of the inputs, the model is more robust [93].

B. Random Forest

Before providing a brief explanation about RF applied in regression problems, it is required to know some operation concepts behind Decision Trees (DT). When using this method (DT), a single prediction is made as a result of questions that are produced based on a splitting method. The decision starts at the root node, on the top of the tree, and it progresses through the tree considering the answers to the questions at each decision node. This process runs until reaching the best prediction, that is found at the terminal node, also known as leaf node, as presented by Figure 17.

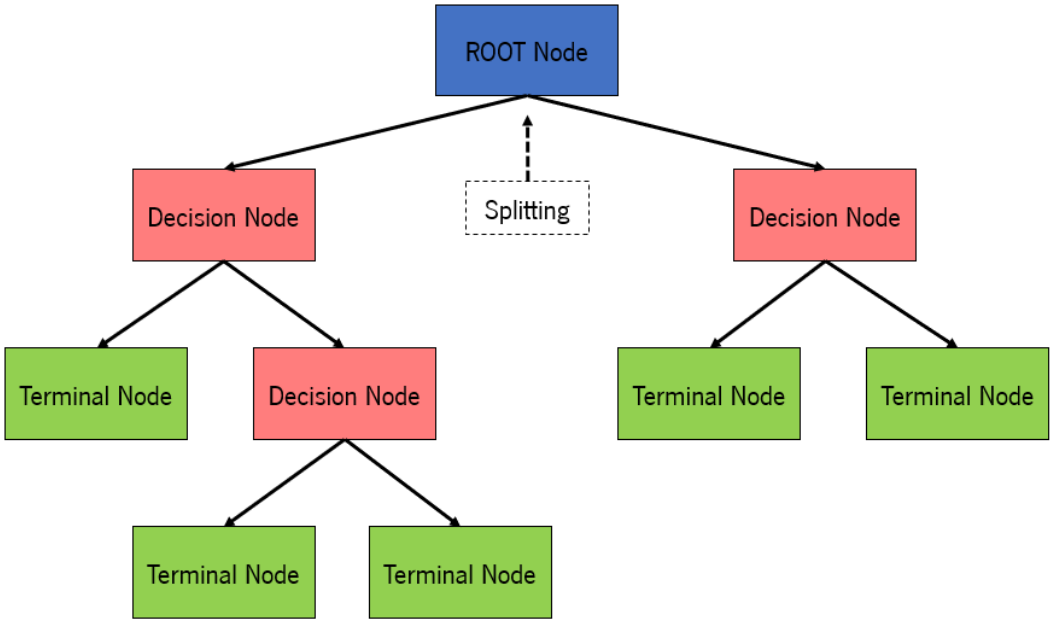

Figure 17. Example of an architecture of a DT.

During the training process, the DT learns the best questions/decisions to ask/perform, as well as the order to ask, with the final purpose of achieving the most accurate estimation. The decision criteria related to the splitting method is normally based on the mean squared error and, thus, according to this value, during the training process, the model decides if it is required to split a node [99]. However, the

major problem related with DT is overfitting, because when training, the model tends to adapt itself too much to the training data. Another negative aspect of this method is the instability, producing a model with high variance. In these cases, small variations in the data imply a generation of a different DT. These issues can be overpassed using RF. This regression method aggregates many trees that are trained with different random parts of the same training dataset, in order to reduce the high variance, using a technique called **bagging**. This technique enables better predictions, since the different trees are not correlated. In this sense, this means that the average performance of many trees is less sensitive to noise, while the prediction of a single tree is considerably sensitive [99].

C. Artificial Neural Networks: Multilayer Perceptron

ANN are composed by three layers: input, hidden and the output layer, containing independent variables, activation functions and dependent variables, respectively. The input layer is connected to the hidden layer that is composed by hidden neurons. These neurons receive the information from the input layer, they calculate the weights of the variables using activation functions (such as, hyperbolic tangent, sinusoid, logistic, binary step or identity functions) and predict the final output [100]. If the output of one layer serves as input in the next layer and all nodes are fully connected, the network is called feedforward neural network and the information never fed back in the neural network because there are no loops in its architecture [101]. Figure 18 represents an example of an architecture of a feedforward neural network with two hidden layers.

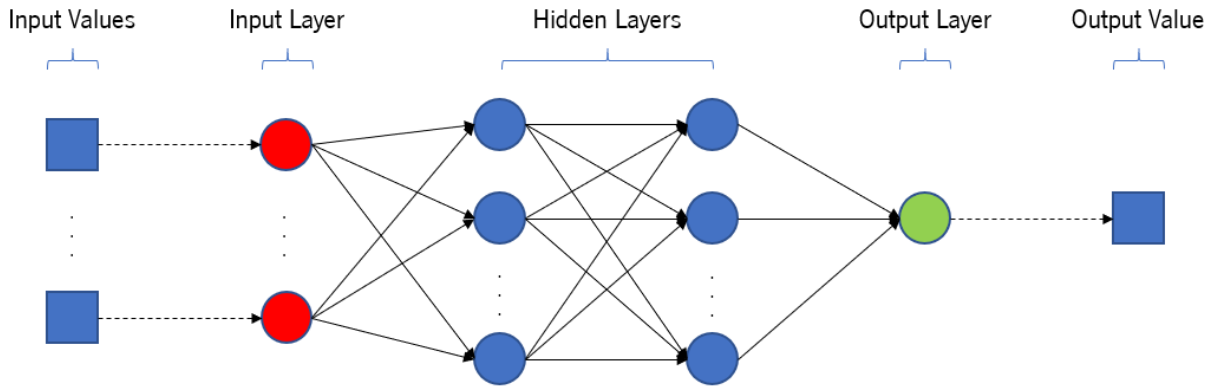

Figure 18. Feedforward neural network architecture with two hidden layers.

Based on these characteristics, and according to [102]–[104], MLP is the most used ANN in the majority of the fields due to its simplicity. Thus, a MLP neural network was applied in this dissertation.

The training process of MLPs has been widely used along with backpropagated algorithms, since the convergence of the neural network is improved [105]. The principle behind MLPs with backpropagation algorithms is based on the error gradient computation with respect to the weights and

it comprehends two phases: **(i)** to process the data from the input layer to the output layer, passing through the hidden layer(s); **(ii)** having the outputs, a comparison between the estimated and the real signal is done, computing an error. This error is backpropagated through the neural network based on the gradient descendent techniques. Thus, the weights are updated according with the error between the difference of the predicted output and the real signal. This can enable the achievement of predictive values closer to the target [101], [106]. Mathematically, the error/cost function in backpropagation algorithms can be calculated as the sum of squares, using Equation (4).

$$C_{(T,O)} = \frac{1}{N}\sum_{k=1}^{N}(T_k - O_k)^2 \tag{4}$$

Where *C* represents the cost function between the target (*T*) and the predicted output (*O*) for each output neuron, *N*. As reported by [107], for a network with only one layer with one neuron and a rectified linear unit activation, the prediction/target of the model corresponds to the activation of the neuron. In this case, the activation function is described by Equation (5).

$$activation(X) = max\ (0, w \cdot X + b) \tag{5}$$

Where, *w* and *b* represent the parameters of the model (weight and bias, respectively) and *X* represents the model inputs. As a result, the cost function can be reformulated by Equation 6 and 7:

$$C_{(T,O,w,b)} = \frac{1}{N}\sum_{k=1}^{N}(T_k - activation(X_k))^2 \tag{6}$$

$$\mathrm{C_{(T,O,w,b)}} = \frac{1}{\mathrm{N}}\sum_{\mathrm{k=1}}^{\mathrm{N}}(\mathrm{T_k} - \max\,(0, \mathrm{w} \cdot \mathrm{X_k} + \mathrm{b}))^2 \tag{7}$$

Differentiating Equation (7) with respect to the weights, it is possible to update the current weights, at instant *t*, considering the error gradient descent and the weights of the previous instant *t – 1*, obtaining Equation (8). The derivation steps to achieve Equation 8 can be consulted in [107].

$$w_t = w_{t-1} - \frac{\delta C}{\delta w_{t-1}} \tag{8}$$

Notwithstanding the prediction can achieve better performances, the gradient descent algorithms used to backpropagate the error can stuck in a local minimum, as presented in Figure 19.

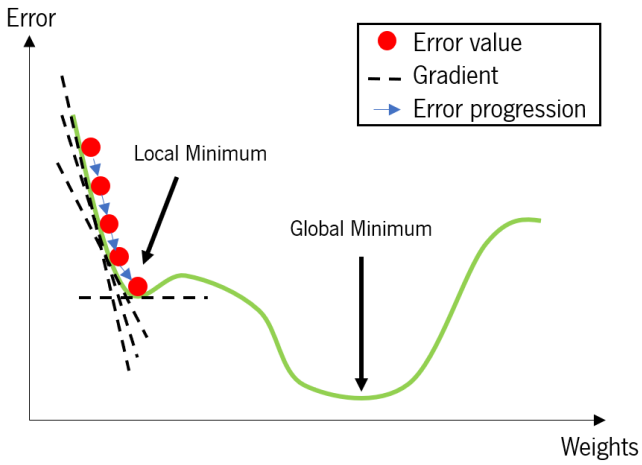

Figure 19. Gradient descent algorithm getting stuck in a local minimum.

To solve this problem, two new parameters can be considered, namely *learning rate*, η and *momentum*, α, as represented by Equation (9).

$$w_t = w_{t-1} - \eta \frac{\delta C}{\delta w_{t-1}} - \alpha w_{t-1} \quad (9)$$

With these parameters, the effect of the error gradient on the weights update is controlled. Moreover, the performance of the neural network and its time of convergence are also dependent on these parameters. Regarding the learning rate, it is required to consider that if this parameter is set too small, the algorithm will take too much time to converge, because the gradient descent algorithm will work slowly. In these cases, the convergence of the model is compromised and it is possible to stop again in a local minimum. On the other hand, if the learning rate is set too high, the algorithm will converge rapidly but with no stability. Thus, low values of learning rate are preferable, also considering the momentum parameter to escape from local minimums, since this parameter adds a percentage to the last update, improving the current update [108].

However, the error on the training set can be small, but when the neural network predicts responses to unknown data, the error is large. This means that the neural network is not generalized and it cannot provide good responses to new situations. According with [109], in MLP, the generalization performance is better using Bayesian regularization. Another regularization technique that provides a generalized neural network is the Levenberg-Marquardt [100].

In this sense, using the neural network toolbox of *MATLAB®*, in this dissertation, a MLP with backpropagation algorithm is applied, investigating two different training algorithms: *trainbr* and *trainlm*, corresponding to the Bayesian regularization method and Levenberg-Marquardt method, respectively. In both cases, the learning rate and momentum parameters were used as default. Moreover, based on

[109], the performance of the neural network can increase, obtaining a stable learning if the learning rate is updated during the training process. In this sense, another training algorithm, namely, *traingdx* was implemented to update the learning rate parameter.

D. Artificial Neural Networks: Deep Learning

Ankle joint torque is a continuous signal that is dependent on the time and, thus, it can be recognized as a Time-Series signal. In this field, studies reported that the use of Deep Learning methods, such as LSTM and CNN, can provide satisfactory results [110], [111].

LSTM consists of a type of recurrent neural networks. As described in the previous sub-section, the behavior of the activation functions existing on the neurons of the hidden layers of a feedforward neural networks depends on the behavior of the activation functions of neurons of the previous hidden layers. In contrast, with the architecture of recurrent neural networks, the behavior of the activation functions of the hidden neurons depends not only on the behavior of the previous activation functions, but also on the behavior at an earlier time. For this reason, neural networks where the behavior of the activation functions is dependent of the time are called by recurrent neural networks and, thus, Time-Series data is learned in an efficient way [101]. Normally, these architectures are used to predict the future using past information. However, if the interval in time between the current prediction and the previous information is too large, the predictions of the recurrent neural network are not promising. According to [101], if the time to run of a recurrent neural network is too long, the gradient will become tremendously unstable and the capacity to learn will be minimal. To solve this problem, LSTM neural networks were proposed. These kind of neural networks are a conjugation of recurrent neural networks with gradient descendent learning algorithms, making easier to obtain good results with unstable gradient problems under control [112]. Information relative to the train of the LSTM neural network can be found in [112].

CNN are another type of neural networks that is trained based on backpropagation algorithms. The architecture of these neural networks was inspired in the mammalian visual cortex, since according to [113], the first processing stages in the visual cortex consist in the detection of simple features, such as edges and bars. In the following processing stages, more complex associations are done and the object that is being seen is recognized. The behavior of CNN is identical, since these neural networks are composed by three layers (convolutional, pooling and fully-connected layers) and during the training process, the objective is to reduce the dimensionality of the representation based on feature extraction methods, in order to capture the most relevant spatial and temporal dependencies of an image [113], [114]. Thus, this neural network was used to extract the most relevant features to achieve the most proximal ankle joint torque.

The convergence and generalization performance of neural networks can be a difficult task to accomplish due to the difficulty into find the best learning rate and momentum value. Moreover, if only one learning rate and momentum value is applied to all weights, the weight update is the same to all neural network, causing the convergence performance less efficient. To improve the convergence performance, some gradient descendent algorithms have been emerged, such as, the Adaptive Moment Estimation (ADAM). With this algorithm, the weights of the neural network are updated using adaptive learning rates, avoiding the existence of a global one. Thus, the convergence performance is increased, while the learning error is reduced, obtaining a versatile neural network [115]. In Deep Learning algorithms explored in this dissertation, ADAM was used. In the neural network toolbox of *MATLAB®* is not possible to apply this algorithm when using MLP neural network and thus, the most proximal algorithm found was *traingdx*.

5.2.2. Data Preparation

The data collected in the Chapter 4 was used to train the implemented machine learning models. To train all the models, the data were randomly divided int blocks, where 60% of the data were used for training, 20% for validation and 20% for testing, corresponding to 10, 3 and 3 subjects, respectively. The inputs of the models were the ankle joint angles, angular velocity, angular acceleration, body height and walking speed. The output of the models was the ankle joint torque normalized by the body mass. A *k*-fold cross-validation algorithm was implemented to analyze the robustness of the models. The number of folds was set to 4.

Table 13 presents the maximum range and the units revealed by the input and output features. In accordance to these values, it is possible to infer that there is a discrepancy in the magnitude order of each feature.

Table 13. Units and Maximum Variation Range of each model feature

Feature	Unit	Maximum Range
Ankle Angle	degrees	76.0
Ankle Angular Velocity	degrees/s	3.75×10^{2}
Ankle Angular Acceleration	degrees/s^2	3.68×10^{3}
Body Height	m	0.320
Walking Speed	km/h	3.00
Ankle Torque	N·m/kg	2.18

Due to the difference in the range of each feature, if these data were applied in regression models, the model's learning process would take a long time to find a global minimum and to converge. In this sense, before the training process, it is required to apply a normalization step to the input data to achieve better results with faster calculations [116]. In a small dataset, four types of normalization were examined: **(i)** Min – Max normalization between 0 and 1; **(ii)** Min – Max normalization between -1 and 1; **(iii)** Z – Score normalization; and **(iv)** Median normalization. Table 14 resumes the mathematical formulas of each normalization method.

Table 14. Normalization methods

Normalization Method	Formula
Min-Max Normalization between 0 and 1	$X_{norm} = \frac{X - min\,(X)}{max(X) - min\,(X)}$
Min-Max Normalization between -1 and 1	$X_{norm} = -1 + 2 \times \frac{X - min\,(X)}{max(X) - min\,(X)}$
Z-Score Normalization	$X_{norm} = \frac{X - mean\,(X)}{std(X)}$
Median Normalization	$X_{norm} = \frac{X - median\,(X)}{Interquartile\ Range}$

The Min – Max normalization implies a linear transformation of the data between the maximum and the minimum of the feature. In this sense, the maximum and the minimum value of each feature correspond to 1 and 0 (in case **(i)**) or to 1 and -1 (in case **(ii)**), respectively and, thus, all values of the feature are contained into range of [0,1] (in case **(i)**) or [–1,1] (in case of **(ii)**). Z – Score normalization consists into remove the mean of the feature to each value, dividing by the standard deviation. In this connection, after Z – Score normalization, the data present null mean and a unitary standard deviation. Regarding the Median normalization, the median of each feature is removed to each data point of that feature and then, the result is divided by the interquartile range, that correspond to the subtraction of the first quartile from the third quartile. The Min – Max normalization is more affected by outliers that, as reported by [117], reduce the performance of the models. In fact, this was verified in a previous study and, besides that, with the Median normalization, better results were achieved. Thus, this normalization method was used.

5.2.3. Machine Learning Evaluation Metrics

To evaluate the performance of the regression models, two metrics were used: GOF and NRMSE between the predicted and the expected torque. The choice of these evaluation metrics was because **(i)** the GOF evaluates the performance of the fit achieved with each model, including a correlation and a similarity analysis between curves; and **(ii)** the NRMSE provides a percentage of the RMSE in the range of the experimental data.

Thus, along the next section, the model parameterization and optimization, as well as their respective results are presented.

5.3. Results

5.3.1. Support Vector Regression

SVR model is composed by five main hyperparameters: **Box Constraint**, **Kernel Scale**, **Epsilon**, **Kernel Function** and **Polynomial Order**. With recourse to optimization steps, the best model hyperparameters can be found. In this dissertation, these model parameters were optimized and the results of this optimization step are presented in Table 15.

Table 15. SVR best hyperparameters

Hyperparameter	Range	Hyperparameter value
Box Constraint	$[1e^{-3}, 1e^{3}]$	5.20
Kernel Scale	$[1e^{-3}, 1e^{3}]$	0.461
Epsilon	$[1e^{-3}, 1e^{3}]$	$1.70e^{-3}$
Kernel Function	Gaussian, Linear, Polynomial	Gaussian
Polynomial Order *	2, 3 or 4	

*Only when the Kernel Function is Polynomial

Table 16 presents the results of the SVR model trained without and with the optimization step.

Table 16. SVR results without (in red) and with (in green) hyperparameters optimization

Model Parameters Optimized?	GOF (%)		NRMSE (%)	
	Validation mean (std)	Test	Validation mean (std)	Test
✗	28.7 (1.45)	28.6	15.5 (0.531)	15.1
✓	69.4 (9.52)	68.7	5.97 (2.01)	6.59

Based on the collected results, without the optimization of the parameters, the SVR model is not able to produce a good fit between the predicted and the real ankle joint torque, since the GOF and the NRMSE evaluation metrics presented low and high percentages, respectively. After the optimization step, an increment of 40.1 % in the fit performance for the test dataset was observed, along with a decreasing of 8.51 % in the NRMSE.

5.3.2. Random Forest

RF method is composed by six main hyperparameters, namely **Ensemble Aggregation Method**, **Number of Learning Cycles**, **Learning rate**, **Minimum Leaf Size**, **Maximum Number of Splits** and **Number of Variables to Sample**. As in the SVR method, a hyperparameters optimization was done and the results can be consulted in Table 17.

Table 17. RF best hyperparameters

Hyperparameter	Range	Hyperparameter value
Ensemble Aggregation Method	Bag LSBoost	Bag
Number of Learning Cycles	[10, 500]	39
Learning rate	$[1e^{-3}, 1]$	
Minimum Leaf Size	$\left[1, \frac{\text{Number of Observations}}{2}\right]$	1
Maximum Number of Splits	$\left[1, \frac{\text{Number of Observations}}{2}\right]$	24748
Number of Variables to Sample	[1, 5]	4

The performance of the RF method was evaluated with and without optimization steps and the results are presented in Table 18.

Table 18. RF results without (in red) and with (in green) hyperparameters optimization

Model Parameters Optimized?	GOF (%)		NRMSE (%)	
	Validation mean (std)	Test	Validation mean (std)	Test
✗	69.4 (1.20)	67.9	6.66 (0.321)	6.75
✓	73.9 (1.95)	73.6	5.68 (0.470)	5.56

In accordance with the results, RF method provides satisfactory performances without hyperparameters optimization. Nonetheless, the hyperparameters optimization was investigated and the results of GOF and NRMSE of the test dataset presented an increase of 5.7 % and a decrease of 1.19 %, respectively.

5.3.3. Multilayer Perceptron

In MLP neural network, the main characteristics imposed in the training process are presented in Table 19. In this sense, the stopping criteria was based on the maximum number of epochs, maximum validation failures, minimum performance gradient or maximum momentum update (*mu*). If one of these values was reached, the training process ended.

Table 19. Key parameters for MLP neural network

Parameter	Value
Maximum number of epochs	10000
Performance goal	0
Maximum validation failures	10
Minimum performance gradient	$1e^{-7}$
Maximum time to train	Infinite
Initial *mu*	0.001
mu decrease factor	0.1
mu increase factor	10
Maximum *mu*	$1e^{10}$

To determine the best structure of the neural network to obtain a most close ankle joint torque, three training functions were studied (*trainbr*, *trainlm* and *traingdx*), as already referred. Different numbers

of neurons (10, 70 and 110) and hidden layers (1 and 2) were explored. Table 20 presents the achieved results with this neural network under the conditions referred. The worst and the best results are colored in red and green, respectively.

Table 20. MLP results

Method	Hidden Layers	Hidden Neurons	GOF (%)		NRMSE (%)	
			Validation mean (std)	Test	Validation mean (std)	Test
MLP (*trainlm*)	1	10	57.8 (1.05)	55.3	9.17 (0.320)	9.41
		70	67.3 (2.12)	66.8	7.10 (0.395)	7.00
		110	68.7 (2.12)	69.0	6.79 (0.395)	6.54
	2	10	66.1 (2.32)	67.8	7.37 (0.475)	6.78
		70	70.4 (1.26)	69.4	6.44 (0.313)	6.44
		110	70.5 1.26)	69.8	6.37 (0.314)	6.36
MLP (*trainbr*)	1	10	59.3 (1.65)	58.8	8.85 (0.390)	8.67
		70	69.9 (1.58)	69.1	6.53 (0.355)	6.50
		110	70.7 (1.57)	69.9	6.36 (0.360)	6.33
	2	10	67.3 (1.54)	67.0	7.10 (0.380)	6.95
		70	**67.3** (1.57)	**70.9**	**7.10** (0.380)	**6.13**
		110	70.1 (1.31)	69.2	6.48 (0.328)	6.50
MLP (*traingdx*)	1	10	45.9 (1.19)	46.9	11.8 (0.403)	11.2
		70	34.2 (3.68)	36.8	14.3 (0.801)	13.3
		110	28.4 (5.66)	32.5	15.6 (1.37)	14.2

	10	47.1 (0.880)	45.1	11.5 0.194)	11.6
2	70	38.2 (2.59)	40.5	13.4 (0.778)	12.5
	110	**28.4** (0.944)	**28.3**	**15.6** (0.160)	**15.1**

Based on an overview of the results achieved with *trainlm* and *trainbr* training functions, the regression performance of both is similar. Generally, an increment in the number of hidden neurons is reflected by an improvement of the fit. Moreover, increasing the number of hidden layers increased the regression performance. However, it was noticed that this performance's improvement caused when 2 hidden layers are considered became less appreciable when the number of hidden neurons is higher.

Using *traingdx* as training function, it would be expectable to achieve better performances, considering that an adaptive learning rate during the training process produces better results [109]. However, with this training function, the worst results were achieved and, thus, this training function must not be used to predict the ankle joint torque.

In accordance to the obtained regression performance, a **MLP with 2 hidden layer**, **70 hidden neurons** and trained with ***trainbr*** as **training function is the architecture that provides the better performance to the predict the reference ankle joint torque**. It should be noticed that when more than 110 hidden neurons are considered, the neural network does not offer better results upon the results achieved with this number of hidden neurons, having been verified a stabilization or a decrease in the model performance.

5.3.4. Long Short-Term Memory Neural Network

The main options defined during the training process of the LSTM neural network are presented in Table 21. The neural network trained while the number of maximum epochs or the number of maximum validation failures were not reached. The initial learning rate value, the drop period, drop factor and the batch size were set according with the default values.

Table 21. Key parameters for LSTM neural network

Parameter	Value
Maximum number of epochs	10000
Maximum validation failures	10
Gradient Descendent Algorithm	ADAM
Initial Learning Rate	0.01
Learning Rate Drop Period	50
Learning Rate Drop Factor	0.2
Batch Size	64

The results of the LSTM neural network with the parameters defined in Table 21 are presented in Table 22.

Table 22. LSTM results with default parameters, where the worst and best results are colored in red and green, respectively

Batch Size	Hidden Neurons	GOF (%)		NRMSE (%)	
		Validation mean (std)	Test	Validation mean (std)	Test
64	10	78.1 (0.400)	77.7	4.76 (0.121)	4.70
	70	77.2 (2.71)	78.4	4.96 (0.634)	4.55
	110	79.4 (0.195)	79.6	4.92 (0.117)	4.31

Considering the regression performance achieved with LSTM, an increment of the number of neurons does not offer significative improvements. The best results were achieved for a LSTM neural network with 110 hidden neurons.

The effect of the batch size was studied in this neural network, increasing and the decreasing its value, in order to find the architecture that provided the best results. Due to the high time consumption encountered during the initial developments of this neural network, the batch size was only varied for the LSTM with 110 hidden neurons, since that was the architecture that provided the best performance in default parameters. The results achieved are presented in Table 23, where the worst and the best performances are colored in red and green, respectively.

Table 23. LSTM results with batch size variation

Batch Size	Hidden Neurons	GOF (%)		NRMSE (%)	
		Validation mean (std)	Test	Validation mean (std)	Test
128	110	79.3 (0.200)	79.5	4.95 (0.125)	4.57
64	110	79.4 (0.195)	79.6	4.92 (0.117)	4.31
32	110	77.4 (0.352)	76.8	4.92 (0.155)	4.87

According with Table 23, with a decreasing of the batch size, the performance of the neural network started to decrease. On the other side, considering a larger batch size, the performance of the neural network remains similar. Thus, an **LSTM with 110 hidden neurons and trained with a batch size of 64 can provide good performances**.

5.3.5. Convolutional Neural Network

Generally, CNN are used for image processing and thus, this neural network operates with 3 – dimensional matrices. In this sense, the input data were treated as images, having suffered a transformation. Once there are five input features and several gait cycles, the data was organized in 3 – dimensional matrices, as follows: **width** – number of each gait cycle samples; **height** – number of input features; **depth** – number of gait cycles.

Concerning the training process, this neural network also trained while the number of maximum epochs or the number of maximum validation failures were not reached. At the beginning, the initial learning rate value, the drop period, drop factor and the batch size were set according with the default values. The defined parameters are presented in Table 24.

Table 24. Key parameters for CNN

Parameter	Value
Maximum number of epochs	10000
Maximum validation failures	10
Gradient Descendent Algorithm	ADAM
Initial Learning Rate	0.01
Learning Rate Drop Period	50
Learning Rate Drop Factor	0.2
Batch Size	64
Number of Convolutional Layers	3 (with 8, 16 and 32 filters applied)
Kernel Size	5×5
Pooling (Pool Size)	Average (2)
Stride	2
Fully Connected Layers (Number of outputs)	1 (1)

According to [118], with smaller kernel sizes, the computational performance is more efficient than with larger kernel sizes and the neural network is able to learn more complex non-linear features. In this sense a kernel size of 3 was also experienced and the results are presented in Table 25.

Table 25. CNN results with kernel size variation

Kernel Size	GOF (%)		NRMSE (%)	
	Validation mean (std)	Test	Validation mean (std)	Test
5×5	81.1 (0.721)	80.5	4.10 (0.122)	4.10
3×3	81.0 (1.08)	80.7	4.13 (0.188)	4.06

Based on the achieved results, the performance of the neural network with both kernel sizes was identical, achieving smaller better results in the test dataset with a kernel size of 3.

Since the last layer of CNN is a fully connected layer identical to a MLP and considering that an increment in the number of hidden neurons in MLP caused an improvement in the regression performance, another fully connected layer was added to CNN. Since at the end of the last convolutional layer, a vector with a length of 32×3 is created and considering the desired output torque value, the

number of neurons of the fully connected layer added was set to 32. The results achieved with this new architecture are presented in Table 26.

Table 26. CNN results with two fully connected layers

Kernel Size	GOF (%)		NRMSE (%)	
	Validation mean (std)	Test	Validation mean (std)	Test
3×3	80.6 (0.596)	80.0	4.20 (0.0814)	4.22

In contrast to the expectable, the performance of CNN decreases with the addition of another fully connected layer. Thus, only one fully connected layer should be considered. In this neural network, the batch size was also varied. The performances achieved are exhibited in Table 27, where the worst and best performances are colored in red and green, respectively.

Table 27. CNN results with batch size variation

Kernel Size	Batch Size	GOF (%)		NRMSE (%)	
		Validation mean (std)	Test	Validation mean (std)	Test
3×3	128	81.6 (0.533)	81.2	3.99 (0.137)	3.97
	64	81.0 (1.08)	80.7	4.13 (0.188)	4.06
	32	79.9 (0.548)	79.7	4.36 (0.137)	4.27

By analyzing Table 27, a reduction of the batch size is not favorable, since the regression performances started to decrease. On the other side, with an increment of the batch size, better results were achieved. Thus, a **CNN with 3 convolutional and 1 fully connected layer, a kernel size of 3×3 and a batch size of 128 was found as the architecture that provides better results**.

5.4. Discussion and General Conclusions

Machine learning algorithms have been used in the last years to model nonlinear relationships of the walking. However, to the best of the author's knowledge, there are no literature evidences on the using of machine learning to predict the ankle joint torque oriented to the subject. In this sense, the most

used regression models applied to model nonlinear relationships, namely SVR, RF, MLP, LSTM and CNN, were used to predict the reference ankle joint torque based on five inputs: ankle angle, angular velocity, angular acceleration, body height and walking speed.

Table 28 presents the best results obtained per each machine learning algorithm.

Table 28. Best results of the implemented regression models where the best model performances achieved are colored in green, while the worst are colored in red

Method	GOF (%)		NRMSE (%)	
	Validation mean (std)	Test	Validation mean (std)	Test
SVR	69.4 (9.52)	68.7	5.97 (2.01)	6.59
RF	73.9 (1.95)	73.6	5.68 (0.470)	5.56
MLP	67.3 (1.57)	70.9	7.10 (0.380)	6.13
LSTM	79.4 (0.195)	79.6	4.92 (0.117)	4.31
CNN	81.6 (0.533)	81.2	3.99 (0.137)	3.97

In addition to the best results summarized and presented by Table 28, Figure 20 exhibits the ground truth ankle joint torque and the predictions achieved with each one of the models for a random selected range of the test dataset.

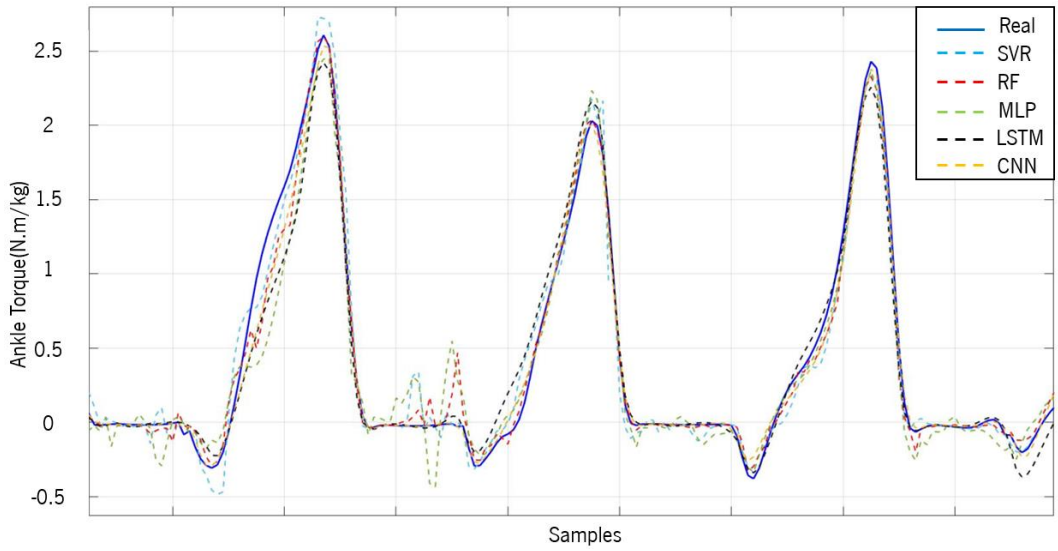

Figure 20. Predictions of the SVR, RF, MLP, LSTM and CNN machine learning models in comparison with the real ankle joint torque.

In accordance to Figure 20, it is possible to infer that the predictions made by LSTM and CNN models produced an ankle joint torque closer to the expected one, when compared to the remaining regression models. This fact is confirmed by the higher GOF and lower NRMSE value presented by these models, in Table 28. Nonetheless, performing a deeper analysis centered on the gait cycle, during the stance phase, it was verified that all the models present capacity to model the ankle joint torque. However, in the swing phase, irregularities and sudden peaks were verified for the predictions achieved by the SVR and MLP. This phenomenon can be confirmed by the lowest evaluation metrics presented by these two models. Thus, considering the obtained results, **the CNN was the model chosen to predict the reference ankle joint torque oriented to the subject**.

CHAPTER 6 – AAN EMG-BASED CONTROL STRATEGY

This chapter describes the proposed AAN EMG-based control strategy presented on Chapter 2. The importance of the regression models developed in Chapter 4 and Chapter 5 is investigated. Additionally, it is developed a method to estimate the real ankle joint torques based on EMG signals and joint angles. The performance of the ankle joint torque estimation is evaluated and the chapter ends with a discussion of the achieved results.

6.1. Introduction

The literature analysis in Chapter 2 demonstrated that the EMG-based control strategies integrated into WPADs only follow the intentions of the user and, consequently, it may be possible that individuals with impairments of the lower limbs and whose EMG signals are weak do not receive the required support to walk. AAN control strategies integrating EMG signals represent a recent alternative to overcome these limitations, taking advantage of the anticipatory performance of these signals. Thus, this dissertation aims to construct an AAN EMG-based control strategy for a future integration at SmartOs.

To advance with the proposed strategy, it is required to determine two parameters: a **reference** and a **real joint torque**, as represented in Figure 4. Regarding the reference ankle joint angle determined in Chapter 4, its impact is determinant on the prediction of the reference ankle joint torque. According to [77], the joint torque about the ankle joint is dependent on the angular acceleration. Since this parameter corresponds to the second derivative of the joint angle, the prediction of the reference ankle

joint torque is dependent on the reference ankle joint angle prediction. In this sense, through this chapter, the connection between the Chapter 4 and Chapter 5 is evaluated: i.e., the prediction of the reference ankle joint torques with the best model found in Chapter 5 fed with the predicted ankle joint kinematics determined at Chapter 4.

Considering the collected works responsible for converting the EMG signals into joint torque values, the study developed by [64] was chosen to perform this conversion due to present the shortest conversion time, offering promising results. Furthermore, the toolbox to perform this estimation is open source, programmed in *C++* language and it is available on [119]. Thus, in this chapter, the code of the toolbox is adapted to the architecture of SmartOs, in order to estimate the real ankle joint torque in real-time.

6.2. Reference Ankle Joint Torque Prediction

The prediction of the reference ankle joint torque ($\tau_{ref}(t)$) was based on the prediction of kinematic data for each subject. Five inputs were involved, namely, *BH, WS,* $\theta_{ref}(t)$, $\omega_{ref}(t)$ and $\alpha_{ref}(t)$, as presented in Figure 2.

To evaluate the performance of the reference ankle joint torque prediction, two cases are analyzed: **(i)** the worst; and **(ii)** the best ankle joint angle prediction. Based on the results achieved in Chapter 4, the worst prediction was verified for a subject with a body height of 1.79 m, walking at 1 km/h, while the best results were achieved for a subject with a body height of 1.65 m, walking at 4 km/h. For each case, the body mass was 81.9 and 60.0 kg, respectively. Thus, for both cases it was predicted the reference ankle joint torque using the best regression model found in Chapter 5, namely, CNN with a kernel size of 3×3, 3 convolutional and 1 fully connected layers, trained with a batch size of 128. The results of the predictions are represented in Figures 21.

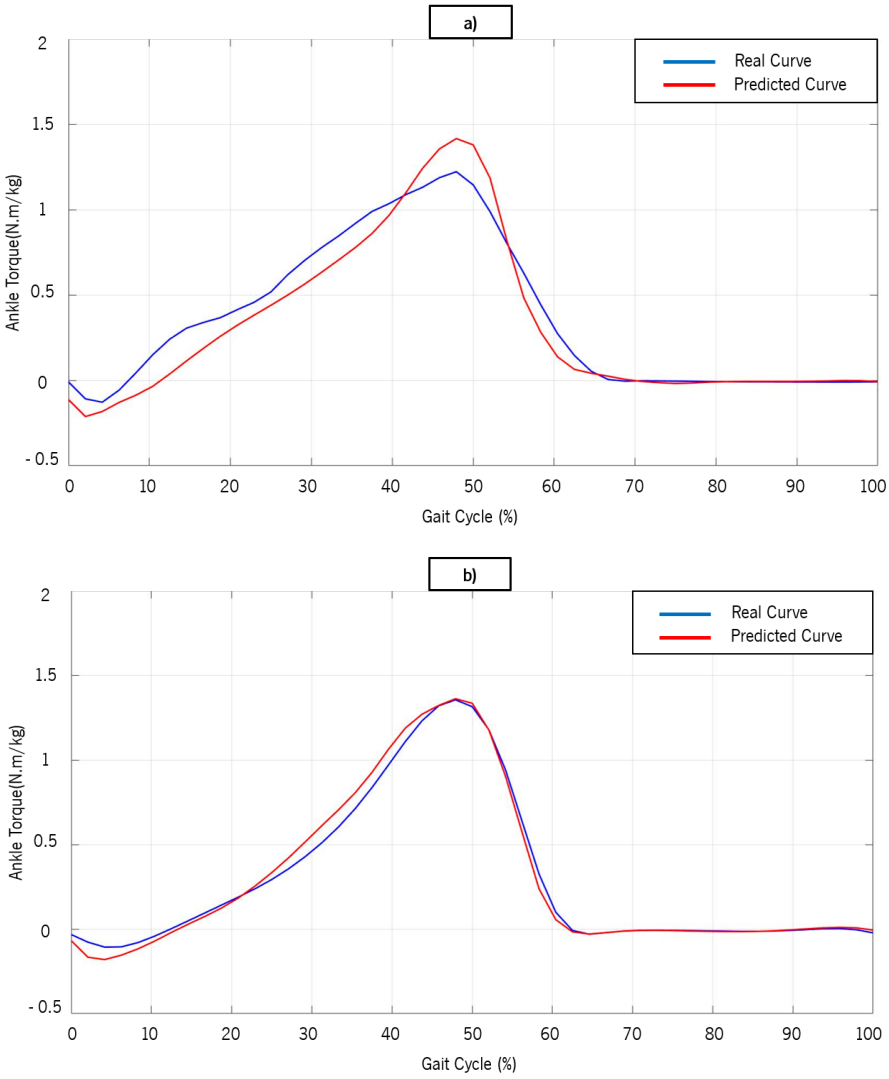

Figure 21. Reference ankle joint torque prediction based on the worst (**a)**) and best (**(b)**) reference ankle joint angle prediction.

Although the ankle joint angle prediction for the first case (**(i)**) has been less favorable, the prediction of the torque for this joint is acceptable and comparable with the real joint torque, presenting a GOF of 74.7 % and a NRMSE of 8.02 %. Based on Figure 15 – a), (that represents the worst ankle joint angle prediction), the ankle joint angle predicted presents a wider range of motion (ROM) when compared with the real ROM. Hence, the angular acceleration also presents a wider range and, since the joint torque is directly dependent on this parameter, it would be expectable that the predicted joint torque could present higher values than the real one. In fact, this phenomenon occurred, as it is proven by Figure 21 – a). Concerning the second case (**(ii)**), the prediction of the joint torque is quite similar to the real joint torque, presenting a GOF of 89.8% and a NRMSE of 3.16%.

Overall, even the predicted reference ankle joint kinematics present less favorable fits, the implemented machine learning algorithm (CNN) can model the reference ankle joint torques with high accuracy.

6.3. EMG-based Real Joint Torque Estimation

Once the prediction of the reference ankle joint torque has been achieved, it was required to estimate the real ankle joint torque of a subject, in real-time. Along this section, all the algorithms implemented are exhibited, ending the chapter with the validation of the proposed estimation.

6.3.1. Model Presentation

Figure 22 presents the block diagram to estimate the real ankle joint torque, based on real EMG signals and real ankle joint angles.

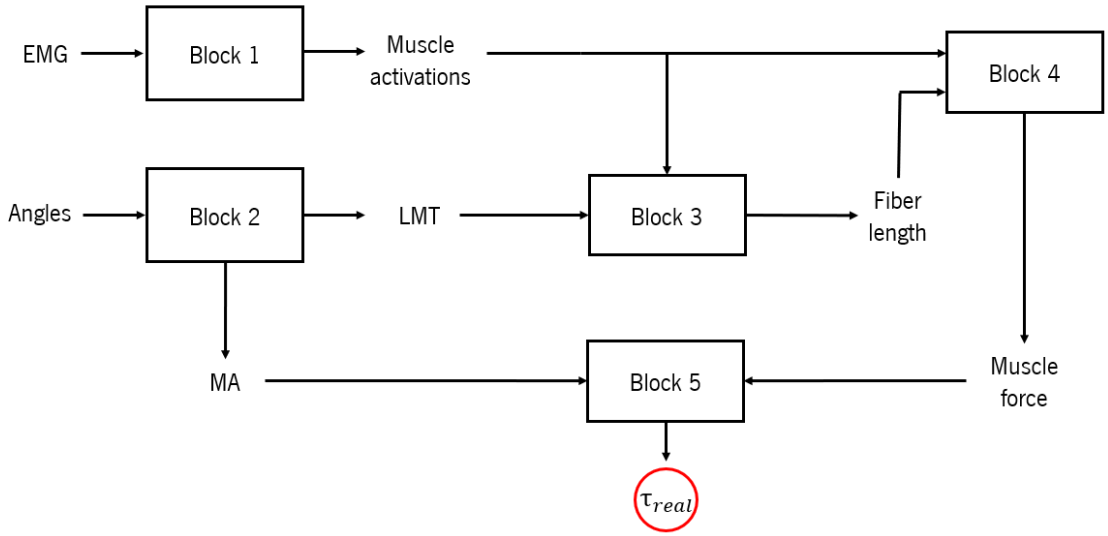

Figure 22. Block diagram to estimate the real ankle joint torque, τ_{real}.

The toolbox available on [119] performs the conversions illustrated in the Blocks 1, 3, 4 and 5 of Figure 23. However, it does not calculate the musculotendon lengths (LMTs), neither the moment arms (MAs) illustrated in Block 2, both required to estimate the real ankle joint torque. To solve this problem, an algorithm presented by [120] and adapted by [121] was used to obtain the LMTs and MAs based on real ankle joint angles. To determine these two parameters, a calibration step is required, in order to identify six calibration parameters, namely, F^{max}, V^{max}, L_0^m, optimal length of the tendon (L_{slack}), ϕ and type / fibers percentage. In the work advanced by [121], these six parameters (presented in Table 29) were found for a healthy subject with 1.80 m and 80 kg.

Table 29. Muscle parameters

Calibration Parameter	Muscle	
	GL	TA
F^{max} (N)	1500	800
v^{max} (m/s)	12.0	12.0
L_0^m (m)	0.0500	0.0600
L_{slack} (m)	0.400	0.240
ϕ	0.700	0.700
Type I fibers percentage	0.810	0.500

6.3.2. Model Adaptation

The study presented by [64] used six muscles to estimate the ankle joint torque: TA, SOL, GASM, GASL, PL and PT. Considering the information reviewed in Chapter 2, the most important muscles to perform dorsiflexion and plantar flexion of the ankle joint are the TA and the GAS or the SOL, respectively. In this connection, during the data collection exhibited in Chapter 4, only data from TA and GASL were collected. Thus, the model of [64] was adapted to receive data only from these two muscles.

Considering the hierarchical control and the non-centralized architecture presented in SmartOs, the proposed AAN EMG-based control strategy will be executed by the CCU of SmartOs into a SmartOs-dedicated program. However, it is not possible to implement the proposed EMG-based torque estimation model into the SmartOs program, given the no compatibilities between this framework and the SmartOs program. Thus, a bidirectional Transmission Control Protocol/Internet Protocol (TCP/IP) was developed to simulate the communication between the EMG-based torque estimation model and the CCU of SmartOs. In Figure 23 is presented the flowchart of the proposed communication.

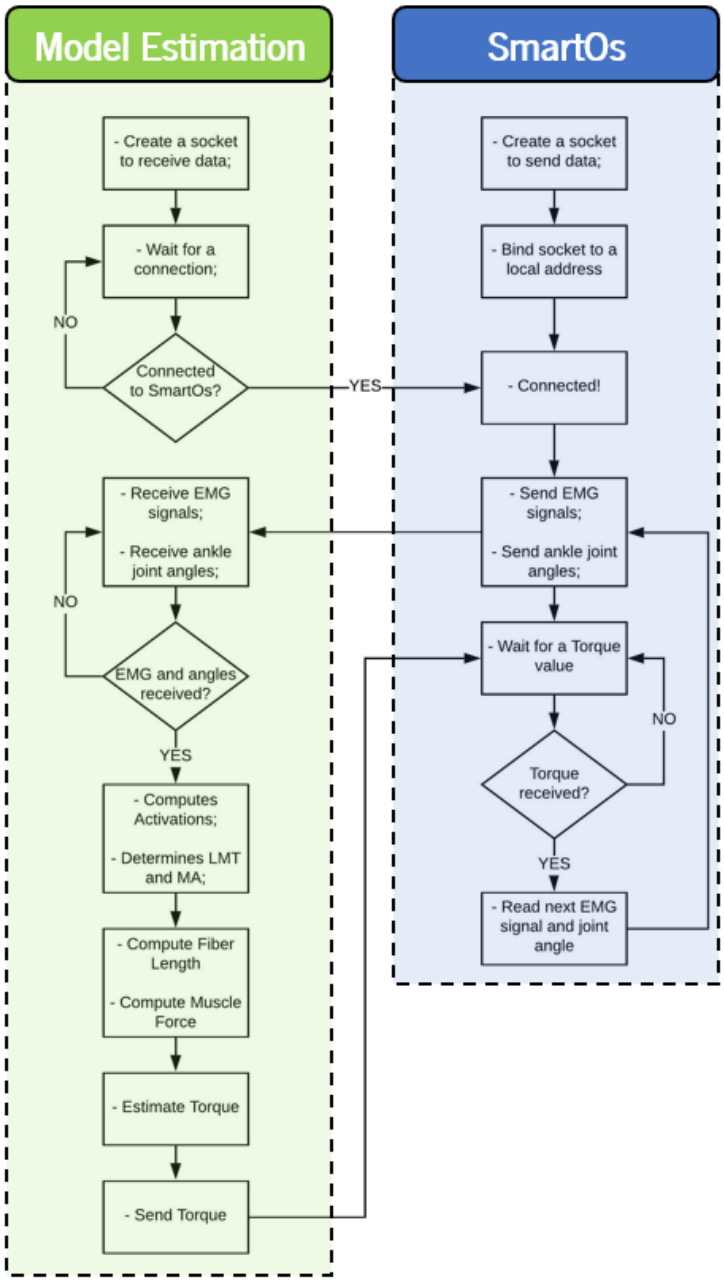

Figure 23. Flowchart with the implemented TCP/IP communication.

To explain the flowchart of Figure 23, it is required to remember the AAN EMG-based control strategy proposed in Chapter 3 and the EMG-based torque estimation exhibited in Figure 3. The inputs required to estimate the real ankle joint torque are the real EMG signals and the real ankle joint angles. In a future integration, the EMG signals will be acquired with recourse to the EMG boards developed in Chapter 3, integrated into SmartOs. On the other side, the joint angles will be provided by the potentiometer also integrated into SmartOs. In this sense, in the beginning, the proposed estimation model waits for a connection with the orthosis. If a connection is established, the communication starts and the EMG signals along with the ankle joint angles are sent from SmartOs to the EMG-based torque

estimation model. After the operational computations schematized in Figure 23, the joint torque is estimated and sent to SmartOs, which is waiting for a real torque value to be compared with the reference ankle joint torque. Once received, the next EMG signal and ankle joint angles are sent to the model and another estimation is performed.

6.3.3. Model Validation

Once established the TCP/IP communication to simulate the connection between the proposed EMG-based torque estimation and the CCU of SmartOs, it was required to validate the adapted model. Since the calibration parameters already enounced were found for a subject with 1.80 m and 80 kg, EMG signals from TA and GASL along with ankle joint angles from a subject with the same physical characteristics was used to serve as input in the model.

The results of the torque estimation for a walking speed of 1 km/h are presented in Figure 24 and compared with the expected ankle joint torque. Varying the walking speed, the model estimation presents the same behavior.

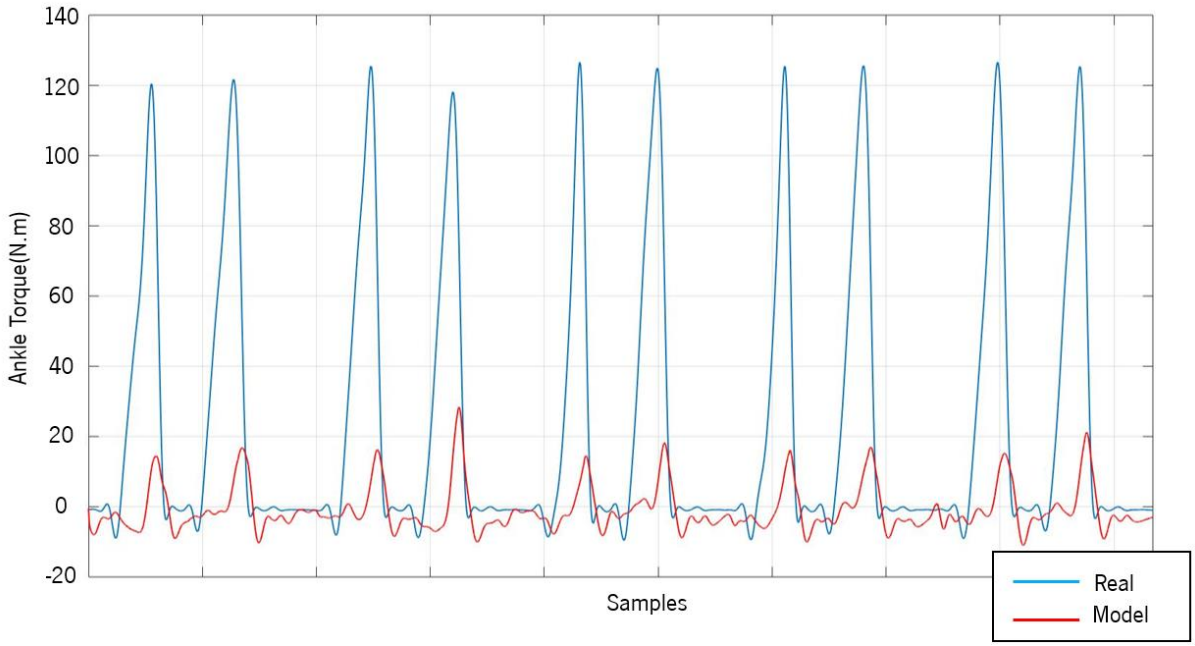

Figure 24. Comparison between the real (blue) and the ankle joint torque estimated by the model (red), considering TA and GASL.

Based on the assumption that only two muscles were considered to estimate the real joint torque, it would be expectable that the obtained values reveled a lower magnitude, when compared to the real ankle joint torque. However, since TA and GASL are the muscles that provide the most relevant ankle joint motion, it would also be expectable that the magnitude of the estimated values was lower but not too much inferior to the real value. Nonetheless, based on Figure 24, the obtained results presented a

magnitude much smaller than the expected one. In order to try to understand this phenomenon, a third muscle was considered, namely, GASM and fed with the data of the GASL. The results of this modification are presented in Figure 25.

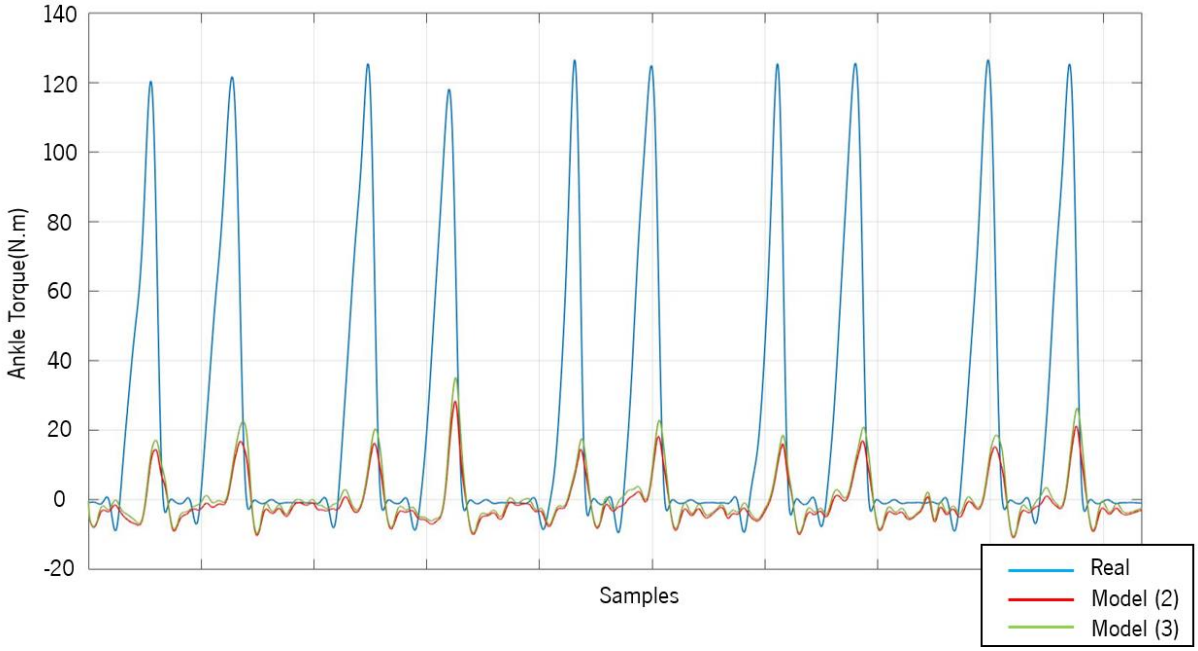

Figure 25. Comparison between the real (blue) and the ankle joint torque estimated by the model, considering TA and GASL (Model 2 – red) and considering TA, GASL and GASM (Model 3 – green).

Results of Figure 25 show that an increment in the number of muscles, produces a higher magnitude. However, this increment of the magnitude was not enough to achieve the expected ankle joint torque. In order to try to find the reason behind this phenomenon, the LMTs and MAs achieved were compared with the results presented in [64], [122]. The pattern and magnitude of the curves achieved for both cases was identical to the pattern of the curves presented in the literature. Since the computation of the muscle activations, fiber lengths and muscle forces were performed based on [64], the reason that can justify the magnitude difference between the results achieved and the results presented by [64] is the use of a small number of muscles. Furthermore, a delay around 100 ms was verified between both curves. However, this phenomenon requires a deeper investigation, since studies [64], [120] reported a delay of 3 ms in their implementations.

Overall, the model requires more EMG signals from other muscles to achieve the real ankle joint torque, since only two muscles are not recommended, despite being the main muscles that act in the ankle joint.

6.4. General Conclusions

This chapter presents the implementation and validation of the two main blocks of the proposed AAN EMG-based control strategy: **(i)** the prediction of a reference ankle joint torques oriented to each user; and **(ii)** the estimation of the real ankle joint torques for each user, based on real EMG signals and real ankle joint angles.

In what concern to the first point, considering the worst and the best scenario for the reference ankle joint torque prediction, good results were demonstrated. With the regression model proposed in Chapter 4 responsible to predict the reference ankle joint angles, along with the architecture of the CNN developed in Chapter 5, reference ankle joint torques with a GOF ranging from 74.7 to 89.8 % and a NRMSE between 3.16 and 8.02 % can be achieved for a subject with **(i)** a body height from 1.51 m to 1.83 m, **(ii)** a body weight between 52.0 kg and 83.7 kg and **(iii)** walking with a speed ranging from 1 to 4 km/h. Moreover, it was verified that the implemented machine learning algorithm (CNN) can model the reference ankle joint torques with high accuracy, even considering predicted reference ankle joint kinematics with less favorable fits.

In relation to the EMG-based torque estimation, a musculoskeletal model was applied, using EMG signals from TA and GASL muscles and ankle joint angles. Based on the obtained results and comparing with the results achieved in [64], it is concluded that more muscles must be considered, in order to obtain magnitude values of torque similar to the real ones. On the other hand, a more in-depth investigation is required to understand the delay around 100 ms, introduced by the model. The proposed musculoskeletal model depends on calibration parameters. This fact conducts to a limitation of the implemented EMG-based torque estimation, since only one subject was used to validate the proposed model.

CHAPTER 7 – CONCLUSIONS

Neurological diseases, such as stroke, can be the origin of disabilities in the lower limbs and, thus, producing abnormal gait patterns. In this field, WPADs, such as orthosis or exoskeletons, have been widely used to promote adequate assistance to neurological patients or patients with motor injuries, aiming to restore the lower limb functions.

Human-machine interactions integrating EMG signals has been explored, based on the construction of bioinspired control architectures with user-oriented control strategies, considering the motor intention and condition of the patient. Nonetheless, in cases of disabilities of the lower limbs, the use of these EMG-based control strategies into WPADs may not provide the assistance required by the patient, since the EMG signals are weaker when compared with healthy subjects. Thus, AAN EMG-based control strategies have emerged to provide a personalized assistance, considering the motor condition of the user and what the user should perform under healthy conditions.

In this master dissertation, an AAN EMG-based control strategy was proposed to assist the ankle joint and its future insertion in SmartOs (a bioinspired, modular and time-effective WPAD) was explored. The future integration of the proposed strategy into SmartOs comprehends an innovative aspect, since there are few studies where AAN EMG-based control strategies are used to manage the assistance provided by the WPAD to the user.

In the first step, a literature analysis was performed in order to identify the main muscles responsible for the motion of the ankle joint. The knee joint was also investigated for a future implementation. TA, GAS and SOL were the muscles identified that provide a major contribution in the dorsiflexion and plantar flexion movement of the ankle joint. After that, an extensive literature search was

performed to identify the EMG-based and AAN EMG-based control strategies already developed, as well as the most relevant methodologies to estimate the joint kinetics based on EMG signals, since this conversion is performed in the majority of the control strategies using EMG signals. Proportional myoelectric, musculoskeletal and empirical models were investigated as methods to convert the EMG signals into torque values. Empirical models may be more appropriated to perform the desired conversion for disable persons, since calibration steps are not required.

An EMG system was projected, implemented and validated with a healthy subject walking at 1 km/h. The results achieved when compared with a commercial system and with literature findings, revealed a good performance.

In this dissertation, a regression model was explored to predict the reference ankle joint kinematics trajectory for a specific subject in the sagittal plane, based on the walking speed and body height. The results achieved were satisfactory and similar to the results obtained in [82]. However, improvements related to **(i)** the data collection; and **(ii)** the regression model must be done. Regarding the first point, during the data collection, it was verified that at slow walking speeds, the postural stability of most of the subjects was compromised. During the regression model training, in the presence of slow walking speeds, the regression model learned irregular ankle joint trajectories. Regarding the second point, it was verified that the proposed regression model attributes the same reference ankle joint angle for subjects with the same body height and walking at the same walking speed. However, the inter-subject variation is considerable and, for this reason, it is recommended to develop a model oriented to the user, considering more data, such as body mass.

Based on ankle joint kinematics, body height of the subject and walking speed, machine learning-based methods were explored to generate the reference ankle joint kinetics. The performance of five machine learning models was explored, namely: SVR, RF, MLP, LSTM and CNN, where the best results were achieved for a CNN.

The results demonstrated that CNN can accurately predict the reference ankle torque trajectories, even considering reference ankle joint kinematics with less favorable predictions. The correct prediction of the reference ankle joint torque oriented to the user based on predicted reference ankle joint kinematics, body height and walking speed is utmost importance in the AAN EMG-based control strategy, in order to compare the reference ankle joint torque with the real one. In this field, considering the best acknowledge of the author, there is no evidence on the literature regarding the ankle joint torque prediction oriented to the subject.

To estimate the real ankle joint torque, an EMG-based torque estimation was performed, based on a musculoskeletal model presented in [64]. Only two muscles were used to perform the estimation, in contrast to the six muscles used in [64]. Thus, EMG data from TA and GASL were used with real ankle joint angles to estimate the real ankle joint torque. Since the model depends on calibration parameters that were found for a subject with 1.80 m and 80 kg, the validation of this methodology was performed only considering one subject with the referred physical characteristics. Based on the obtained results, it was verified that the magnitude of the torque provided by the model was inferior to the real magnitude, indicating that only two muscles are not enough to estimate the ankle joint torque. Thus, it is necessary to include more EMG contributions from GASM, SOL, PT and PL muscles.

Aiming the future integration of the proposed AAN EMG-based control strategy into SmartOs and considering that the EMG-based torque estimation was developed as a standalone framework, a TCP/IP communication was created to simulate the protocol between the EMG-based torque estimation model and the CCU of SmartOs.

Furthermore, with the developed master thesis, the goals that were established in Chapter 1 were all achieved and the RQ can be answered:

- RQ1: *Which are the contributions and the main differences of the EMG-based control and the AAN EMG-based control strategies?*

  This RQ was addressed in Chapter 2. Both strategies contributed to muscular activity improvement and endurance, avoiding muscle atrophy. Most of the EMG-based control strategies verified a decreased muscular activity while the joint angles were controlled. However, these reviewed strategies were only tested in healthy subjects. Thus, the joint angles were controlled given the motor ability of the healthy subjects. Nonetheless, it is not expectable that these strategies have the potential to assist the lower limbs of disabled subjects. In contrast, the AAN EMG-based control strategies compare, in real-time, the user's motor performance with the desired user's motion to ensure a sufficient level of assistance oriented to the user's needs. Thus, AAN EMG-based control strategies have the potential to assist and rehabilitate the lower limbs, such that the user can achieve autonomy to perform their daily life activities.

- RQ2: *Is it possible to obtain joint torque measures only using EMG signals?*

  This RQ was addressed in Chapter 2. Based on the reviewed information, it was concluded that most of the control methods which use EMG signals to control WPADs convert these EMG signals into torque values. Nonetheless, there are literature evidences that only EMG

readings are not enough to obtain the accurate values of joint torques, being necessary to fuse EMG data with biomechanical data, such as, joint angles, velocities, accelerations.

- **RQ3:** *Is it possible to predict reference walking kinematics and kinetics trajectories relying exclusively on the walking speed and anthropometric data?*

  This RQ was approached in Chapters 4, 5 and 6. Based on the results achieved in Chapter 4, it is possible to predict reference walking kinematics using exclusively walking speed and anthropometric data. The results of this dissertation show the needed for adding more anthropometric data (such as, the body mass) to avoid the attribution of the same ankle joint angle to subjects with the same body height, walking at the same walking speed. However, based on the results achieved in Chapter 5 and Chapter 6, this is not a limitation to predict the reference walking kinetics, since good performances were obtained.

- **RQ4:** *Can EMG-based torque estimation strategy present a good performance?*

  This RQ was approached in Chapter 6. Based on the results achieved in the literature [64], the EMG-based torque estimation with joint angles can be performed in real-time with good performances, when six muscles are considered. In this dissertation, only EMG data from two muscles (TA and GASL) and ankle joint angles were considered. Based on the achieved results, the magnitude of the estimated ankle joint torque was inferior to the expectable. With the addition of one more muscle (GASM), higher magnitudes were achieved. Thus, more muscles must be considered to estimate the real ankle joint torques, considering EMG signals and real ankle joint angles.

7.1. Future Work

Future work in the scope of this dissertation include: (1) the improvement of the regression model to predict reference ankle joint angles, in order to avoid the attribution of the same trajectory for subjects with the same body height and walking speed; (2) the improvement of the quality of the data acquisition by performing walking test in a treadmill with force platforms to avoid loss of the balance, specially at slow walking speeds; (3) the inclusion of more muscles to estimate the real ankle joint torque based on EMG signals and joint angles; (4) the exploration of machine learning algorithms operating in real-time to estimate the real ankle joint torque based on EMG signals and joint angles, since these empirical methods may

be more appropriated to perform the conversion in motor impaired persons, because calibration steps are not required.

REFERENCES

[1] W. Johnson, O. Onuma, M. Owolabi, and S. Sachdev, "Bulletin of World Health Organization," *Stroke: a global response is needed*, 2016. [Online]. Available: https://www.who.int/bulletin/volumes/94/9/16-181636/en/. [Accessed: 05-Jun-2019].

[2] F. A. Loterio, "Análise do Padrão de Ativação Muscular de Indivíduos Hemiparéticos Pós-AVC em Marcha Assistida por Andador Robótico," Universidade Federal do Espírito Santo, 2015.

[3] S. H. Jang, "The recovery of walking in stroke patients: a review," *Int. J. Rehabil. Res.*, vol. 33, no. 4, pp. 285–289, Dec. 2010.

[4] D. G. da Saúde, "Programa Nacional de Prevenção e Controlo das Doenças Cardiovasculares," *Dgs*, p. 28, 2006.

[5] A. H. NeuroHealth, "A Parent's Quick Guide to Hemiplegia and Hemiparesis," 2017. [Online]. Available: https://neurohealthah.com/guide-to-hemiplegia-hemiparesis/. [Accessed: 05-Jun-2019].

[6] J. Cao, S. Q. Xie, R. Das, and G. L. Zhu, "Control strategies for effective robot assisted gait rehabilitation: The state of art and future prospects," *Med. Eng. Phys.*, vol. 36, no. 12, pp. 1555–1566, Dec. 2014.

[7] G. Colombo, M. Joerg, R. Schreier, and V. Dietz, "Treadmill training of paraplegic patients using a robotic orthosis.," *J. Rehabil. Res. Dev.*, vol. 37, no. 6, pp. 693–700, 2000.

[8] A. Kaelin-Lang, L. Sawaki, and L. G. Cohen, "Role of Voluntary Drive in Encoding an Elementary Motor Memory," *J. Neurophysiol.*, vol. 93, no. 2, pp. 1099–1103, 2004.

[9] M. Lotze, “Motor learning elicited by voluntary drive,” *Brain*, vol. 126, no. 4, pp. 866–872, Apr. 2003.

[10] L. Marchal-Crespo and D. Reinkensmeyer, “Review of control strategies for robotic movement training after neurologic injury,” *J. Neuroeng. Rehabil.*, 2009.

[11] K. Gui, H. Liu, and D. Zhang, “A Practical and Adaptive Method to Achieve EMG-Based Torque Estimation for a Robotic Exoskeleton,” *IEEE/ASME Trans. Mechatronics*, vol. 24, no. 2, pp. 483–494, Apr. 2019.

[12] C. Ma, N. Chen, Y. Mao, D. Huang, R. Song, and L. Li, “Alterations of Muscle Activation Pattern in Stroke Survivors during Obstacle Crossing,” *Front. Neurol.*, vol. 8, no. MAR, Mar. 2017.

[13] P. N. Fernandes *et al.*, “EMG-based Motion Intention Recognition for Controlling a Powered Knee Orthosis,” in *2019 IEEE International Conference on Autonomous Robot Systems and Competitions (ICARSC)*, 2019, pp. 1–6.

[14] P. Artemiadis, “EMG-based Robot Control Interfaces: Past, Present and Future,” *Adv. Robot. Autom.*, vol. 1, no. 2, pp. 1–3, 2012.

[15] P. R. Cavanagh and P. V. Komi, “Electromechanical delay in human skeletal muscle under concentric and eccentric contractions,” *Eur. J. Appl. Physiol. Occup. Physiol.*, vol. 42, no. 3, pp. 159–163, Nov. 1979.

[16] S. Olney and C. Richards, “Hemiparetic gait following stroke. Part I: Characteristics,” *Gait Posture*, vol. 4, pp. 136–148, 1996.

[17] C. Fleischer and G. Hommel, “A Human-Exoskeleton Interface Utilizing Electromyography,” *IEEE Trans. Robot.*, vol. 24, no. 4, pp. 872–882, Aug. 2008.

[18] S. Jezernik, G. Colombo, and M. Morari, “Automatic Gait-Pattern Adaptation Algorithms for Rehabilitation With a 4-DOF Robotic Orthosis,” *IEEE Trans. Robot. Autom.*, vol. 20, no. 3, pp. 574–582, Jun. 2004.

[19] R. M. Singh, S. Chatterji, and A. Kumar, “Trends and challenges in EMG based control scheme of exoskeleton robots—a review,” *Int. J. Sci. Eng. Res*, vol. 3, no. 8, pp. 933–940, 2012.

[20] L. L. M. e Silva, C. E. M. de Moura, and J. R. P. de Godoy, “A marcha no paciente hemiparético,” *Univ. Ciências da Saúde*, vol. 3, no. 2, pp. 261–273, Apr. 2008.

[21] B. Balaban and F. Tok, “Gait Disturbances in Patients With Stroke,” *PM&R*, vol. 6, no. 7, pp. 635–642, Jul. 2014.

[22] C. A. Johnson, J. H. Burridge, P. W. Strike, D. E. Wood, and I. D. Swain, “The effect of combined use of botulinum toxin type A and functional electric stimulation in the treatment of spastic drop

foot after stroke: a preliminary investigation," *Arch. Phys. Med. Rehabil.*, vol. 85, no. 6, pp. 902–909, Jun. 2004.

[23] J. Perry, *Gait Analysis: Normal and Pathological Function*. Thorofare: SLACK Incorporated, 1992.

[24] K. P. Parekh and J. B. Vyas, "Myoelectric Leg for Transfemoral Amputee," *Int. J. Sci. Res. Dev.*, vol. 1, no. 5, pp. 12–15, 2013.

[25] B. S Rajaratnam, "A Comparison of EMG Signals from Surface and Fine-Wire Electrodes During Shoulder Abduction," *Int. J. Phys. Med. Rehabil.*, vol. 02, no. 04, 2014.

[26] D. L. Waite, R. L. Brookham, and C. R. Dickerson, "On the suitability of using surface electrode placements to estimate muscle activity of the rotator cuff as recorded by intramuscular electrodes," *J. Electromyogr. Kinesiol.*, vol. 20, no. 5, pp. 903–911, Oct. 2010.

[27] M. Solomonow *et al.*, "Surface and wire EMG crosstalk in neighbouring muscles," *J. Electromyogr. Kinesiol.*, vol. 4, no. 3, pp. 131–142, Jan. 1994.

[28] R. Bogey, K. Cerny, and O. Mohammed, "Repeatability of Wire and Surface Electrodes in Gait," *Am. J. Phys. Med. Rehabil.*, vol. 82, no. 5, pp. 338–344, May 2003.

[29] R. A. Bogey, J. Perry, E. L. Bontrager, and J. K. Gronley, "Comparison of across-subject EMG profiles using surface and multiple indwelling wire electrodes during gait," *J. Electromyogr. Kinesiol.*, vol. 10, no. 4, pp. 255–259, Aug. 2000.

[30] C. J. De Luca, "Surface electromyography: Detection and recording," *DelSys Inc.*, vol. 10, no. 2, pp. 1–10, 2002.

[31] B. Gerdle, S. Karlsson, S. Day, and M. Djupsjöbacka, "Acquisition, Processing and Analysis of the Surface Electromyogram," in *Modern Techniques in Neuroscience Research*, Berlin, Heidelberg: Springer Berlin Heidelberg, 1999, pp. 705–755.

[32] D. A. Gabriel, "Effects of monopolar and bipolar electrode configurations on surface EMG spike analysis," *Med. Eng. Phys.*, vol. 33, no. 9, pp. 1079–1085, Nov. 2011.

[33] R. Merletti and P. Parker, *Electromyography: Physiology, Engineering and Noninvasive Applications*. New Jersey: John Wiley & Sons, Inc, 2004.

[34] A. Suresh, "Body swarm interface (BOSI): Controlling Robotic Swarms Using Human Bio-Signals," Boston University, 2016.

[35] L. Shaw and S. Bagha, "Online EMG Signal Analysis for diagnosis of Neuromuscular diseases by using PCA and PNN," *Int. J. Eng. Sci. Technol.*, vol. 4, pp. 4453–4459, 2012.

[36] C. ADInstruments, "Trigno EMG Sensors." [Online]. Available: https://www.adinstruments.com/products/trigno-emg-sensors. [Accessed: 02-Sep-2019].

[37] Delsys Incorporated, *Trigno ™ Wireless Biofeedback System*. 2018.

[38] Noraxon, *Ultium™ EMG System: Sensor and Receiver User Manual*. .

[39] I. Motion Lab Systems, *Motion Lab Systems: User Guide*. 2004.

[40] BITalino: Biomedical Equipment, *MuscleBAN BE Data Sheet*. 2015.

[41] BITalino: Biomedical Equipment, *OpenSignals: User Manual*. 2012.

[42] D. P. Ferris and C. L. Lewis, "Robotic lower limb exoskeletons using proportional myoelectric control," in *2009 Annual International Conference of the IEEE Engineering in Medicine and Biology Society*, 2009, pp. 2119–2124.

[43] H. Kawamoto and Y. Sankai, "Comfortable power assist control method for walking aid by HAL-3," in *IEEE International Conference on Systems, Man and Cybernetics*, 2003.

[44] D. Ao, R. Song, and J. Gao, "Movement Performance of Human–Robot Cooperation Control Based on EMG-Driven Hill-Type and Proportional Models for an Ankle Power-Assist Exoskeleton Robot," *IEEE Trans. Neural Syst. Rehabil. Eng.*, vol. 25, no. 8, pp. 1125–1134, Aug. 2017.

[45] Rong Song, Kai-yu Tong, Xiaoling Hu, and Le Li, "Assistive Control System Using Continuous Myoelectric Signal in Robot-Aided Arm Training for Patients After Stroke," *IEEE Trans. Neural Syst. Rehabil. Eng.*, vol. 16, no. 4, pp. 371–379, Aug. 2008.

[46] A. V. Hill, "The heat of shortening and the dynamic constants of muscle," *Proc. R. Soc. London. Ser. B - Biol. Sci.*, vol. 126, no. 843, pp. 136–195, Oct. 1938.

[47] M. G. Hoy, F. E. Zajac, and M. E. Gordon, "A musculoskeletal model of the human lower extremity: The effect of muscle, tendon, and moment arm on the moment-angle relationship of musculotendon actuators at the hip, knee, and ankle," *J. Biomech.*, vol. 23, no. 2, pp. 157–169, Jan. 1990.

[48] D. G. Lloyd and T. F. Besier, "An EMG-driven musculoskeletal model to estimate muscle forces and knee joint moments in vivo," *J. Biomech.*, vol. 36, no. 6, pp. 765–776, Jun. 2003.

[49] M. Sartori, D. G. Lloyd, M. Reggiani, and E. Pagello, "A stiff tendon neuromusculoskeletal model of the knee," in *2009 IEEE Workshop on Advanced Robotics and its Social Impacts*, 2009, pp. 132–138.

[50] M. Sartori, M. Reggiani, A. J. van den Bogert, and D. G. Lloyd, "Estimation of musculotendon kinematics in large musculoskeletal models using multidimensional B-splines," *J. Biomech.*, vol. 45, no. 3, pp. 595–601, Feb. 2012.

[51] N. Karavas, A. Ajoudani, N. Tsagarakis, J. Saglia, A. Bicchi, and D. Caldwell, "Tele-impedance based assistive control for a compliant knee exoskeleton," *Rob. Auton. Syst.*, vol. 73, pp. 78–90,

Nov. 2015.

[52] Suncheol Kwon, Yunjoo Kim, and Jung Kim, "Movement Stability Analysis of Surface Electromyography-Based Elbow Power Assistance," *IEEE Trans. Biomed. Eng.*, vol. 61, no. 4, pp. 1134–1142, Apr. 2014.

[53] H. He and K. Kiguchi, "A Study on EMG-Based Control of Exoskeleton Robots for Human Lower-limb Motion Assist," in *2007 6th International Special Topic Conference on Information Technology Applications in Biomedicine*, 2007, pp. 292–295.

[54] T. Yan, M. Cempini, C. M. Oddo, and N. Vitiello, "Review of assistive strategies in powered lower-limb orthoses and exoskeletons," *Rob. Auton. Syst.*, vol. 64, pp. 120–136, Feb. 2015.

[55] K. Kiguchi and Y. Imada, "EMG-based control for lower-limb power-assist exoskeletons," in *2009 IEEE Workshop on Robotic Intelligence in Informationally Structured Space*, 2009, pp. 19–24.

[56] W. Hassani, S. Mohammed, H. Rifaï, and Y. Amirat, "Powered orthosis for lower limb movements assistance and rehabilitation," *Control Eng. Pract.*, vol. 26, pp. 245–253, May 2014.

[57] C. Fleischer and G. Hommel, "Torque Control of an exoskeletal knee with EMG signals," in *Proceedings of the joint conference on robotics*, 2006.

[58] C. Fleischer and G. Hommel, "Calibration of an EMG-Based Body Model with six Muscles to control a Leg Exoskeleton," in *IEEE International Conference on Robotics and Automation*, 2007, pp. 2514–2519.

[59] W. Hassani, S. Mohammed, and Y. Amirat, "Real-Time EMG Driven Lower Limb Actuated Orthosis for Assistance As Needed Movement Strategy," in *Robotics: Science and Systems IX*, 2013.

[60] W. Hassani, S. Mohammed, H. Rifai, and Y. Amirat, "EMG based approach for wearer-centered control of a knee joint actuated orthosis," in *2013 IEEE/RSJ International Conference on Intelligent Robots and Systems*, 2013, pp. 990–995.

[61] M. Moltedo, T. Baček, T. Verstraten, C. Rodriguez-Guerrero, B. Vanderborght, and D. Lefeber, "Powered ankle-foot orthoses: the effects of the assistance on healthy and impaired users while walking," *J. Neuroeng. Rehabil.*, vol. 15, no. 1, p. 86, Dec. 2018.

[62] C. Fleischer, C. Reinicke, and G. Hommel, "Predicting the intended motion with EMG signals for an exoskeleton orthosis controller," in *2005 IEEE/RSJ International Conference on Intelligent Robots and Systems*, 2005, pp. 2029–2034.

[63] L. Liu, M. Luken, S. Leonhardt, and B. J. E. Misgeld, "EMG-driven model-based knee torque estimation on a variable impedance actuator orthosis," in *IEEE International Conference on Cyborg and Bionic Systems (CBS)*, 2017, vol. 2018–Janua, pp. 262–267.

[64] G. Durandau, D. Farina, and M. Sartori, "Robust Real-Time Musculoskeletal Modeling Driven by Electromyograms," *IEEE Trans. Biomed. Eng.*, vol. 65, no. 3, pp. 556–564, Mar. 2018.

[65] M. Chandrapal, X. Chen, W. Wang, B. Stanke, and N. Le Pape, "Investigating improvements to neural network based EMG to joint torque estimation," *Paladyn, J. Behav. Robot.*, vol. 2, no. 4, pp. 185–192, Jan. 2011.

[66] M. E. Hahn, "Feasibility of estimating isokinetic knee torque using a neural network model," *J. Biomech.*, vol. 40, no. 5, pp. 1107–1114, Jan. 2007.

[67] P. A. Huijing and G. C. Baan, "Stimulation level-dependent length-force and architectural characteristics of rat gastrocnemius muscle," *J. Electromyogr. Kinesiol.*, vol. 2, no. 2, pp. 112–120, Jan. 1992.

[68] K. N. An, K. Takahashi, T. P. Harrigan, and E. Y. Chao, "Determination of Muscle Orientations and Moment Arms," *J. Biomech. Eng.*, vol. 106, no. 3, pp. 280–282, 1984.

[69] W. Meng, Q. Liu, Z. Zhou, Q. Ai, B. Sheng, and S. S. Xie, "Recent development of mechanisms and control strategies for robot-assisted lower limb rehabilitation," *Mechatronics*, vol. 31, pp. 132–145, Oct. 2015.

[70] Y. H. Yin, Y. J. Fan, and L. D. Xu, "EMG and EPP-Integrated Human–Machine Interface Between the Paralyzed and Rehabilitation Exoskeleton," *IEEE Trans. Inf. Technol. Biomed.*, vol. 16, no. 4, pp. 542–549, Jul. 2012.

[71] J. S. Campos Figueiredo, "Smart Wearable Orthosis to Assist Impaired Human Walking," University of Minho, 2019.

[72] STMicroelectronics, "UM1472: STM32F407VG MCU - User Manual." 2017.

[73] J. Wang, L. Tang, and J. E Bronlund, "Surface EMG Signal Amplification and Filtering," *Int. J. Comput. Appl.*, vol. 82, no. 1, pp. 15–22, Nov. 2013.

[74] C. J. De Luca, "The Use of Surface Electromyography in Biomechanics," *J. Appl. Biomech.*, vol. 13, no. 2, pp. 135–163, May 1997.

[75] A. Abdelouahad, A. Belkhou, A. Jbari, and L. Bellarbi, "Time and frequency parameters of sEMG signal — Force relationship," in *2018 4th International Conference on Optimization and Applications (ICOA)*, 2018, no. 1, pp. 1–5.

[76] F. D. Farfán, J. C. Politti, and C. J. Felice, "Evaluation of EMG processing techniques using Information Theory," *Biomed. Eng. Online*, vol. 9, no. 1, p. 72, 2010.

[77] D. A. Winter, *Biomechanics and Motor Control of Human Movement*. Hoboken, NJ, USA: John Wiley & Sons, Inc., 2009.

[78] J. L. Lelas, G. J. Merriman, P. O. Riley, and D. C. Kerrigan, "Predicting peak kinematic and kinetic parameters from gait speed," *J. Gait Posture*, vol. 17, pp. 106–112, 2003.

[79] C. A. Fukuchi and M. Duarte, "A prediction method of speed-dependent walking patterns for healthy individuals," *Gait Posture*, vol. 68, no. December 2018, pp. 280–284, 2019.

[80] M. Hanlon and R. Anderson, "Prediction methods to account for the effect of gait speed on lower limb angular kinematics," *Gait Posture*, vol. 24, no. 3, pp. 280–287, Nov. 2006.

[81] C. B. Beaman, C. L. Peterson, R. R. Neptune, and S. A. Kautz, "Differences in self-selected and fastest-comfortable walking in post-stroke hemiparetic persons," *Gait Posture*, vol. 31, no. 3, pp. 311–316, Mar. 2010.

[82] B. Koopman, E. H. F. van Asseldonk, and H. van der Kooij, "Speed-dependent reference joint trajectory generation for robotic gait support," *J. Biomech.*, vol. 47, no. 6, pp. 1447–1458, Apr. 2014.

[83] M. P. Kadaba, H. K. Ramakrishnan, and M. E. Wootten, "Measurement of Lower Extremity Kinematics During Level Walking," *J. Orthop. Res.*, vol. 8, pp. 383–392, 1990.

[84] H. & M. E. Roithner R. Schwameder, "Determination of optimal filter parameters for filtering kinematic walking data using butterworth low pass filter," in *Proceedings of the 18th International Symposium on Biomechanics in Sports*, 2000.

[85] MathWorks, "Least Squares Fitting." [Online]. Available: https://ch.mathworks.com/help/curvefit/least-squares-fitting.html.

[86] L. Moreira *et al.*, "Study of Gait Cycle Using a Five-Link Inverted Pendulum Model: First Developments *," in *2019 IEEE 6th Portuguese Meeting on Bioengineering (ENBENG)*, 2019, pp. 1–4.

[87] M. Branco, R. Santos-Rocha, and F. Vieira, "Biomechanics of Gait during Pregnancy," *Sci. World J.*, vol. 2014, pp. 1–5, 2014.

[88] P. M. Quesada, L. J. Mengelkoch, R. C. Hale, and S. R. Simon, "Biomechanical and metabolic effects of varying backpack loading on simulated marching," *Ergonomics*, vol. 43, no. 3, pp. 293–309, Mar. 2000.

[89] P. DeVita and T. Hortobágyi, "Obesity is not associated with increased knee joint torque and power during level walking," *J. Biomech.*, vol. 36, no. 9, pp. 1355–1362, Sep. 2003.

[90] D. T. H. Lai, P. Levinger, R. K. Begg, W. L. Gilleard, and M. Palaniswami, "Automatic Recognition of Gait Patterns Exhibiting Patellofemoral Pain Syndrome Using a Support Vector Machine Approach," *IEEE Trans. Inf. Technol. Biomed.*, vol. 13, no. 5, pp. 810–817, Sep. 2009.

[91] M. Yang, H. Zheng, H. Wang, S. McClean, J. Hall, and N. Harris, "A machine learning approach to assessing gait patterns for Complex Regional Pain Syndrome," *Med. Eng. Phys.*, vol. 34, no. 6, pp. 740–746, Jul. 2012.

[92] H. Asadi, R. Dowling, B. Yan, and P. Mitchell, "Machine Learning for Outcome Prediction of Acute Ischemic Stroke Post Intra-Arterial Therapy," *PLoS One*, vol. 9, no. 2, p. e88225, Feb. 2014.

[93] M. Awad and R. Khanna, *Efficient Learning Machines: Theories, Concepts and Applications for Engineers and System Designers*. Apress Open, 2015.

[94] Q. Duan, J. Zeng, K. Chakrabarty, and G. Dispoto, "Accurate Predictions of Process-Execution Time and Process Status Based on Support-Vector Regression for Enterprise Information Systems," *IEEE Trans. Comput. Des. Integr. Circuits Syst.*, vol. 34, no. 3, pp. 354–366, Mar. 2015.

[95] C. Lv *et al.*, "Levenberg–Marquardt Backpropagation Training of Multilayer Neural Networks for State Estimation of a Safety-Critical Cyber-Physical System," *IEEE Trans. Ind. Informatics*, vol. 14, no. 8, pp. 3436–3446, Aug. 2018.

[96] I. Goodfellow, Y. Bengio, and A. Courville, *Deep learning*, vol. 1. MIT press Cambridge, 2016.

[97] V. N. Vapnik, *The Nature of Statistical Learning Theory*. New York, NY: Springer New York, 1995.

[98] R. G. Brereton and G. R. Lloyd, "Support Vector Machines for classification and regression," *Analyst*, vol. 135, no. 2, pp. 230–267, 2010.

[99] G. Louppe, "Understanding Random Forests: From Theory to Practice," University of Liège, 2014.

[100] M. Kayri, "Predictive Abilities of Bayesian Regularization and Levenberg–Marquardt Algorithms in Artificial Neural Networks: A Comparative Empirical Study on Social Data," *Math. Comput. Appl.*, vol. 21, no. 2, p. 20, May 2016.

[101] M. Nielsen, "Neural Networks and Deep Learning," in *Artificial Intelligence*, 2015.

[102] J. F. Mas and J. J. Flores, "The application of artificial neural networks to the analysis of remotely sensed data," *Int. J. Remote Sens.*, vol. 29, no. 3, pp. 617–663, Feb. 2008.

[103] H. Chan *et al.*, "Assessing Gait Patterns of Healthy Adults Climbing Stairs Employing Machine Learning Techniques," *Int. J. Intell. Syst.*, vol. 28, no. 3, pp. 257–270, Mar. 2013.

[104] A. P. Piotrowski and J. J. Napiorkowski, "A comparison of methods to avoid overfitting in neural networks training in the case of catchment runoff modelling," *J. Hydrol.*, vol. 476, pp. 97–111, Jan. 2013.

[105] M. T. Hagan and M. B. Menhaj, "Brief Papers," *Brain Cogn.*, vol. 32, no. 2, pp. 273–344, Nov. 1996.

[106] E. Tosun, K. Aydin, and M. Bilgili, "Comparison of linear regression and artificial neural network model of a diesel engine fueled with biodiesel-alcohol mixtures," *Alexandria Eng. J.*, vol. 55, no. 4, pp. 3081–3089, Dec. 2016.

[107] T. Parr and J. Howard, "The Matrix Calculus You Need For Deep Learning," no. March, 2018.

[108] P. N. Lopes Fernandes, C. P. Santos, and J. C. Moreno, "Feedback-Error Learning Control for Powered Assistive Devices," University of Minho, 2019.

[109] H. Demuth, M. Beale, and M. Hagan, "Neural network toolbox™ 6," *User's Guid.*, 2008.

[110] J. C. B. Gamboa, "Deep Learning for Time-Series Analysis," 2017.

[111] H. Ismail Fawaz, G. Forestier, J. Weber, L. Idoumghar, and P.-A. Muller, "Deep learning for time series classification: a review," *Data Min. Knowl. Discov.*, vol. 33, no. 4, pp. 917–963, Jul. 2019.

[112] S. Hochreiter and J. Schmidhuber, "Long Short-Term Memory," *Neural Comput.*, vol. 9, no. 8, pp. 1735–1780, Nov. 1997.

[113] I. Hadji and R. P. Wildes, "What Do We Understand About Convolutional Networks?," 2018.

[114] K. O'Shea and R. Nash, "An Introduction to Convolutional Neural Networks," pp. 1–11, 2015.

[115] D. P. Kingma and J. Ba, "Adam: A Method for Stochastic Optimization," pp. 1–15, Dec. 2014.

[116] J. Sola and J. Sevilla, "Importance of input data normalization for the application of neural networks to complex industrial problems," *IEEE Trans. Nucl. Sci.*, vol. 44, no. 3, pp. 1464–1468, Jun. 1997.

[117] V. R. Patel and R. G. Mehta, "Impact of Outlier Removal and Normalization Approach in Modified k-Means Clustering Algorithm," *Int. J. Comput. Sci. Issues*, vol. 8, no. 5, pp. 331–336, 2011.

[118] D. Killampilli, "https://towardsdatascience.com/deciding-optimal-filter-size-for-cnns-d6f7b56f9363," 2018. .

[119] M. Reggiani, "CEINMS," 2018. [Online]. Available: https://github.com/CEINMS/CEINMS.

[120] H. Geyer and H. Herr, "A Muscle-Reflex Model That Encodes Principles of Legged Mechanics Produces Human Walking Dynamics and Muscle Activities," *IEEE Trans. Neural Syst. Rehabil. Eng.*, vol. 18, no. 3, pp. 263–273, Jun. 2010.

[121] F. Dzeladini, J. van den Kieboom, and A. Ijspeert, "The contribution of a central pattern generator in a reflex-based neuromuscular model," *Front. Hum. Neurosci.*, vol. 8, no. JUNE, pp. 1–18, Jun. 2014.

[122] E. M. Arnold and S. L. Delp, "Fibre operating lengths of human lower limb muscles during walking," *Philos. Trans. R. Soc. B Biol. Sci.*, vol. 366, no. 1570, pp. 1530–1539, May 2011.